ER-0609

Overview of oxidation phenomena in Boom Clay around galleries of the HADES URF – Status 2019

In-situ and leachate pore water geochemistry, mineralogy and modelling assessment

Authors: Miroslav Honty, Mieke De Craen, Lian Wang and Eef Weetjens

Contract name: ONDRAF/NIRAS, Contrat de R&D "gestion à long terme des dechets radioactifs" (2015-2020)
Contract number: SCK CEN: CO-90-14-3690-00;
ONDRAF: CCHO 2015-0304/00/00;
Specification sheet RS15-SCK-NFE-12
Publication date: 2020-04-23

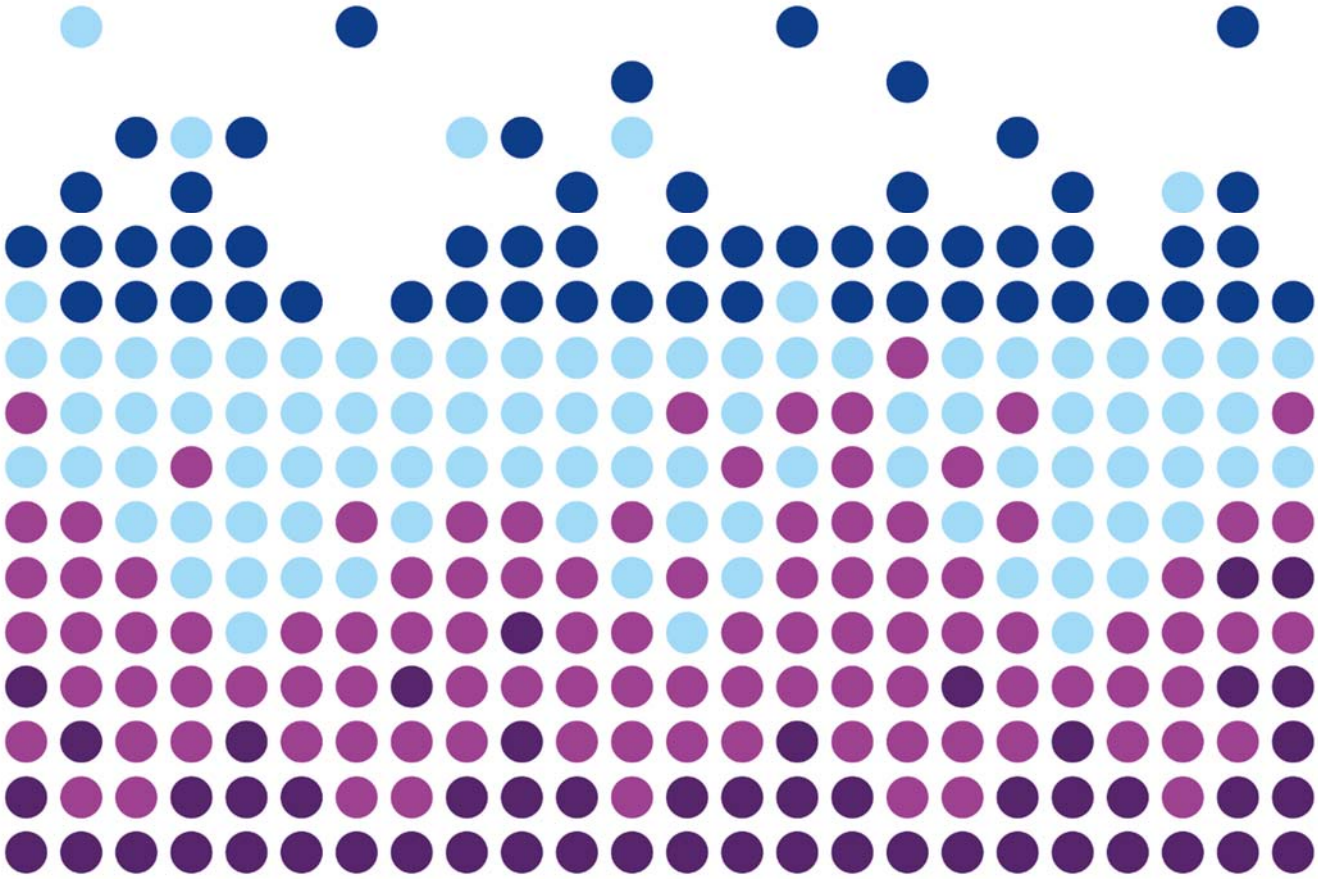

sck cen

Exploring
a better tomorrow

Registered Office:
Avenue Herrmann Debroux 40 - 1160 Brussel – Belgium

Research Centres:
Boeretang 200 - 2400 Mol - Belgium
Chemin du Cyclotron 6 - 1348 Ottignies-Louvain-la-Neuve - Belgium

www.sckcen.be

Copyright rules

Table of Content

Glossary of Abbreviations

CEC	Cation Exchange Capacity
CG	Connecting Gallery
DOC	Dissolved Organic Carbon
EDZ	Excavation Damaged Zone
EXAFS	Extended X-ray Absorption Fine Structure
FTIR	Fourier Transform Infrared Spectroscopy
GC-MS	Gas Chromatography – Mass Spectroscopy
GPC-HPLC	Gel Permeation Chromatography – High Performance Liquid Chromatography)
HADES	High Activity Disposal Experimental Site
ICP-AES	Inductively Coupled Plasma – Atomic Emission Spectroscopy
NF-PRO	Near Field Processes (EC funded project)
PDF	Powder Diffraction File
PG	Praclay Gallery
PRACLAY	PReliminAry demonstration test for CLAY disposal of high radioactive waste
TD	Test Drift
URF	Underground Research Facility
VHLW	Vitrified High Level Waste
XANES	X-ray Absorption Near Edge Structure
XRD	X-ray Diffraction

Abstract

The *in-situ* and leachate pore water geochemistry, mineralogy, (reactive) transport modelling and geochemical modelling data were used in this study in order to evaluate oxidation phenomenon in the Boom Clay around the galleries of the HADES URF. In general, the new data confirm the previously established conceptual model in that oxidation occurs immediately in the course of the gallery excavation due to the creation of the fractures. The extent of these fractures dictates the extent of the oxidation in the host rock, which is limited to a maximum of 1.2 m ahead of the galleries of the HADES URF. After self-sealing of these fractures, a combined diffusion-advection regime redistributes the oxidation products around the galleries. Indeed, the sulphate radial concentration profiles show the decrease of the sulphate concentrations in the deep filters and concomitant increase of their concentrations in the filters nearest to the gallery in the 6 year observation period. The results suggest that the concentrations of sulphates remain relatively high (2560 mg/L at a distance of 0.4 m) in the near field even 25 years after the excavation. This indicates that the sulphates are not easily degradable (reducible) in the course of the open drift phase. Low concentrations of thiosulphates are generally observed (<1 mg/L) and tend to decrease with time confirming their metastable character. The high sulphate concentrations are accompanied with the increased concentrations of Na, K, Ca and Mg. The geochemical model reproduced fairly well the pore water chemistry data and can be explained by mineral dissolution/precipitation and ion-exchange reactions. The gypsum and jarosite are the most common oxidation products based on the XRD, FTIR, Mossbauer spectroscopy and XANES investigation. In samples with jarosite, no carbonates were detected indicating partial or complete loss of pH buffering capacity of the clay. Nevertheless, these mineralogical changes are limited to first few cm from the concrete lining.

Keywords

Oxidation, pore water chemistry, mineralogy, sulphates, Excavation Damaged Zone, Boom Clay, Underground Research Facility

1 Introduction

In Belgium, geological disposal in clay is the primary option for the final disposal of high-level radioactive waste and spent fuel. For the construction and operation of a geological repository for radioactive waste disposal, the excavation and ventilation of galleries is necessary. As such, oxidation of the host rock is unavoidable. Oxidation can affect the favourable host rock characteristics and indirectly influence the engineered barrier system through interactions with the oxidised host rock. Adequate understanding oxidation processes and their effect on the host rock properties is therefore required.

The studies reported here consider oxidation phenomena observed in the Boom Clay. The Boom Clay is an anoxic sediment and is very sensitive to oxidation due to the presence of pyrite and organic matter. The effects of oxidation of Boom Clay were recognised in earlier laboratory work by Henrion et al. (1985), Baeyens et al. (1985) and Griffault et al. (1996) who reported high and variable amounts of sulphate and thiosulphate in their experiments as a result of pyrite oxidation. De Craen et al. (2004a) reported high sulphate concentrations in squeezed Boom Clay pore water and related it to the oxidation of badly-preserved clay cores. Van Geet (2003) described oxidation phenomena observed in the clay at the HADES Underground Research Facility (URF). In the frame of the EC project NF-PRO, De Craen et al. (2008, 2011) performed in-situ experiments in the HADES URF in order to systematically study the effect of oxidation of the Boom Clay as a result of excavation and ventilation of galleries. Blanchart (2011) studied the effect of oxidation on the Boom Clay organic matter. The results of these previous studies are briefly described in chapter 2 of this report.

The scope of this report is to focus on results which were obtained in the period 2008-2013 and have not been reported yet. These mainly relate to a detailed investigation around the PRACLAY gallery. In addition, the periodic sampling and analyses of pore water of various piezometers provided time series and enabled to study the evolution of the pore water chemistry in the oxidised zone around the URF. Furthermore, additional analytical techniques used for mineralogical investigation improved our basic understanding. The work programme performed between 2008 and 2013 is presented in chapter 3.

Chapters 4 and 5 present the location of the experimental setups within the HADES URF and the installation of the experimental equipment respectively. The sampling and analysis protocols are presented in chapter 6.

The results are presented and discussed in chapter 7. General conclusions are provided in chapter 8 and open questions and some recommendations to address these are presented in chapter 9.

2 Result of previous studies on oxidation in Boom Clay

The effects of oxidation of Boom Clay were recognised in earlier experimental work in the laboratory by Henrion et al. (1985), Baeyens et al. (1985) and Griffault et al. (1996) who reported high and variable amounts of sulphate and thiosulphate in their experiments as a result of pyrite oxidation.

Undisturbed Boom Clay pore water at the Mol site is a $NaHCO_3$-type water (De Craen et al., 2004b), in which sulphates are normally absent. However, pyrite oxidation results in the release of Fe^{2+}, SO_4^{2-} and acidity into the pore water. The pore water chemistry has a quick response towards oxidation, and the presence of sulphate in the pore water is a good indicator of oxidation processes.

De Craen et al. (2004a) reported high sulphate concentrations in Boom Clay pore water squeezed out of clay samples and related it to the oxidation of badly-preserved clay cores. As Boom Clay is extremely susceptible to oxidation because of the presence of pyrite, the methodology of sampling, sample preservation and sample treatment is crucial. Nevertheless, despite the precautions that were taken to avoid oxidation, sulphate and thiosulphate concentrations were still measured in squeezed Boom Clay pore waters. The lowest sulphate concentrations were measured in pore waters squeezed out of clay samples immediately after core drilling and retrieval from the boreholes. Higher sulphate concentrations were often measured in the pore water when the clay cores have been preserved for a few months or years. A relation between sulphate concentration and time of preservation (storage) of the clay cores could not be found. Most likely, the initial amount of pyrite in each core, and the conditions of core preservation (good sealing of the aluminium-coated PE bags) are more crucial than the duration of the storage of the samples.

Blanchart (2011) studied the effect of oxidation on the Boom Clay organic matter. Both naturally and artificially oxidized sample sets were studied. The evolution of the geochemical data of solid and dissolved organic matter of the two series was compared using Rock-Eval pyrolysis, bitumen extraction by soxhlet, GC-MS and GPC-HPLC analysis. It was shown that total organic carbon contents in the solid samples were decreasing with oxidation, while dissolved organic carbon contents in the pore waters were increasing upon oxidation: dissolved organic matter was generated during oxidation of the kerogen. Furthermore, the chemical composition of the organic matter changed as well. More details can be found in Blanchart (2011).

For the construction of the Connecting gallery, starting from the second shaft (enlargement of the HADES URF), the temporary concrete wall in the Northern Starting Chamber near the base of the second shaft was removed and the clay was investigated. Oxidation phenomena were observed. Macroscopic investigation clearly indicated the presence of Fe-oxides around fractures created during the excavation of the shaft and starting chamber (rusty halos around the fractures). A microscopic study of this clay indicated that oxidation products (mainly Fe-oxides and gypsum) were always associated with the fractures, and that they were never observed in the clay matrix itself. Based on these observations, Van Geet (2003) concluded that a relation exists between oxidation and fracturing.

Within the frame of the EC project NF-PRO, *in-situ* experiments were performed in the HADES URF (De Craen *et al.*, 2008, 2011). These *in-situ* experiment aimed at comparing the oxidation around the Test Drift (excavated in 1987) and around the Connecting Gallery (excavated in 2002) of the HADES URF. The experimental setups consists of two identical horizontal multi-piezometers installed in the clay from both galleries with filters at different distances to the concrete/clay interface (filters at 0.4 m, 0.7 m, 1.2 m, 2.7 m, 5.7 m and 8.2 m). For the detailed analyses close to the gallery, the first 0.4 m of clay was sampled as well. The drilling of the boreholes for the installation of these piezometers was performed with nitrogen instead of compressed air, in order to prevent any oxidation due to the installation of the experimental setups.

The most striking result of this *in-situ* experiment is definitely the similarity between the radial oxidation profiles observed from the Test Drift and the Connecting Gallery. For both parts of the HADES URF, sampling of Boom Clay pore water indicates that undisturbed conditions still prevail beyond a distance of about 1 m away from the gallery. Within the first metre of clay, a trend of increasing sulphate concentrations towards the gallery is observed. This trend is corroborated by analysis of the pore waters obtained from the leaching of the clay cores taken from this zone. Very close to the gallery lining, the effect of oxidation is the most pronounced and sulphate concentrations up to 31000 mg/l are reached. The high concentrations of sulphate are associated with high concentrations of major[1] cations. This can be explained by mineral precipitation/dissolution reactions and cation exchange. The effect of oxidation on the mineralogy of the Boom Clay has also been investigated, by analysing thin slices from ~50 cm long cores taken with a hollow stainless steel tube with a cutting edge. Pyrite and calcite are still present in the clay close to the gallery lining, but the presence of gypsum, and occasionally jarosite, suggests that oxidation processes indeed affected the mineralogy of the Boom Clay. Nevertheless, the extent of change in mineralogical composition is much smaller than the extent of change in pore water composition. Changes in mineralogy have been

[1] Major cations are Na, K, Ca and Mg

observed on thin slices originating from the first 5 cm of clay ahead of the concrete/clay interface, both in the old and the new gallery. Beyond this distance, the analyses of the thin slices reveals that Boom Clay mineralogy resembles that of the undisturbed clay.

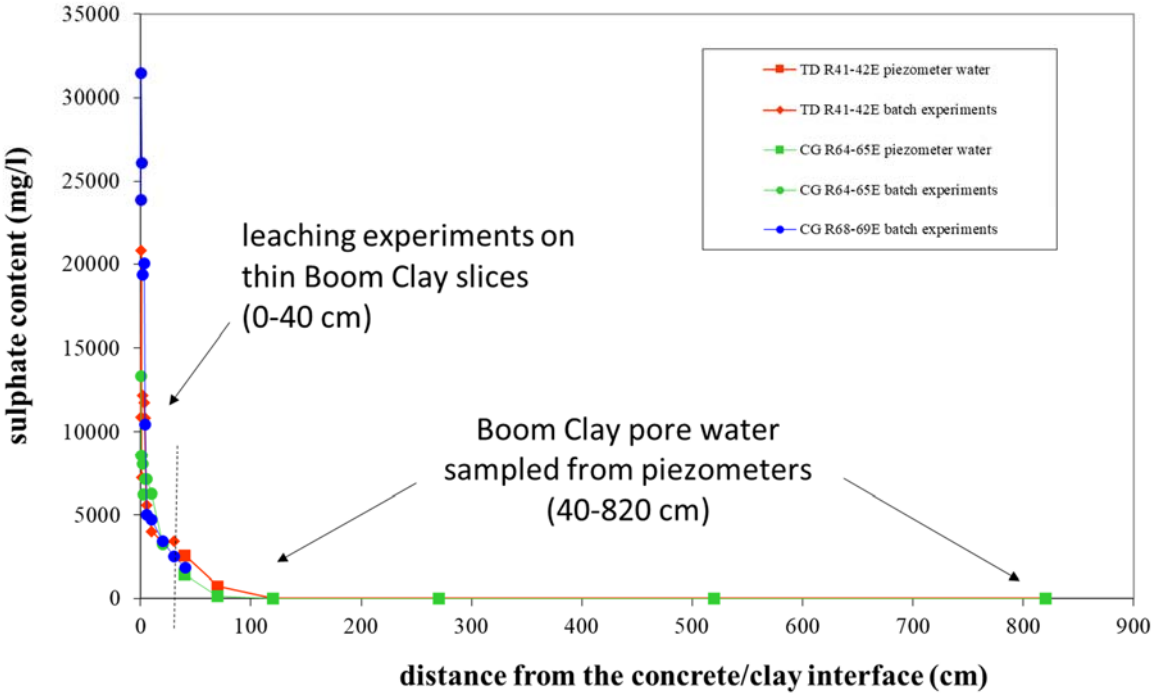

Figure 1: Radial profiles of the sulphate concentration in the Boom Clay pore water around the Test Drift and the Connecting Gallery in function of the distance from the concrete/clay interface. The sulphate concentrations at a distance of 0-40 cm from the concrete/clay interface are calculated from the leaching experiments on the thin clay slices, the sulphate concentrations at a distance of 40-820 cm are measured from piezometer water (modified after De Craen *et al.*, 2008).

Scoping calculations were performed regarding the extent of the oxidised zone in the host formation around a deep repository in Boom Clay. Two types of calculations were performed: 1) oxygen in-diffusion into the host rock, and 2) redistribution of sulphate. Oxygen in-diffusion into the Boom Clay is very limited, as diffusion of dissolved oxygen is a slow process and also because pore water is continuously being drained towards the (open) gallery, opposing the effect of diffusion. Conservative calculations have shown that, even after 20 years, the extent of oxygen in-diffusion into the Boom Clay is limited to less than 1 m. Moreover, when taking into account reactive transport, simulations indicate that the in-diffusing oxygen would be quickly consumed due to pyrite oxidation which would occurs in the first millimetres of clay behind the concrete lining. Concerning the oxidation products, i.e. sulphates, it is shown that the sulphate concentration within the EDZ diminishes fast. While the gallery is open, the majority of the sulphates are transported towards the gallery by the drained pore water[2].The transport of the sulphates further into the Boom Clay is limited, even if the gallery is left open for 50 years.

[2] It should be noted, however, that unlike pore water which evaporates as it enters the gallery and is evacuated by the ventilation system, sulphates will accumulate at or close to the gallery wall under the form of salts.

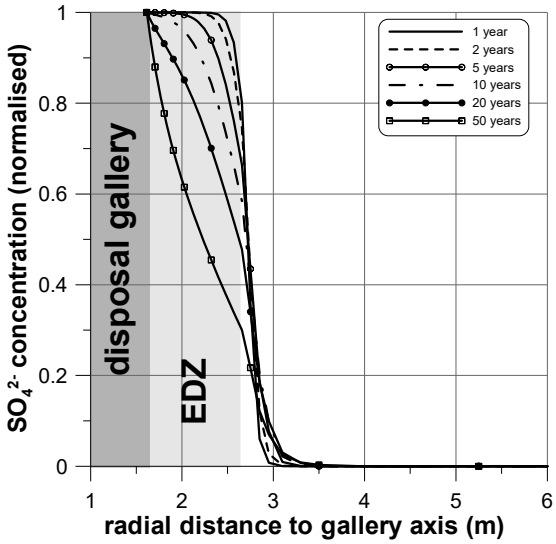

Figure 2: Radial SO_4^{2-} concentration profiles as a function of the distance to the gallery axis (De Craen *et al.*, 2008).

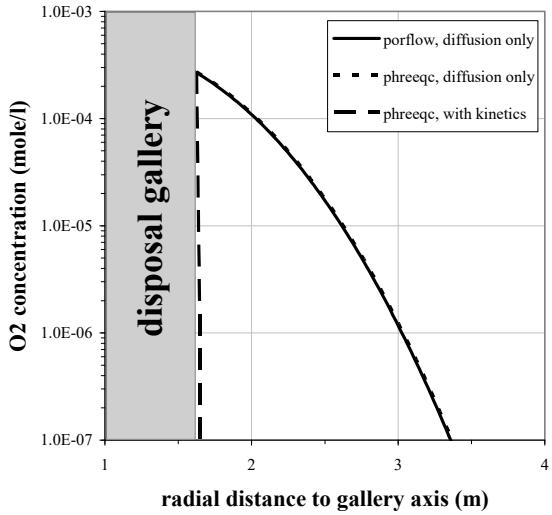

Figure 3: Radial oxygen profiles as function of the distance from the gallery after 20 years (semi-logarithmic plot), for a simulation including diffusion only (the codes PORFLOW and PHREEQC yield similar profiles) and another simulation also including kinetic dissolution of pyrite (with the reactive transport code PHREEQC), (De Craen et al., 2008).

Based on the results of this *in-situ* experiment and the scoping calculations, a storyboard could be worked out for oxidation around HADES Galleries:

1. During excavation of the HADES galleries, fractures are created in the surrounding host rock to a depth of about 1 m (Bastiaens *et al.*, 2003; Bernier *et al.*, 2007). These are open fractures in contact with air. At that moment an instantaneous oxidation occurs along these fractures. Hence, this oxidation extends for about 1 m.
2. Within the plastic Boom Clay sealing of the fractures occurs fast (Bernier *et al.*, 2005, 2007). The oxidation products are then trapped within this first metre around the gallery. A combined diffusion-advection regime is present around the galleries and the oxidation products will be re-distributed. Because the pore water is continuously drained towards the open gallery, the diffusion of the oxidation products further into the undisturbed Boom Clay is extremely limited, and the majority of the oxidation products are transported towards the gallery. Hence, the extent of the oxidised zone still remains limited to about 1 m. During the operational phase after the construction, while the gallery is left open and ventilated, a continuous oxygen supply from the gallery towards the clay massif is maintained. Because the Boom Clay remains fully saturated with pore water, oxygen migration into the clay is controlled by dissolution in the water and diffusion, which is a slow process. Moreover, a combination of processes, namely oxygen consumption by mineral and organic matter oxidation and advection in the opposite direction (due to pore water being drained towards the gallery) strongly limits the oxygen transport further into the Boom Clay. Hence, the extent of the oxidation affected zone remains limited (to about 1 m), even after 20 years as demonstrated by the data collected around the Test Drift.

3 Work programme 2008-2013 on Boom Clay oxidation

The prime objective of this report is to present and integrate new data gathered in the period 2008-2013 and compare them with the data obtained in the context of the previous studies performed on oxidation.

New data involve the detailed investigation of Boom Clay pore waters obtained from various piezometers around the PRACLAY Gallery: PG-70S and PG-70D, CG-30E (previously P30E) and CG-35E (previously P35E). These new data serve to refine and validate the conceptual model elaborated by De Craen *et al.* (2008, 2011) in the frame of the studies performed in the Belgian RD&D programme on geological disposal and in the NF-PRO project.

In addition to the piezometers installed around the PRACLAY gallery, we also used the pore water data from the piezometers CG13U (R13U) and CG13D (R13D) in order to assess the evolution of the oxidized pore waters with time. The initial composition of these pore waters was affected by the drilling with air of the boreholes in which these piezometers were installed. Pore water sampled from the filters closer to the gallery is also affected by the oxidation induced by excavation. The evolution of the pore water composition with time is also assessed in the nitrogen installed piezometers CG-68E (N2CG), TD-41E (N2TD), CG-30E and CG-35E where the initial composition of the pore water is in principle solely affected by oxidation induced by gallery excavation. Old and new data from various piezometers enabled to study the evolution of the pore water composition as a function of time (several years).

The fate of dissolved organic carbon (DOC) in the oxidized zone is evaluated based on numerous analysis of pore waters from piezometers installed using both conventional air drilling and nitrogen drilling procedure. To this moment, only limited data sets were published from air-installed piezometer TD-11D (MORPHEUS, Van Geet, 2004) and nitrogen-installed piezometers CG-30E and CG-35E (P30E and P35E in De Craen *et al.*, 2011).

In addition, the presence of the filters at variable distance from the gallery in the vertical direction allowed to assess the role of the Boom Clay layering on the concentration of oxidation markers (sulphates and DOC) in the vertical profile. It is expected that, for boreholes drilled with air, in the layers with relatively higher pyrite and organic matter content, the concentrations of sulphates and DOC will also be higher in the pore water compared to pore waters associated with layers with relatively lower pyrite and organic matter content. This hypothesis is tested in the light of numerous pore water data from the vertically oriented piezometers PG-70D, CG13D and CG-13U.

The geochemical and transport models, established previously as a part of the conceptual model of Boom Clay oxidation, were revised in the light of the integrated (old and new) data set.

Apart from the pore water chemistry, mineralogical analysis was performed on core material in order to search for the secondary mineral phases formed as a result of oxidation. Some of these techniques were applied for the very first time (XANES/EXAFS) to study speciation of the Fe in the oxidised zone of the Boom Clay.

Based on the work programme 2008-2013, an integration of both old and new results has been done to advance the understanding of oxidation processes in the Boom Clay and their effect on the Boom Clay (pore water composition and mineralogy).

4 The HADES URF and location of the experiments

Figure 4 shows the location of the studied piezometers within the HADES URF.

Piezometers TD-41E (N2TD), CG-64E (N2CG), CG-30E, CG-35E have been installed in N_2-drilled boreholes. Piezometers CG-13U, CG-13D, PG-70S andPG-70D are installed in air-drilled boreholes. In addition to *in-situ* pore water sampling, the leaching extraction technique has been applied to core samples taken with tubes with cutting edges from the Test Drift close to TD-41E (denoted here as TD-41E cores), the Connecting Gallery (CG64E and CG-68E) and the PRACLAY Gallery (PG-70D). More detailed specification of the piezometers is available in Chapter 5.

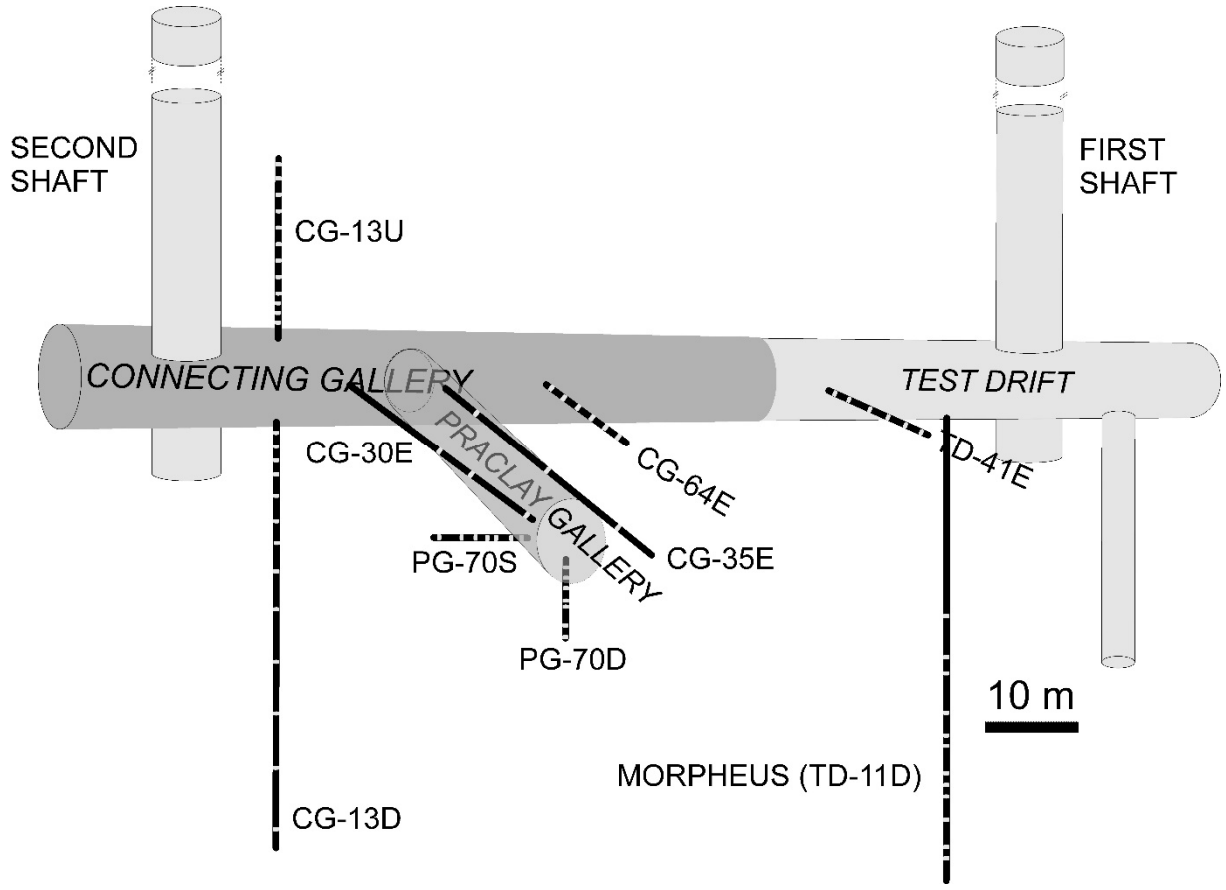

Figure 4. Schematic view of the studied piezometers within the HADES URF in Mol.

5 Borehole drilling, installation of piezometers and the experimental equipment

In general, boreholes in the HADES URF are drilled with pressurised air. However, in the frame of the NF-PRO project (De Craen *et al.*, 2008, 2011, see also chapter 2 of this report), in which the extent of oxidation was studied around the HADES galleries as a result of excavation, additional oxidation due to the drilling of boreholes had to be avoided. Therefore, boreholes for this project were drilled with N_2 instead of air. Also during the installation of the associated piezometers, the boreholes were continuously flushed with N_2 to avoid oxidation as much as possible. This methodology was applied for the first time for piezometers TD-41E (N2TD) and CG-64E (N2CG). These piezometers were furthermore equipped with a dedicated pore water sampling system including a circulation loop, for sampling under in situ conditions. This system is described in the section on sampling and analysis. The same procedure was applied for the drilling of two boreholes close to the PRACLAY gallery and the installation of the associated piezometers CG-30E and CG-35E. These piezometers were installed in advance, from the Connecting Gallery, with the aim to follow the oxidation phenomenon around the PRACLAY gallery while it was excavated. After the PRACLAY gallery excavation and before the start of the heater test, these piezometers allowed to observe the evolution of the pore water composition (including *in-situ* sampling of dissolved gases) during about 7 years. Since 2014, when the PRACLAY heater test was started, these have been used to study the impact of the long-term heating on the pore water composition. This thermal impact will be the subject of another report. A detailed description of these N_2-drilled boreholes and associated piezometers can be found in the report of De Craen *et al.* (2011).

The other piezometers in the vicinity of the PRACLAY Gallery and considered in this report, PG-70D and PG-70S, were both installed in air-drilled boreholes, and were primarily aimed to follow-up the pressure build-up as a result of the long-term heat experiment. Although these piezometers were mainly aimed at THM studies related to the large scale heater test, they provided valuable data to assess the variations of pore water composition in the horizontal and vertical direction.

The piezometers CG-13U and CG-13D (installed in air-drilled boreholes) were initially installed to follow the pressure evolution, but can be used to trace oxygen perturbation inside the boreholes. The piezometer CG-13U is oriented vertically upwards and CG-13D vertically downwards from the Connecting Gallery. In total, they comprise about 60 m of the Boom Clay depth. The detailed characteristics of the piezometers CG-13U and CG-13D is given in De Craen (2005).

Annex 1 gives the Lambert coordinates of the studied piezometer filters.

The Table below summarizes some key characteristics of the piezometers used in this study.

Table 1. List of the piezometers used in this study.

piezometer	Filter GSIS ID	Filter distance from the gallery (extrados) (m, from-to)	orientation (H - horizontal/ V - vertical)	filter material	inner diameter filter mm)	mode of drilling (A - air/N- nitrogen)	mode of PW sampling	leaching of the clay core Y- yes/N - no, total length of the core (m)
TD-41E (N2TD)	TD-41E-1	8,15-8,25	H	SS AISI 304	54	N	circulation	N
	TD-41E-2	5,15-5,25	H	SS AISI 304	54	N	circulation	N
	TD-41E-3	2,65-2,75	H	SS AISI 304	54	N	circulation	N
	TD-41E-4	1,15-1,25	H	SS AISI 304	54	N	circulation	N
	TD-41E-5	0,65-0,75	H	SS AISI 304	54	N	circulation	N
	TD-41E-6	0,35-0,45	H	SS AISI 304	54	N	circulation	Y, 0,365
CG-64E (N2CG)	CG-64E-1	8,15-8,25	H	SS AISI 304	54	N	circulation	N
	CG-64E-2	5,15-5,25	H	SS AISI 304	54	N	circulation	N
	CG-64E-3	2,65-2,75	H	SS AISI 304	54	N	circulation	N
	CG-64E-4	1,15-1,25	H	SS AISI 304	54	N	circulation	N
	CG-64E-5	0,65-0,75	H	SS AISI 304	54	N	circulation	N
	CG-64E-6	0,35-0,45	H	SS AISI 304	54	N	circulation	Y, 0,7
CG-13U (R13U)	CG13U-01	19,575-19,625	V	SS AISI 304	90	A	flow-out	N
	CG13U-02	17,575-17,625	V	SS AISI 304	90	A	flow-out	N
	CG13U-03	15,575-15,625	V	SS AISI 304	90	A	flow-out	N
	CG13U-04	13,575-13,625	V	SS AISI 304	90	A	flow-out	N
	CG13U-05	11,575-11,625	V	SS AISI 304	90	A	flow-out	N
	CG13U-06	9,575-9,625	V	SS AISI 304	90	A	flow-out	N
	CG13U-07	7,575-7,625	V	SS AISI 304	90	A	flow-out	N
	CG13U-08	5,575-5,625	V	SS AISI 304	90	A	flow-out	N
	CG13U-09	3,575-3,625	V	SS AISI 304	90	A	flow-out	N
	CG13U-10	2,575-2,625	V	SS AISI 304	90	A	flow-out	N
	CG13U-11	1,575-1,625	V	SS AISI 304	90	A	flow-out	N
	CG13U-12	0,575-0,625	V	SS AISI 304	90	A	flow-out	N
CG-13D (R13D)	CG-13D-01	39,575-39,625	V	SS AISI 304	88	A	flow-out	N
	CG-13D-02	35,575-35,625	V	SS AISI 304	88	A	flow-out	N
	CG-13D-03	30,575-30,625	V	SS AISI 304	88	A	flow-out	N
	CG-13D-04	25,575-25,625	V	SS AISI 304	88	A	flow-out	N
	CG-13D-05	18,575-18,625	V	SS AISI 304	88	A	flow-out	N
	CG-13D-06	14,575-14,625	V	SS AISI 304	88	A	flow-out	N
	CG-13D-07	11,575-11,625	V	SS AISI 304	88	A	flow-out	N
	CG-13D-08	8,575-8,625	V	SS AISI 304	88	A	flow-out	N
	CG-13D-09	5,575-5,625	V	SS AISI 304	88	A	flow-out	N
	CG-13D-10	3,575-3,625	V	SS AISI 304	88	A	flow-out	N
	CG-13D-11	2,575-2,625	V	SS AISI 304	88	A	flow-out	N
	CG-13D-12	1,575-1,625	V	SS AISI 304	88	A	flow-out	N
	CG-13D-13	0,575-0,625	V	SS AISI 304	88	A	flow-out	N

Table 1 continued. List of piezometers used in this study. *Although the boreholes were drilled from the Connecting Gallery, here the distance from the PRACLAY gallery is indicated as this one is more relevant with respect to EDZ.

piezometer	Filter GSIS ID	Filter distance from the gallery (extrados) (m, from-to)	orientation (H - horizontal/V - vertical)	filter material	inner diameter filter mm)	mode of drilling (A - air/N- nitrogen)	mode of PW sampling	leaching of the clay core Y- yes/N - no, total length of the core (m)
CG-30E	CG-30E-1	1.89*	ID	SS AISI 316L	90	N	circulation	N
	CG-30E-4	0.88*	ID	SS AISI 316L	90	N	circulation	N
	CG-30E-6	0.55*	ID	SS AISI 316L	90	N	circulation	N
CG-35E	CG-35E-2	1.14*	H	SS AISI 316L	90	N	circulation	N
	CG-35E-6	1.00*	H	SS AISI 316L	90	N	circulation	N
	CG-35E-11	0.88*	H	SS AISI 316L	90	N	circulation	N
PG-70S	PG70S-1	9.94	H	SS AISI 316L	75	A	flow-out	N
	PG70S-2	6.96	H	SS AISI 316L	75	A	flow-out	N
	PG70S-3	4.92	H	SS AISI 316L	75	A	flow-out	N
	PG70S-4	2.93	H	SS AISI 316L	75	A	flow-out	N
	PG70S-5	1.94	H	SS AISI 316L	75	A	flow-out	N
	PG70S-6	0.95	H	SS AISI 316L	75	A	flow-out	N
	PG-70S-7	0.45	H	SS AISI 316L	75	A	flow-out	Y, 0,28
PG-70D	PG70D-1	10	V	SS AISI 316L	75	A	flow-out	N
	PG70D-2	8.49	V	SS AISI 316L	75	A	flow-out	N
	PG70D-3	3.50	V	SS AISI 316L	75	A	flow-out	N
	PG70D-4	5.00	V	SS AISI 316L	75	A	flow-out	N
	PG70D-5	6.00	V	SS AISI 316L	75	A	flow-out	N
	PG70D-6	1.50	V	SS AISI 316L	75	A	flow-out	N
	PG70D-7	0.75	V	SS AISI 316L	75	A	flow-out	Y, 0,28

6 Sampling and analyses

6.1 Direct pore water sampling

The pore water samples were acquired either *in-situ* directly from the piezometer filters or *ex-situ* by leaching of clay core material obtained during the drilling of the boreholes (see 6.2).

In-situ pore water sampling from piezometer filters was done via the sampling bypass loop connected to the circulation system via Swagelock quick connectors (flow through system, Figure 5, De Craen *et al.*, 2011) in case of the piezometers TD-41E, CG-64E, CG-30E and CG-35E. From other piezometers not equipped with circulation systems, the pore water was collected directly with the aid of septum bottles connected to the filters by tubing at one end (flow out). The sampling procedure is detailed in the report of De Craen *et al.* (2018).

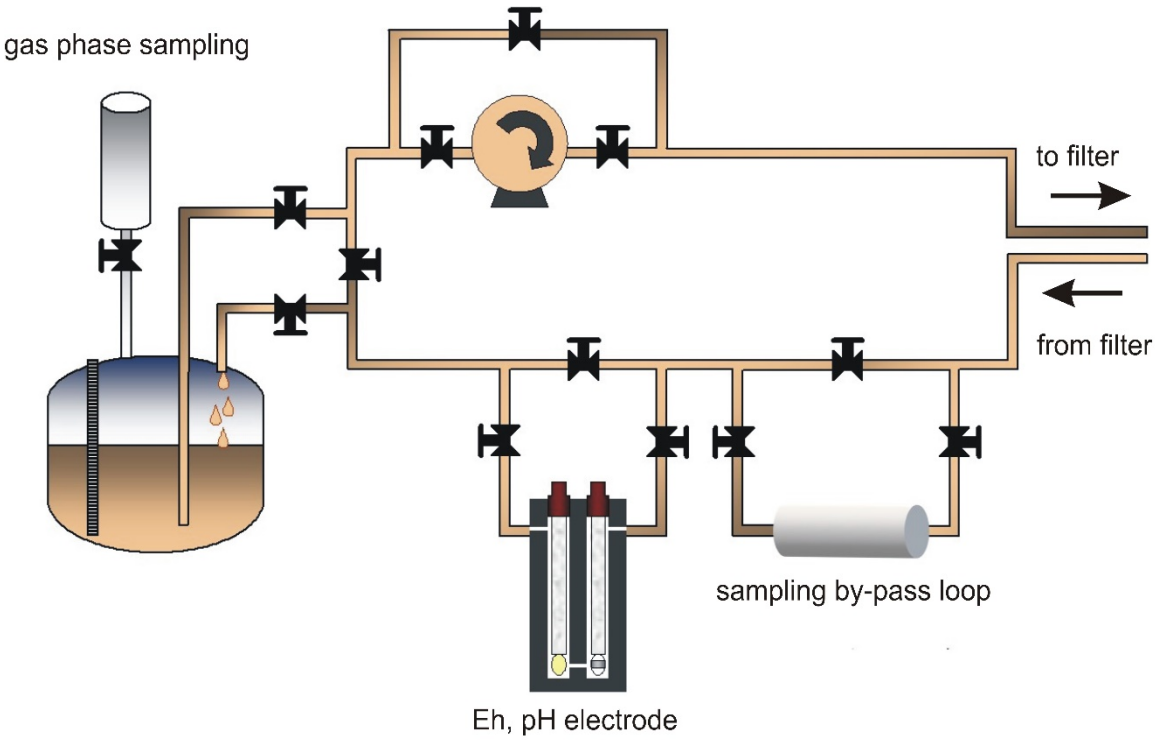

Figure 5. Simplified sketch of the circulation system for *in-situ* pore water and gas sampling connected to piezometers TD-41E and CG-68E in the frame of the NF-PRO project. Currently in use in the piezometers CG-30E and CG-35E around PRACLAY Gallery. Modified after De Craen *et al.* (2011).

6.2 Leaching of clay cores obtained using cutting edges and processing for mineralogical investigation

The core samples were taken with the aid of a hollow stainless steel tube (diameter 4.75 cm, length 50 cm) with a cutting edge on the front side. The cutting edge enables to push the tube into the plastic clay, extruding a clay core into the tube. This strategy prevents oxidation of the clay core except from the two ends of the tube. Upon retrieval, the stainless steel tube with cutting edge containing the clay core was immediately vacuum packed into Al-coated polyethylene bags, and stored at 4°C. The same sampling procedure was undertaken in the Connecting Gallery between rings 64 and 65 towards the east (CG-64E), rings 68 and 69 towards the east (CG-68E), the Test Drift between rings 41 and 42 towards the east (TD-41E) and the PRACLAY Gallery between rings 70 to 71 downwards (PG-70D). Using this technique, clay cores with a total length 70 cm could be retrieved from the CG-64E, 40 cm from the CG-68E, 36.5 cm from the TD41E and 28 cm both in the PG70D and PG70S.

For determination of pore water composition (leaching), the clay cores were pressed out of the tubes and cut into thin slices. The slicing, drying and leaching was performed as described in De Craen *et al.* (2008) in the glove box under Ar atmosphere with 4000 ppm CO_2 to mimic the in situ partial pressure of CO_2. The first 10 cm of clay was cut into slices of 2 mm, further

away, slices of 5 mm were cut. Water content was determined by weighing the samples before and after drying in an oven at 60°C overnight [3].

The leaching technique was performed on clay core material following the procedure of De Craen *et al.* (2004b). For selected samples, different solid/liquid ratios were used: 1/2, 1/5, 1/10, 1/50 and 1/100 (g of dried clay/ml of MilliQ water). All other samples were leached at a S/L ratio of 1/10. The leaching was performed in the thick-walled Nalgene® tubes, shaken continuously for two weeks, after which a steady aqueous concentration of the major ions can be assumed based on previous experiments (De Craen et al, 2004b). After the leaching, the suspensions were centrifuged at 21,255 g for 2 hours and subsequently filtered through 0.45 µm filters, prior to chemical analysis for major cations and anions.

The aliquots from thin slices were dried at 60°C and hand-crushed with the use of pestle and mortar inside a glovebox. The clay powders were further used for mineralogical investigation (XRD, FTIR, Mössbauer spectroscopy, XANES and CEC).

6.3 Analytical techniques

To determine the pore water composition, ion chromatography, ICP-AES (MS), acid-base titration (alkalinity), pH, organic and inorganic carbon analysis were applied. The anions were analyzed using Ion Chromatography, major cations by ICP-AES and trace elements by ICP-MS. Alkalinity measurements were done by titration according to the method described in Rounds and Wilde (2001). The total organic carbon (TOC) and total inorganic carbon (TIC) contents were measured with a high-temperature TOC analyser type Hach-Lange IL 550 TOC. pH measurements were done with the glass electrode InLab 411.

Aliquots of the solid samples were used for XRD and FTIR analysis. The whole-rock samples were hand-crushed in the agate mortar prior to XRD analysis. The whole-rock randomly oriented specimens were scanned using a Philips X'Pert Pro System with the following settings: accelerated voltage 45 kV, beam current 40 mA, mask 10 mm, soller slit 0.04 radians, theta-theta goniometer, CuKα radiation, step size 0.02°2theta, 20s/step and Xcelerator detector. The resulting patterns were evaluated with the aid of X'Pert High Score Plus software and PDF Mineral database. FTIR spectra in the middle infrared region (4000-400 cm^{-1}) were obtained on a Nicolet Magna 750 Fourier transform infrared spectrometer using KBr pressed disk technique (1 mg of sample and 200 mg KBr). Discs were heated in a furnace overnight at 150°C to minimize the amount of the adsorbed water. Spectra manipulations were performed using the OMNIC software package (Nicolet Instruments Corp.).

X-ray absorption spectra were collected on the joint Netherlands-Belgium beam line (BM 26) of the ESRF (European Synchrotron Radiation Facility) with the storage ring operating at 6 GeV and maximum beam current of 200 mA. All spectra were collected at room temperature in fluorescence mode and the intensity of X-rays was monitored by solid state 8-element Ge detector. The energy of the incident beam was tuned with a Si (111) monochromator and the vertical beam height was usually 2 mm. Energy was calibrated using an Fe metal foil and setting the K-edge energy to 7118 eV. The mineral standards were diluted with cellulose and pressed into pellets of ~0.5 cm diameter and 2 mm thickness using the mechanical press and predesigned stainless steel cells.

The collection of Fe containing mineral standards represented the broad range of Fe oxidation states and valences. These are synthetic standards fully described in Majzlan *et al.* (2003a, 2003b) and Majzlan *et al.* (2004). The non-clay Fe mineral standards included hematite (α-Fe2O3), lepidocrocite (γ-FeOOH), akaganeite (β-FeOOH), goethite (α-FeOOH), ferrihydrite ($Fe_2O_3 \times 0.5H_2O$), schwertmannite ~$FeO(OH)_{(3/4)}(SO_4)_{(1/8)}$ and jarosite ($KFe_3(SO_4)_2(OH)_6$). The natural pyrite was extracted from Boom Clay. The other Fe reduced standards were synthetic siderite $FeCO_3$ and pyrhotite FeS.

The clay mineral standards included "Cheto" smectite SAz-1 with the structural formula $(Ca_{0.39}, Na_{0.36}, K_{0.02})(Al_{2.71}, Fe_{0.12}, Mg_{1.11}, Mn_{0.01}, Ti_{0.03})(Si_{8.0})O_{20}(OH)_4$, illite IMt-2 with the structural formula $(K_{1.37}, Mg_{0.09}, Ca_{0.06})(Al_{2.69}, Fe[III]_{0.67}, Fe[II]_{0.06}, Mg_{0.43}, Ti_{0.06})(Si_{6.77}, Al_{1.23})O_{20}(OH)_4$; mixed layer illite-smectite ISCz-1 (70/30 ordered) with the structural formula $(Mg_{0.03}, Ca_{0.1}, Na_{0.09}, K_{0.95})(Al_{3.39}, Fe[III]_{0.12}Mg_{0.48})(Si_{7.19}, Al_{0.81})O_{20}(OH)_4$ and chlorite ripidolite CCa-2 with the structural formula $(Ca_{0.5})(Mg_{4.44}, Fe[III]_{3.47}, Fe[II]_{3.02}, Al_{0.60}, Mn_{0.01}, Ti_{0.06})(Si_{4.51}, Al_{3.49})O_{20}(OH)_{16}$. Because of the high beam energy generated by the synchrotron, the mineral standards had to be diluted by mixing with cellulose to reduce the iron concentration.

Boom Clay natural samples were pressed without mixing with cellulose (as their iron content was low enough) from powders and X-rayed using the same settings as for mineral standards. The sample pellets were fixed on Kapton tape and mounted on plastic rings to fit the sample holder. At least a minimum of 3 scans were collected and averaged for each sample. XANES

[3] There is no consensus on which temperature should be applied in order to determine water content by drying. However for BC, weight loss between 60 and 110°C is considered low (max 1 wt%) compared to total mass loss of 18-20 wt%.

spectra were processed by the ATHENA software (Ravel and Newville, 2005). For the fitting of experimental samples with the standards we used linear combination analysis incorporated in the ATHENA software. The fitting exercise was performed in the range -20 to 80 eV from the E_0 value and E_0 value was allowed to shift between the standards. The quality of the fit can be estimated based on the R-factor which is defined as $\Sigma(\text{data-fit})^2/\Sigma(\text{data})^2$. Alternatively, the relative goodness-of-fit between natural BC samples and standards is described by a reduced χ^2 parameter which is the least square F value divided by the number of independent data points minus the number of varied fit parameters (e.g. O' Day *et al.*, 1994; George and Pickering, 2000 and O' Day *et al.*, 2004).

Mössbauer spectra were obtained at liquid nitrogen temperatures (77 K) and at room temperature (300K) using a Wissel spectrometer equipped with an Oxford Variox 316 cryostat. A ^{57}Co source was moved in constant acceleration mode. Velocity calibration was carried out with respect to the centre of a Fe foil spectrum at room temperature. The spectra were deconvoluted with a least-squares computer program assuming Lorentzian line-shapes.

The cation-exchange capacity (CEC) was determined using a copper(II)triethylenetetramine as an ion-exchanger and distilled water as an electrolyte background solution according to procedure of Amman *et al.* (2005). For the ion-exchange reaction, the 0.01 mol/l solution of the complex copper(II)triethylenetetramine, $[Cu\ Trien]^{2+}$ was used. The 50, 100 and 150 mg of dried Boom clay whole-rock powders were added to 40 ml of distilled water and 10 ml solution of $[Cu\ Trien]^{2+}$. The suspensions of clays were dispersed by an ultrasonic treatment. After ultrasonic treatment, the suspensions were shaken for at least 30 minutes. The supernatant solution was separated by centrifugation at a 2683 g for 20 minutes and the concentration of Cu(II) complex was determined by UV-VIS spectrophotometry (Perkin Elmer, Lambda 40). Solution absorbance was measured at 577 nm (Meier and Kahr, 1999). The amount of $[Cu\ Trien]^{2+}$ adsorbed was determined using Lambert-Beers law. The CEC was then calculated as a difference of added and non-adsorbed copper complex. The standard deviation of the resultant CEC value was calculated based on three independent CEC measurements for 50, 100 and 150 mg weight loads respectively.

7 Results and discussion

7.1 Pore water geochemistry

In this section we 1) briefly describe the general mechanism of the oxidation and its impact on the Boom Clay pore water composition, 2) present the pore water data as a function of distance from the gallery in order to pinpoint the extent of the oxidation 3) evaluate the evolution of the pore water composition as a function of time 4) assess the effect of the Boom Clay layering on the composition of the pore water 5) discuss the impact of oxidation on the dissolved organic matter in the pore water and 6) draw conclusions on the overall effect of the oxidation on the Boom Clay pore water.

In-situ pore water data for this chapter originate from:

- the piezometers installed in N_2-drilled boreholes from the Test Drift (TD-41E) and the Connecting Gallery (CG-68E, CG-30E and CG-35E);
- the piezometers installed in air-drilled boreholes, which include the TD-11D piezometer (MORPHEUS) installed from the Test Drift, piezometers CG-13U and CG-13D installed from the Connecting Gallery and piezometers PG-70S and PG-70D installed from the PRACLAY Gallery;

The *in-situ* pore water data are complemented by the batch pore water chemistry analyses of clay samples collected from boreholes drilled from the Test Drift (TD-41E), the Connecting Gallery (CG-68E) and the PRACLAY Gallery (PG-70D).

The *in-situ* pore water data of the piezometer TD-41E (N2TD) are reported in Annex 2. The data series from 2005 and 2007 are taken as such from De Craen *et al.* (2008), the data are extended with data of 2011. *In-situ* pore water data from the piezometer CG-68E (N2CG) is reported in Annex 3. Similarly to TD-41E, the pore water data from 2005 and 2007 were first published in De Craen *et al.* (2008), the data from 2011 are new data. The pore water chemistries of the piezometers CG-30E and CG-35E are reported in Annex 4 and Annex 5. The data from 2007 originate from the report of De Craen *et al.* (2011). Since then numerous sampling campaigns were carried out on these piezometers and led to the most complete pore water chemistry data set from the nitrogen installed piezometers.

In addition to nitrogen installed piezometers, the *in-situ* pore water chemistry data from the air-drilled piezometers are reported in Annex 6 (CG-13U), Annex 7 (CG-13D) and Annex 8 (PG-70S and PG-70D).

The batch pore water data acquired by aqueous leaching are reported in Annex 9 (TD-41E), Annex 10 (CG-68E) and Annex 11 (PG-70D). They serve to fill the data gaps in the immediate vicinity of the galleries (distance < 40 cm), where no piezometer filters are present. As such they are more sensitive to experimental artefacts introduced in the course of the leaching. Unlike the other elements the sulphate concentrations exhibited a linear relationship with the S/L ratios from the leaching tests, therefore sulphates can be considered as non-reacting during the leaching procedure and may thus be used to complement *in-situ* data in order to construct sulphate concentration profiles around galleries. The combined *in-situ* and batch pore water data are also used as an input for mass balance calculations and transport modelling, presented in section 7.3.

7.1.1 Background: phenomenological description of the oxidation and its impact on the Boom Clay pore water composition

Pyrite and organic matter, both present in Boom Clay are sensitive to oxidation. Pyrite oxidation results in the release of Fe^{2+}, SO_4^{2-} and acidity (protons) into the pore water, as indicated by the following chemical reaction:

$$FeS_2 + 7/2\ O_2(aq.) + H_2O \leftrightarrow Fe^{2+} + 2\ SO_4^{2-} + 2\ H^+$$

The acidity is buffered by water-rock interactions, mainly the dissolution of calcite:

$$CaCO_3 + H^+ \leftrightarrow Ca^{2+} + HCO_3^-$$

Hence, calcium and bicarbonate are released into the pore water. The increase in calcium in the pore water will subsequently induce ion exchange reactions onto clay minerals, and the calcium will be exchanged with sodium, potassium, and magnesium according to following reactions:

$$2\ >X{:}Na + Ca^{2+} \Leftrightarrow >X_2{:}Ca + 2\ Na^+$$
$$2\ >X{:}K + Ca^{2+} \Leftrightarrow >X_2{:}Ca + 2\ K^+$$
$$>X{:}Mg^{2+} + Ca^{2+} \Leftrightarrow >X{:}Ca^{2+} + Mg^{2+}$$

Where >X: stands for the cation exchange site on clay mineral surfaces.

Mineral precipitation/dissolution reactions and cation exchange thus typically result in the decrease of the pH and the increase of sulphate and cation concentrations in the Boom Clay pore water, as observed by De Craen *et al.* (2004b).

Whereas the effect of oxidation on the pyrite and its impact on the composition of the pore water is well studied and documented (e.g. Evangelou, 1995 and references therein), the impact of oxidation on the fate of the soluble part of the organic matter in the pore water is far less understood. The study of Blanchart (Blanchart, 2011, Blanchart *et al.* 2012) on series of naturally and artificially exposed samples showed that the amount of dissolved organic carbon (DOC) in general increased with the duration of exposure to air. In addition, the molecular size distribution of the DOC shifts towards lower molecular weights upon oxidation.

7.1.2 Evolution of the pore water composition as a function of the distance from the gallery

In general, the pore water composition of the studied samples reflects typical features of the oxidation, i.e. elevated sulphate (Figure 6a) and major cation concentrations (Figure 6b to Figure 6d) compared to pore waters of the undisturbed Boom Clay. Irrespectively of the piezometer location, installed from the Test Drift or (younger) Connecting Gallery, the sulphate and major cation contents tend to decrease with the increasing distance from the gallery. The same trend is observed in the piezometers installed with the use of nitrogen and air, although the extent of the oxidation seems to be larger in the latter. It is not surprising bearing in mind the fact that in the piezometers installed in air-installed boreholes, the oxidation related to drilling is superimposed on the oxidation linked to the excavation of the gallery.

We observe from the data on pore water collected from the piezometers CG-64E, TD-41E, CG-30E and CG-35E installed in nitrogen drilled boreholes, plotted as blue diamonds in Figure 6a, that for most of the samples, the sulphate concentration is lower than the upper limit of concentration of 10 mg/L of sulphates proposed by De Craen *et al.* (2004b) for the undisturbed Boom Clay pore water. However, up to a distance of 1.2 metres from the interface between the gallery lining and the clay, a significant number of samples were obtained in which the sulphate concentration was well above this limit. One sample at a distance of 1.89 metres also exhibited a concentration slightly above this limit of 10 mg/L.

This is consistent with the extent of the oxidised zone proposed by De Craen *et al.* (2008) which was up to 0.7 – 1.2 m from the gallery lining. It is also generally consistent with the conceptual model elaborated by De Craen *et al.* (2008) in which the extent of the oxidized zone is assumed to be more or less equal to the extent of the initially open fractures created during excavation in the surrounding host rock, to a depth of about 1 m (Bastiaens *et al.*, 2003; Bernier *et al.*, 2007). These open fractures are initially in contact with the ambient air. As a consequence, the oxidation occurs instantaneously along these fractures. The couple of data points above 10 mg/l at distances between 1 and 1.89 metres could be explained by the variability of the fracture network extension. The fact that even in the first metre, the majority of the data points lie below the 10 mg/L limit suggests that in the matrix, between fractures, the clay remains essentially undisturbed by oxidation.

Radial profiles of major cations are shown on Figure 6b-d. These profiles display the same trend as the sulphate concentrations. As such, these concentrations profiles reflect the effect of cation exchange as explained in the previous section.

Pore water composition data obtained from piezometers installed in air-drilled borehole are also shown on Figure 6 as black circles. Unsurprisingly, oxidation appears to be stronger for these boreholes compared to the N_2-drilled ones. The relatively higher sulphate concentrations can be explained by the additional oxidation incurred during the drilling. Comparison with the profiles obtained from N_2-drilled boreholes suggests that beyond a couple of metres, the sulphate profile obtained from the air-drilled boreholes could be more influenced by the duration of exposure to air during drilling and installation of the equipment rather than by actual distance to the gallery.

In contrast to sulphate and the major elemental composition of the oxidized Boom Clay pore water, which can be explained in terms of relatively simple mechanisms as well as modelled using one of the geochemical codes, the fate of the dissolved organic carbon in the pore waters from the oxidation disturbed zone is less obvious. In the piezometers CG-64E (N2CG) and TD-41E (N2TD) – both installed with the use of N_2 – the DOC values are relatively high (771 and 532 mg/L) close to the gallery compared to the DOC values typical for undisturbed Boom Clay (50-150 mg/L). Remarkably, the highest DOC concentrations were not found in the filters closest to the gallery, at a distance of 0.4 m, but in the filters located at a distance of 0.7 m (Figure 7). No anomalous DOC values were measured in any of the filters of the piezometers CG-30E and CG-35E. It is worth mentioning that these piezometers were also installed with the aid of nitrogen. The DOC values remained stable since 2007 (soon after installation) till the measurements in 2013, before the start of the heating of PRACLAY (see Chapter on Evolution of the pore water composition as a function of time). It can also be noted that, in contrast with sulphates and major cations concentrations, the lowest DOC concentrations were measured in the filters of the air-installed piezometer

PG-70S. Except from some elevated DOC concentrations observed in the piezometers CG-64E and TD-41E, our data indicate that unlike sulphates, there is no apparent link between DOC and the distance from the gallery lining (Figure 7).

In summary, the pore water composition data clearly show that the effect of oxidation is the most pronounced next to the gallery lining and quickly decreases with increasing distance from the gallery, as indicated by sulphate and major cations concentration profiles. Assuming that only pore waters from the nitrogen installed piezometers are relevant to delimit the oxidation disturbed zone, this zone is limited to about 1.2 meters from the gallery lining/clay interface. Further away, the pore water composition resembles the typical composition in undisturbed conditions. Whereas sulphate concentrations tend to rapidly decrease at increasing distances from the gallery, no clear trend could be identified in the case of DOC, although a couple of relatively high DOC concentrations measurements were obtained in some filters close, but not the closest, to the gallery lining. The fact that similar observations are made around the Test Drift and the (younger) Connecting Gallery suggests that most of the oxidation occurs during excavation, with little or no effect of the duration of the open drift phase.

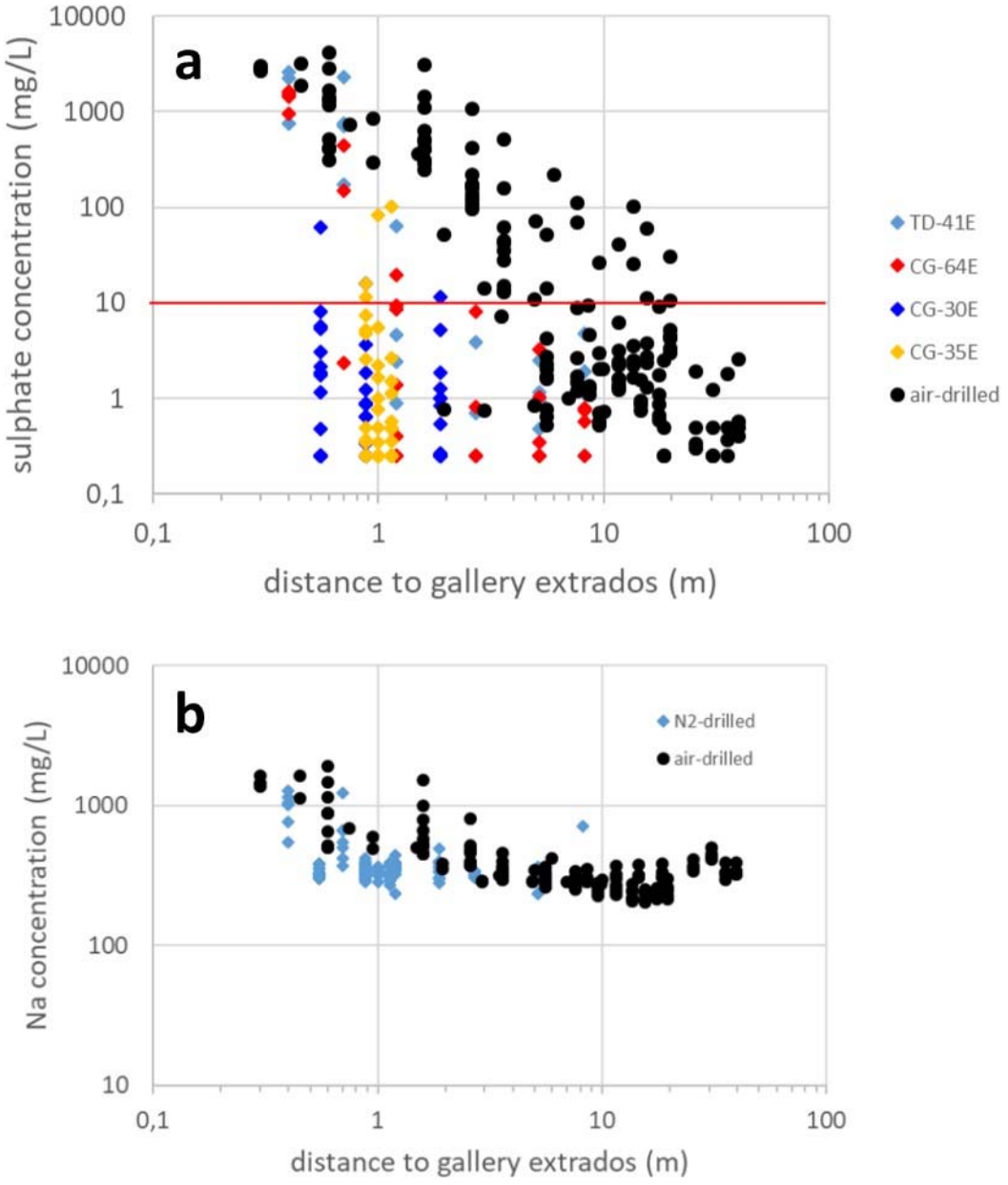

Figure 6. Sulphate (a) and sodium (b) concentration profiles as a function of increasing distance from the gallery. Blue symbols – nitrogen installed piezometers, black symbols – air installed piezometers.

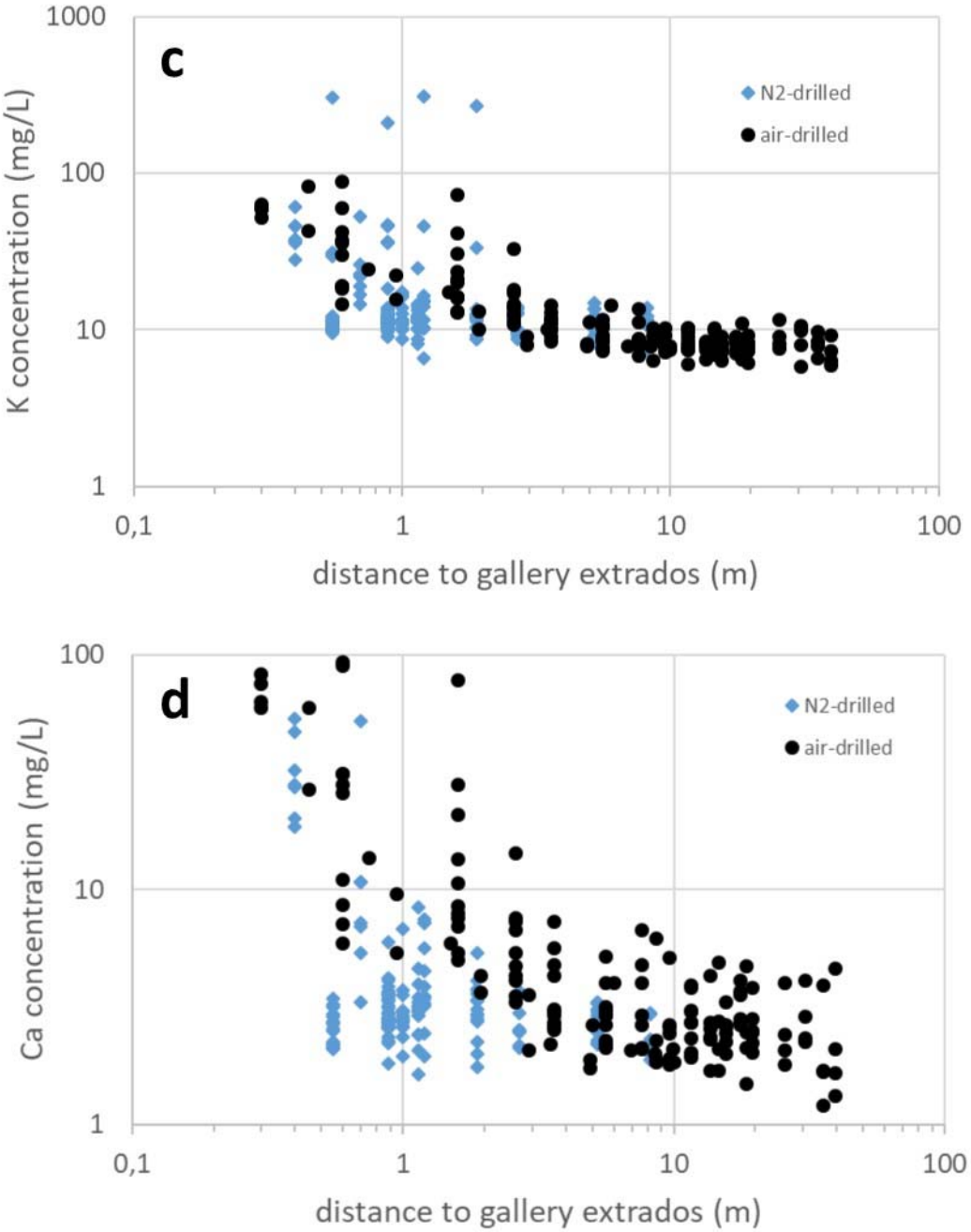

Figure 6 continued. Potassium (c) and calcium (d) concentration profiles as a function of increasing distance from the gallery. Blue symbols – nitrogen installed piezometers, black symbols – air installed piezometers.

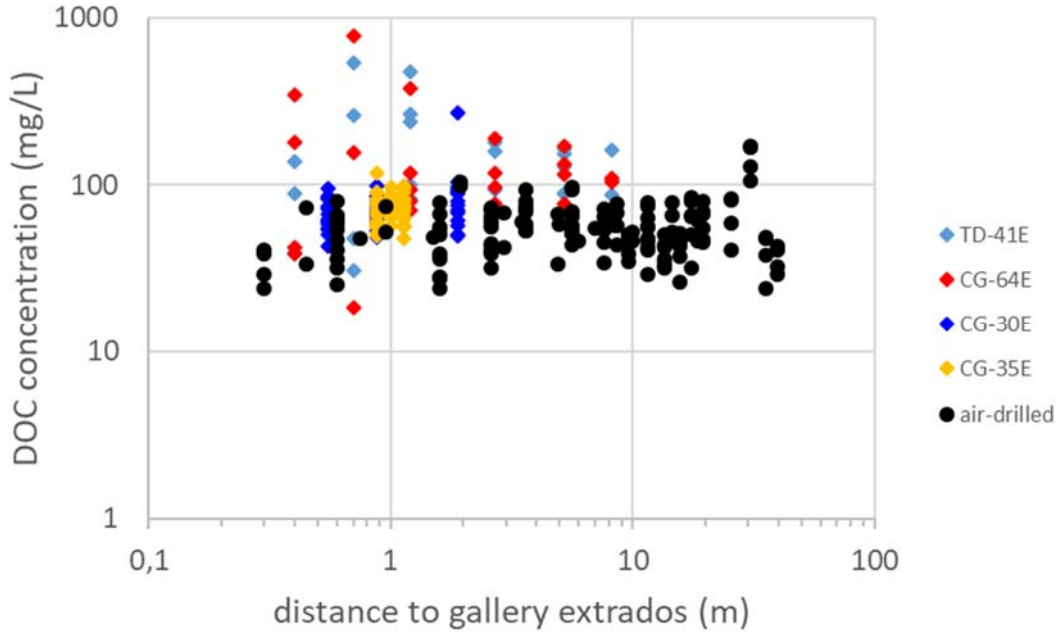

Figure 7. Dissolved organic carbon concentrations in the pore waters as a function of the distance from the concrete/clay interface. Diamond symbols - piezometers installed under nitrogen atmosphere (TD-41E, CG-64E, CG-30E and CG-35E) Air-installed piezometers (CG-13U, CG-13D, PG-70S and PG70D) lumped as black symbols.

7.1.3 Evolution of the pore water composition as a function of time

In order to assess temporal and spatial evolution of the pore water composition around the excavated galleries and boreholes, we have sampled pore waters of individual filters at specific time intervals ranging from a few months after piezometer installation till up to 142 months (~12 years). The evaluation is done by plotting several time series of measured sulphate concentrations against filter distance from the gallery extrados. This is done both for N_2-drilled and air-drilled boreholes.

Air - installed piezometers

If we look at the historical data of the piezometer filters CG-13U (Figure 8a), it is clear that all filters sampled prior to 2007 (piezometer installed in 2003) feed pore waters affected by oxidation as evidenced by sulphate concentrations exceeding 10 mg/L limit up to a distance of more than 15 m in the first sampling campaign (month 10). The increased sulphate concentrations are thus clearly linked to instantaneous oxidation during the borehole (air-) drilling. As such these data cannot be used to assess the extent of the EDZ around Connecting Gallery. However, they still provide valuable information about the fate of the sulphates within the EDZ as demonstrated by the evolution of pore water composition of the filters located near the Connecting Gallery (0.3, 0.6, 1.6 and further away, Table 1, see also first part of the concentration profiles shifting to the left in Fig. 8a). It is also clear that irrespectively of the sampling time, all filters up to the distance of between 4-5 m from the Connecting Gallery show sulphate concentrations >10 mg/L and thus can be considered as permanently disturbed compared to reference pore water composition.

Except from a few exceptions (filter 7 and filter 1 of the CG-13U located at a distance of 7.6 and 19.6 m from extrados of the Connecting Gallery sampled after 22 months) we can state that in all filters a systematic decrease of sulphate concentrations is present as a function of time. Such systematic decrease has been observed in many other piezometer filters and is probably a result of complex interplay between self-sealing process (leading to limited exposure to air), drainage of the water towards galley and continuous sampling, as the water sampled from the filter is replaced by fresh(er) water coming from the clay.
The sulphate concentration profiles and their temporal evolution observed in CG-13U piezometer are consistent with data on CG-13D piezometer (Figure 8b, first sampling after 87 months). It is worth mentioning that the boundary of the chemically disturbed/undisturbed pore waters in CG-13U piezometer set at 4-5 m overlaps with the zone of increased hydraulic conductivity measured in the same piezometer (Chen, 2018).

Unlike sulphates, no general conclusion can be drawn with respect to temporal evolution of the DOC contents in the various piezometer filters of the CG-13U (Figure 9). The differences in DOC among various filters reflect rather vertical variability of organic content in Boom Clay than the various degree of oxidation. The general pattern of the DOC vertical profile remains

more or less preserved over the monitored time period. Though the data are less scattered in the case of the piezometer filters CG-13D, no real trend could be either observed in the evolution of the DOC concentrations as a function of time (not shown).

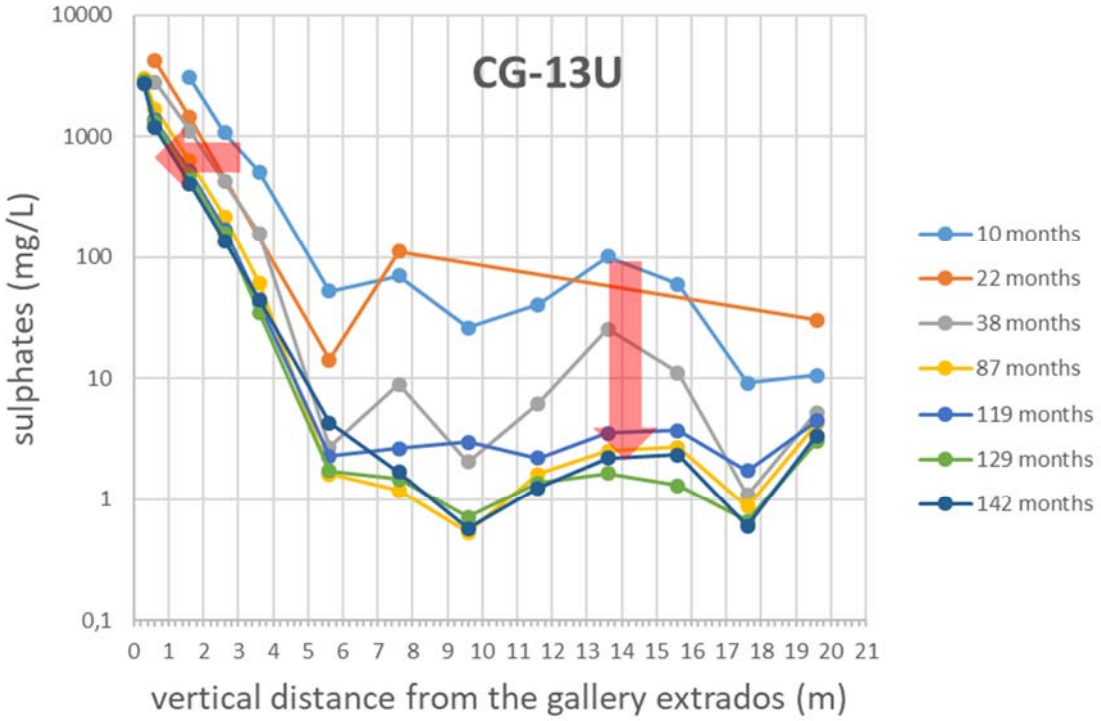

Figure 8a. 2D radial profiles of the sulphate concentrations in the piezometer filters CG-13U at various times after piezometer installation.

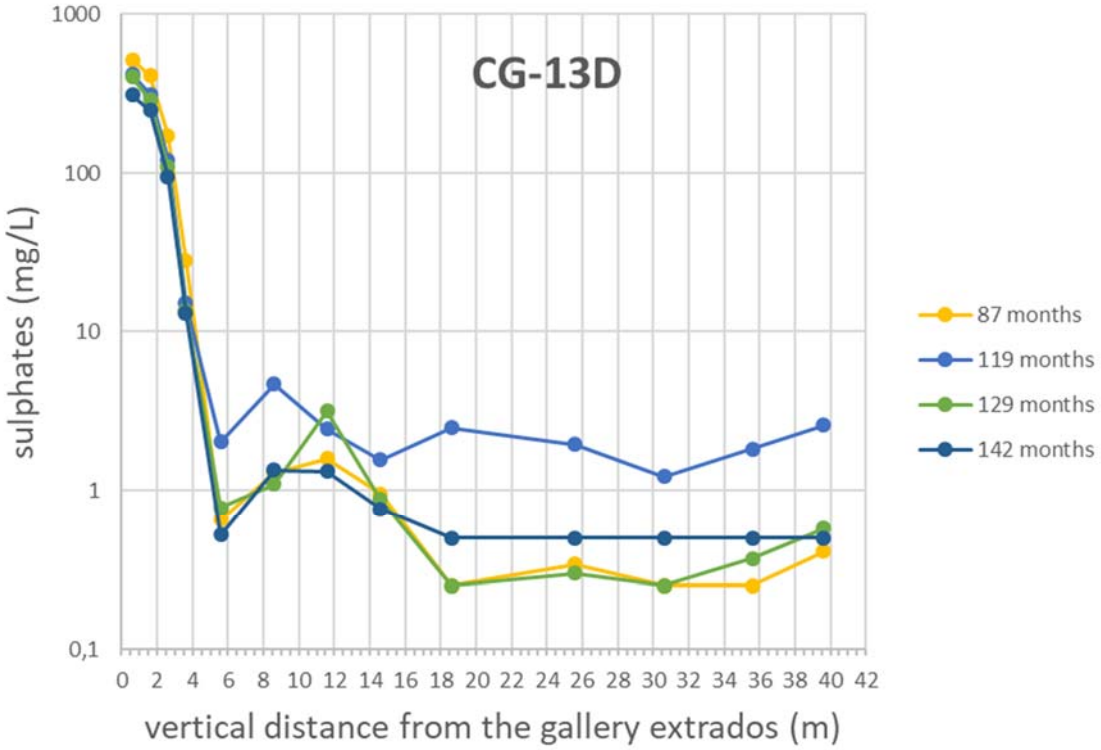

Figure 8b. 2D radial profiles of the sulphate concentrations in the piezometer filters CG-13D at various times after piezometer installation.

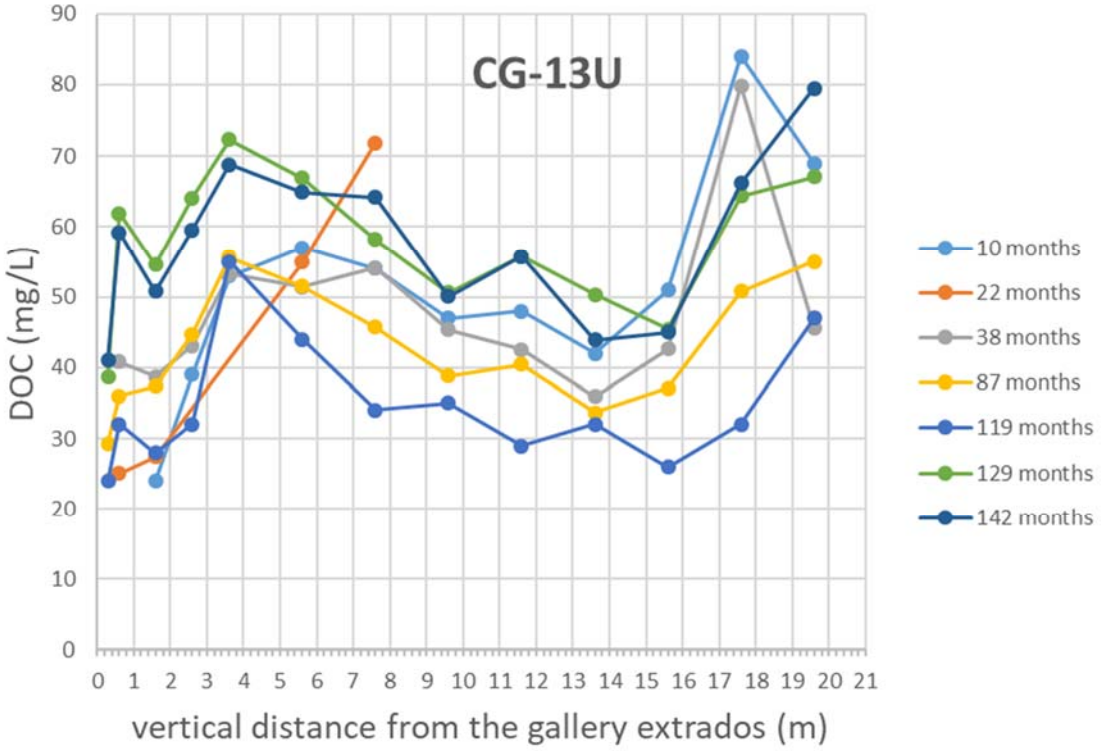

Figure 9. 2D radial profiles of the DOC concentrations in the piezometer filters CG-13U at various times after piezometer installation.

However, it should be mentioned that initial decrease of the total DOC has been observed in the piezometer filters TD-11D (MORPHEUS) and reported in Van Geet (2004). The evolution of DOC as measured in 12 filters as a function of time after piezometer installation is shown in Figure 10. The DOC decrease was explained to be a result of continuous sampling and progressive flush-out of the part of the DOC which was initially present in the pore water as a result of oxidation. It is worth noting that the most significant decrease of DOC is observed before month 10 in these filters, while the first profiles for CG-13U and CG-13D have been obtained at month 10 not allowing to capture an initial transient. Moreover, the MORPHEUS piezometer tube is fabricated from PVC material. Thus, an additional source of organic carbon cannot be fully excluded and adds to the overall complexity of the results.

On the long term, all DOC measurements fall within (or below) the reference range for undisturbed Boom Clay [120-200 mg/l, De Craen *et al.* (2004b)] although observations from MORPHEUS suggest that oxidation around a gallery (or a freshly installed piezometer) might initially produce more mobile, short-chained organic molecules of DOC but that these would quickly be flushed towards the open gallery. The release of aliphatic compounds with relatively lower molecular weight as a result of kerogen oxidation has been reported by Blanchart (2011) and (Blanchart *et al.*, 2012).

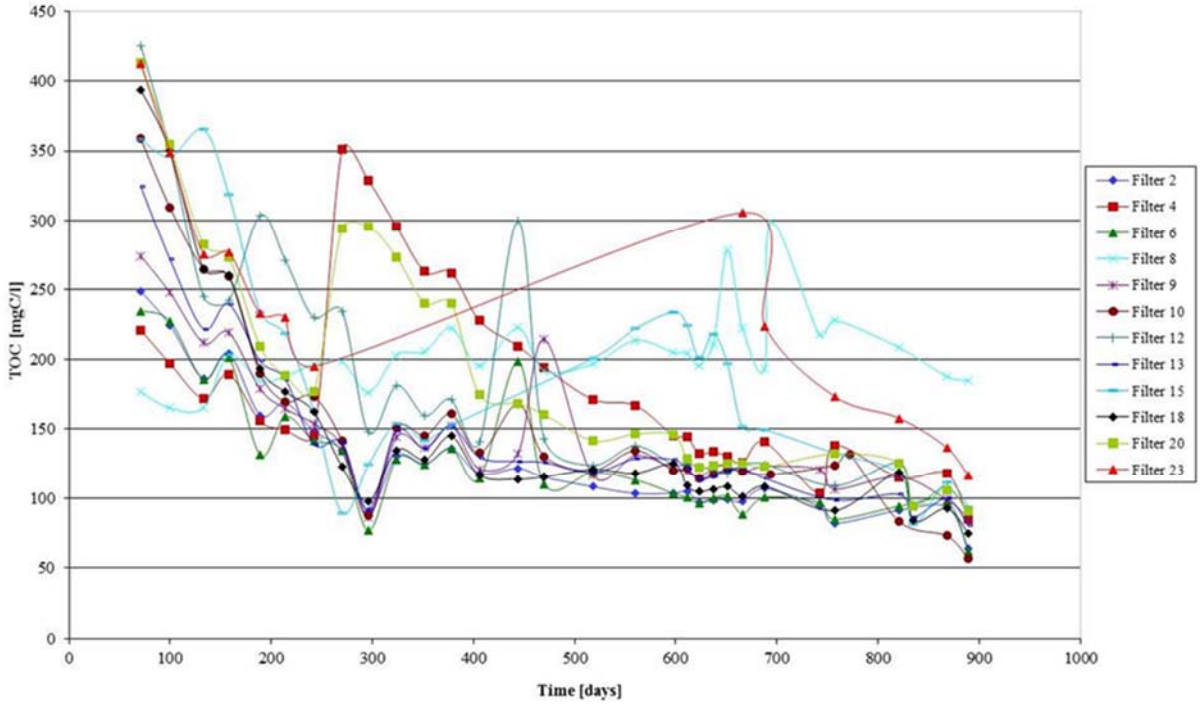

Figure 10. Evolution of the DOC in the different filters of the TD-11D piezometer (MORPHEUS) as a function of time (Van Geet, 2004).

N2 – installed piezometers

The evolution of the sulphate concentrations as a function of time is visualised in Figure 11 (TD-41E), Figure 12 (CG-64E) and Figure 13 (CG-30E and CG-35E, in the EDZ of the PRACLAY gallery).

Comparing the first profiles (up to month 13 after piezometer installation) from TD-41E and CG-64E with corresponding profiles from CG-13U, the effect of N_2 drilling is clearly visible: there is little or no trace of oxidation in the far field of the galleries.

For most of the filters, the general decrease in sulphate concentrations is observed in all piezometers with increasing time. The highest sulphate concentrations has been again observed in the filters close to the gallery. They are related to the initial oxidation caused by the creation of the fractures during the excavation of the galleries. Nevertheless, in the filters located close to the gallery (0.4 m in N2TD & N2CG) the sulphates first increase (from 760 to 2250 mg/L in the N2TD and from 960 to 1530 mg/L in N2CG) and then remain stable in the period between 2007 and 2011 (Figure 14 and Figure 15). The concomitant increase in the sulphates in the filters close to the gallery and decrease in the filters further away can be explained by the transport of the oxidation products towards gallery due to hydraulic gradient. Such mechanism is proposed by the transport modelling (see Chapter 7.3).

It is important to mention that evolution of the sulphate concentrations in the piezometers installed from the Test Drift (TD-41E) and the Connecting Gallery (CG-64E) provide very similar patterns. This is an important argument in support of the statement that time of the ventilation (3 years at the time of the first sampling in the Connecting Gallery and 17 years at the time of the first sampling in the Test Drift) has hardly any impact on either the extent of the EDZ or fate of the sulphates within this zone. Our observations are in line with the conclusions drawn earlier by De Craen *et al.* (2008) with respect to the extent of the oxidized zone around the two galleries.

It should be noted at this point that no such an increase of sulphate concentrations towards gallery could be identified in the piezometers close to the PRACLAY gallery (CG-30E andCG-35E). However, here the distance of the filters relate to the PRACLAY gallery, which has been back-filled 4 years after the excavation (December, 2011) and 7 years after CG-30E and CG-35E piezometer installation. Thus the transport driven by the hydraulic gradient towards the PRACLAY gallery is limited in these filters after 2011 (backfilling with sand) but there is also no in-diffusion of oxygen into the clay from that point on. Another factor that might explain lower (overall) sulphate concentrations in the EDZ of PRACLAY is the smaller diameter of the gallery and perhaps a better controlled convergence that could have led to less open fractures.

Except from the sampling carried out 78 months after the piezometer installation, the overall trend is the decrease in the sulphate concentrations, ultimately leading to a value of 0.25 mg/L (detection limit of the analytical method). The decreasing trend is likely a result of multiple sampling and related flushing out of the sulphate species from the filter environment. Interestingly, unexpectedly high sulphate concentrations observed in the four filters during "78 months sampling campaign" coincides with the period of PRACLAY backfilling and hydration (starting from 02/05/2011). In this view, increased sulphate concentrations may indicate change in the hydraulic gradient. Before back-filling, sulphates could not migrate deeper into the clay due to drainage of the pore water towards empty gallery. However, after backfilling, the migration of sulphates in the opposite direction is possible, thus eventually reaching filters of the piezometer CG-35E. The reason why the maximum sulphate concentrations were reached in the filters at a distance of 1m and 1.14 m, and not in the closer filter at 0.88m is yet to be explained.

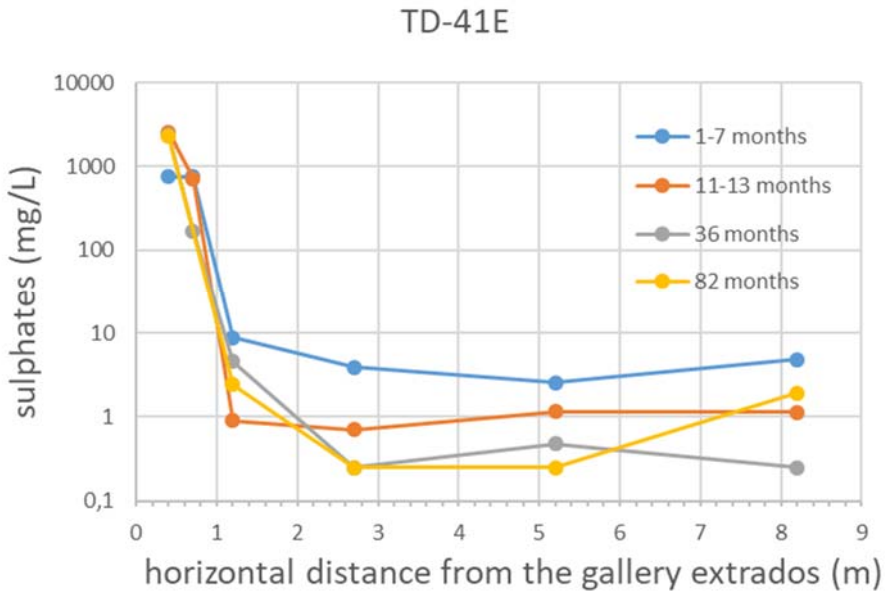

Figure 11. Temporal evolution of the sulphate concentrations profiles as measured in the piezometer filters TD-41E.

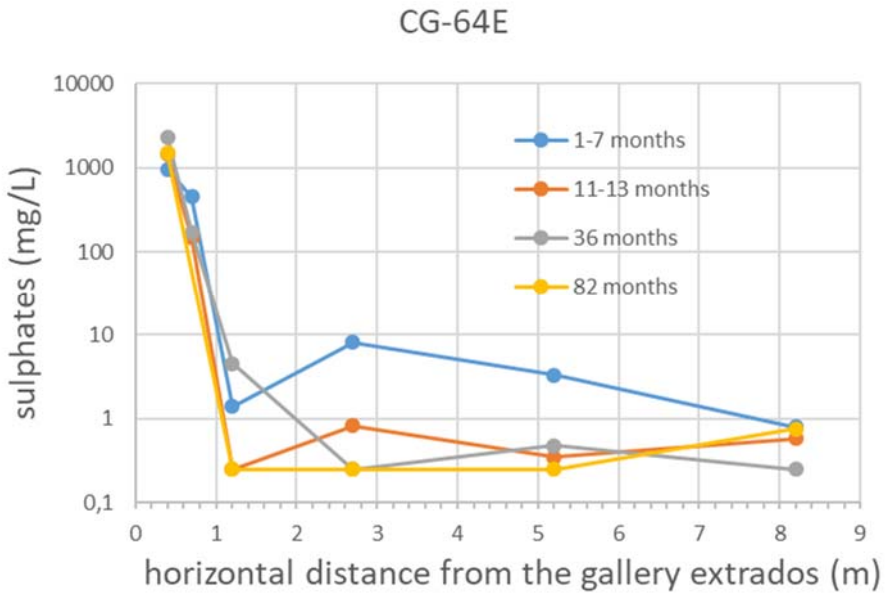

Figure 12. Temporal evolution of the sulphate concentrations profiles as measured in the piezometer filters CG-64E.

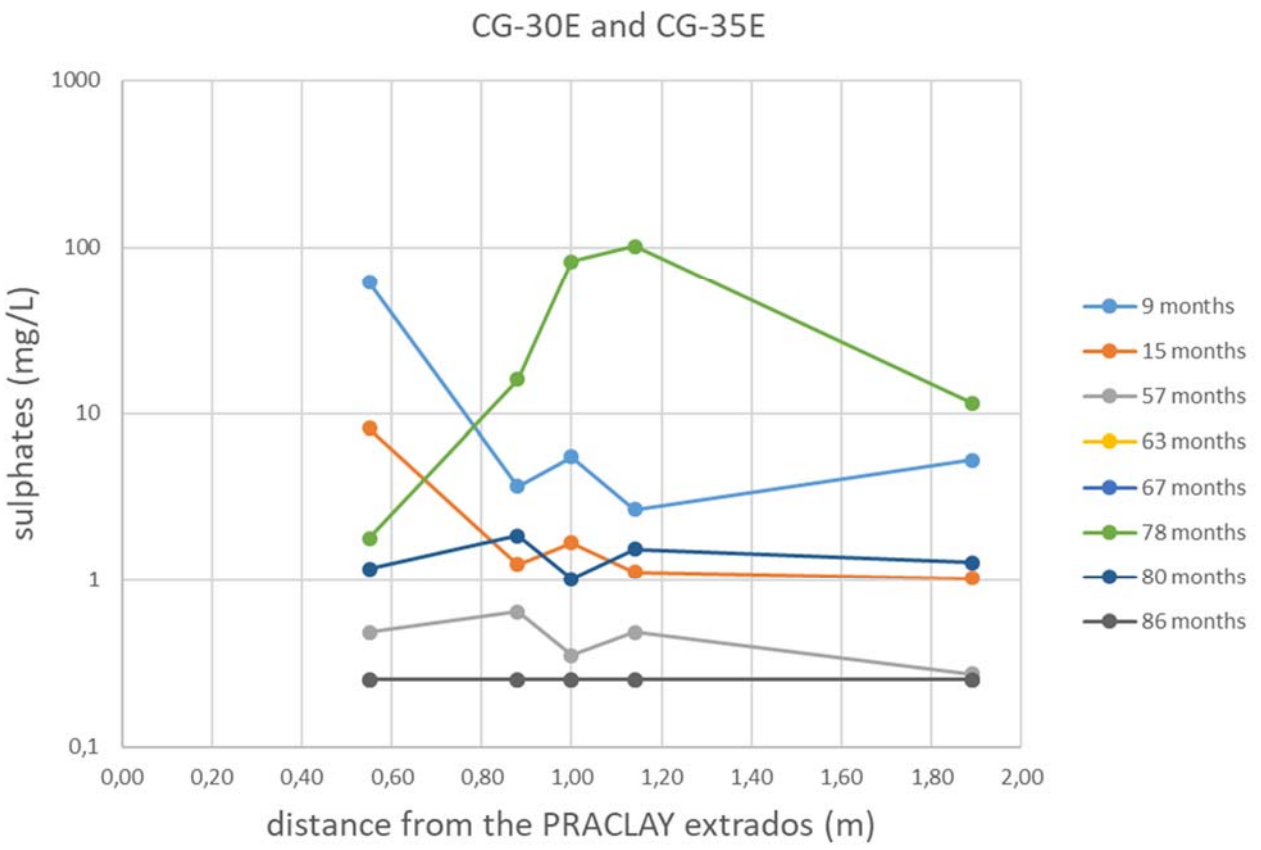

Figure 13. Temporal evolution of the sulphate concentrations as measured in the piezometers CG-30E and CG-35E.

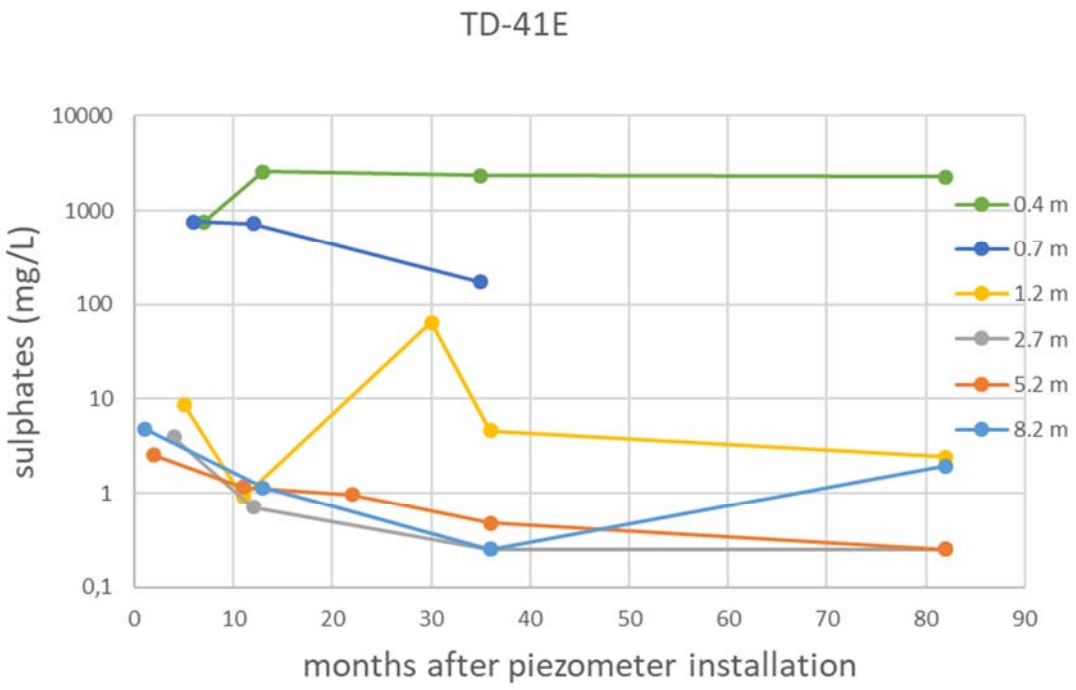

Figure 14. Sulphate concentration as a function of time plotted for the individual filters of the piezometer TD-41E.

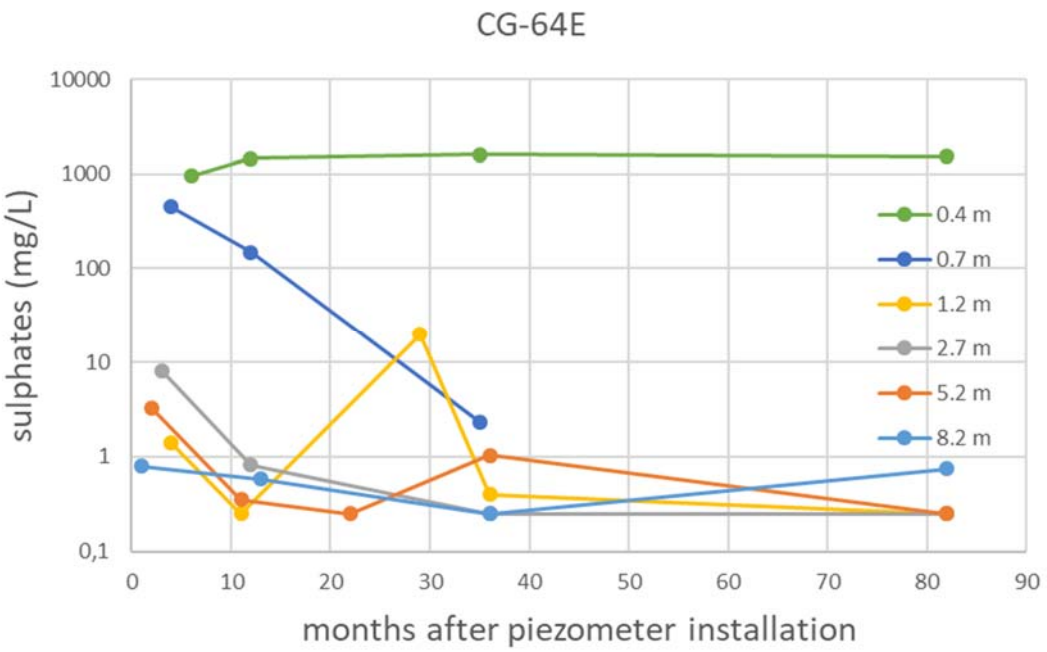

Figure 15. Sulphate concentration as a function of time plotted for the individual filters of the piezometer CG-64E.

The evolution of the DOC concentrations as a function of time is shown in Figure 16 (TD-41E and CG-64E) and Figure 17 (CG-30E and CG-35E, in the EDZ of the PRACLAY gallery).

Figure 16 shows that DOC concentrations are locally higher in the first sampling campaigns (1-7 months) in the filters located close to the Test Drift and the Connecting gallery (0.4, 0.7 and 1.2 m). Interestingly the highest DOC concentrations (771 mg DOC/L in the filter 5 of the CG-64E and 532 mgDOC/L in the filter 5 of the TD-41E) were not detected in the filters closest to the gallery (0.4 m), but in the filters 0.7 m away from the gallery. In the following sampling campaigns, the DOC concentrations in both piezometers approach the values typical for the undisturbed Boom Clay pore water (50-150 mg DOC/L).

Unlike the CG-64E and TD-41E study cases, DOC values from various piezometer filters around PRACLAY gallery show no dependence on the distance from the gallery nor of the time. The only DOC values, which deviate from the rest of the data, correspond to filter CG-30E1 located at a distance of 1.89 m from the PRACLAY gallery. This is a known sampling artefact and relate to leakage of organic polymer based electrode in this specific filter.

It is worth mentioning that a DOC concentration peak in the CG and TD filters number 5 (at a distance of 0.7 m) was detected in the time interval 1-7 months following the piezometer installation, whereas after 11-13 months, the concentration peak disappeared. As the first DOC data from the piezometers located close to the PRACLAY gallery where only obtained 9 months after the piezometer installations, it is possible that an initial peak of oxidation related fraction of DOC could have been missed.

Indeed, when we inspect the DOC data of Van Geet (2004) of the MORPHEUS piezometer, this early DOC release is no longer visible in the data exceeding 200 day time span. Although intensive sampling may lead to flush out of this excess DOC, the piezometer filters CG-64E-5 and TD-41E-5 (0.7 m) were not sampled in the period between 7 and 11 months when significant decrease in DOC seemed to happen. Altogether, these data again suggest that oxidation leads to a production of DOC, which is relatively mobile (lower in molecular weight) and that this fraction can migrate quickly towards the gallery wall. The production of shorter-chained aliphatic products with lower molecular weight due to oxidation of the organic matter was also confirmed by GPC-HPLC (Gel Permeation Chromatography – High Performance Liquid Chromatography) in the study of (Blanchart *et al.*, 2012).

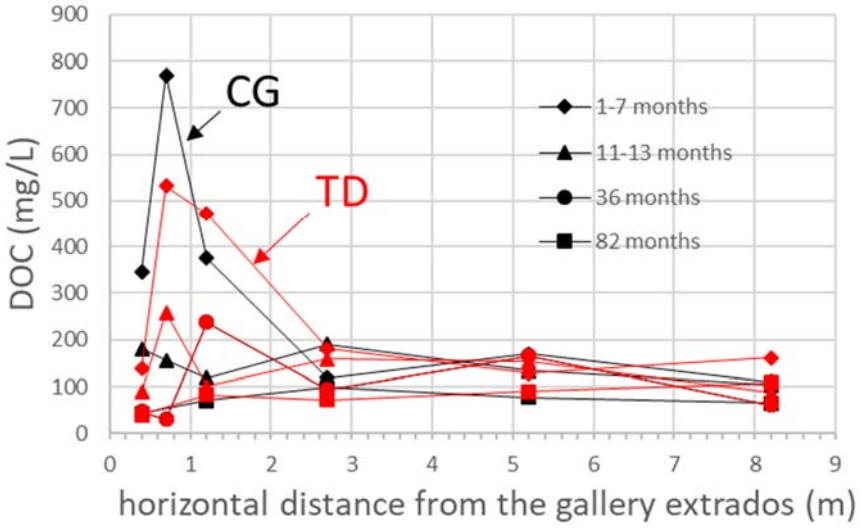

Figure 16. Evolution of the DOC values as a function of time in the piezometer filters CG-64E (black symbols) and TD-41E (red symbols). The different shapes of the symbols correspond to variable times (modified after De Craen *et al.*, 2008).

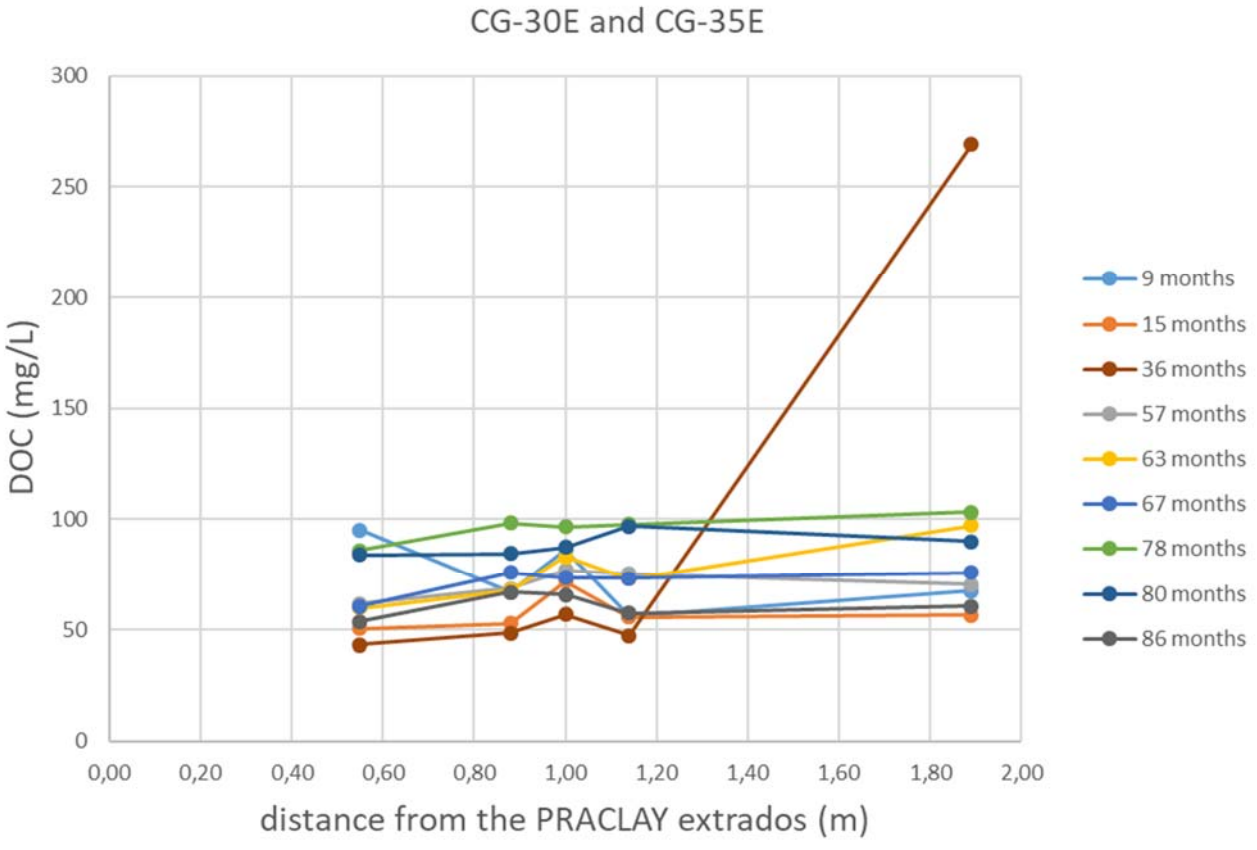

Figure 17. Evolution of the DOC values as a function of time in the piezometer filters CG-30E and CG-35E.

7.1.4 The effect of the Boom Clay layering on the composition of the pore water

Except from the typical exponential shape of the sulphate concentration profiles observed around galleries in the Boom Clay (e.g. CG-68E and TD-41E), some small variations may be superimposed on the shape due to the lithological variations of the Boom Clay (and thus also variability in pyrite and organic matter content), especially in the vertical direction (layered characteristic of the Boom Clay).

The Boom Clay has a layered character which is expressed as variations in grain size, organic matter and carbonate content in the vertical profile. Organic matter and pyrite (both very sensitive to oxidation) are not evenly distributed vertically. As a result, sulphate concentrations may be more variable in the vertical than in the horizontal direction. As an example, Figure 18 shows the concentration profiles of the selected elements for vertically (PG-70D) and horizontally (PG-70S) oriented piezometers installed from the PRACLAY Gallery. Indeed, the sulphate (and exchangeable cations) concentrations obtained from these air-drilled piezometers are more variable in the vertical piezometer compared to the horizontal one. We thus assume that such variations on the vertical scale are the result of the Boom Clay layering and associated variations in the pyrite and organic matter content. In general, pyrite contents in the Boom Clay varies in the range between 0.5 and 3 wt% (Zeelmaekers *et al.*, 2015). Pyrite-rich layers will lead to locally more extensive sulphate production and calcite dissolution relative to the layers containing less pyrite. In the horizontally oriented piezometers, the vertical variability of the Boom Clay has little to no effect.

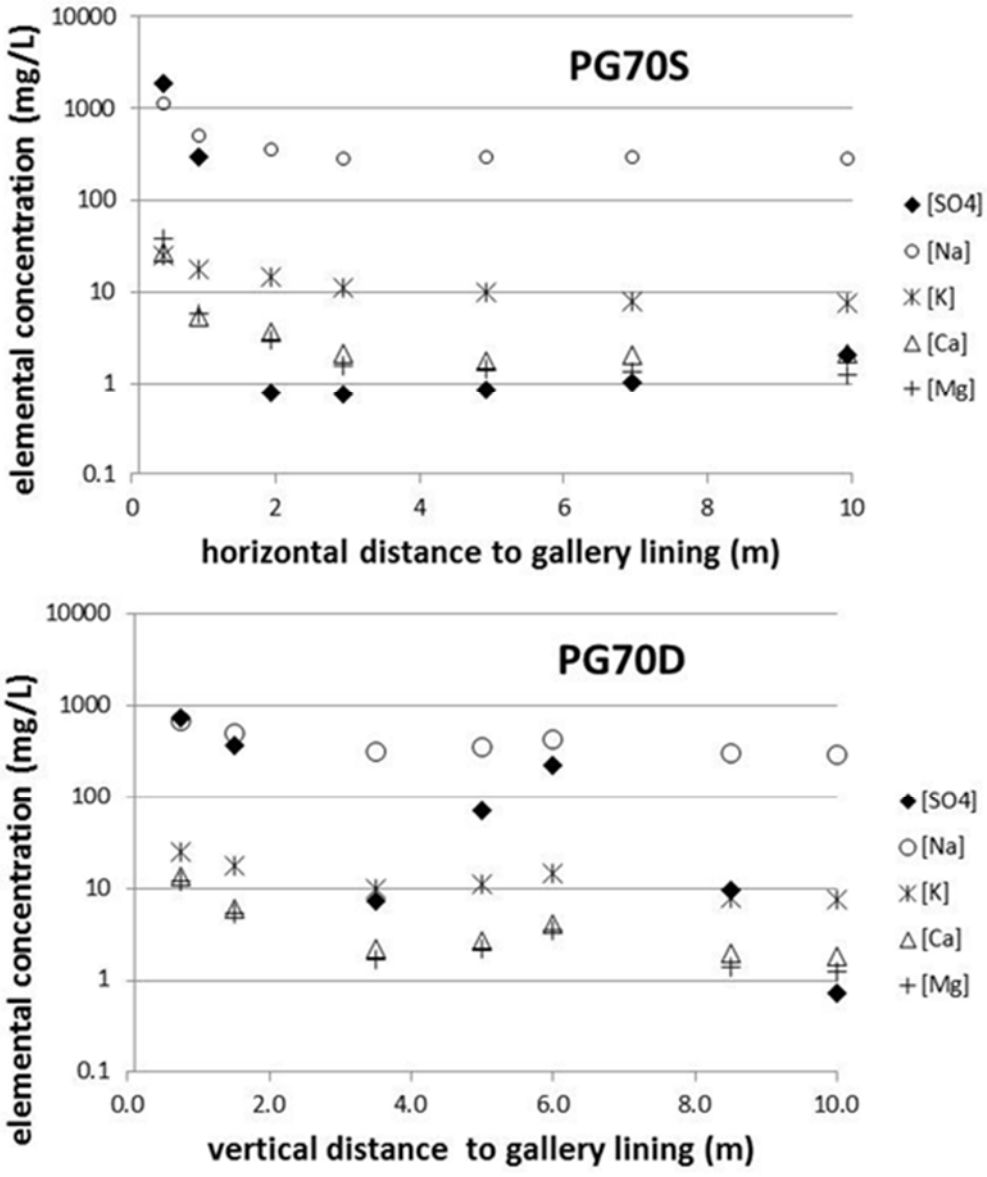

Figure 18. Comparison of the sulfate and exchangeable cations profiles over 10 m distance from the PRACLAY Gallery of the horizontally and vertically oriented piezometers PG-70S (above) and PG-70D (below). More variability is observed in the vertical direction due to natural variability of the Boom Clay (layered character).

The layered character of the Boom Clay is also reflected in the sulphate concentration profiles of the vertically oriented piezometers CG-13U and CG-13D shown previously in Figure 8a and b.

The earlier studies conducted on Boom Clay indicated that organic matter-rich layers in Boom Clay also contain more pyrite (Vandenberghe *et al.*, 2014). Therefore, comparable patterns could be expected for sulphates and dissolved organic matter as a result of oxidation.

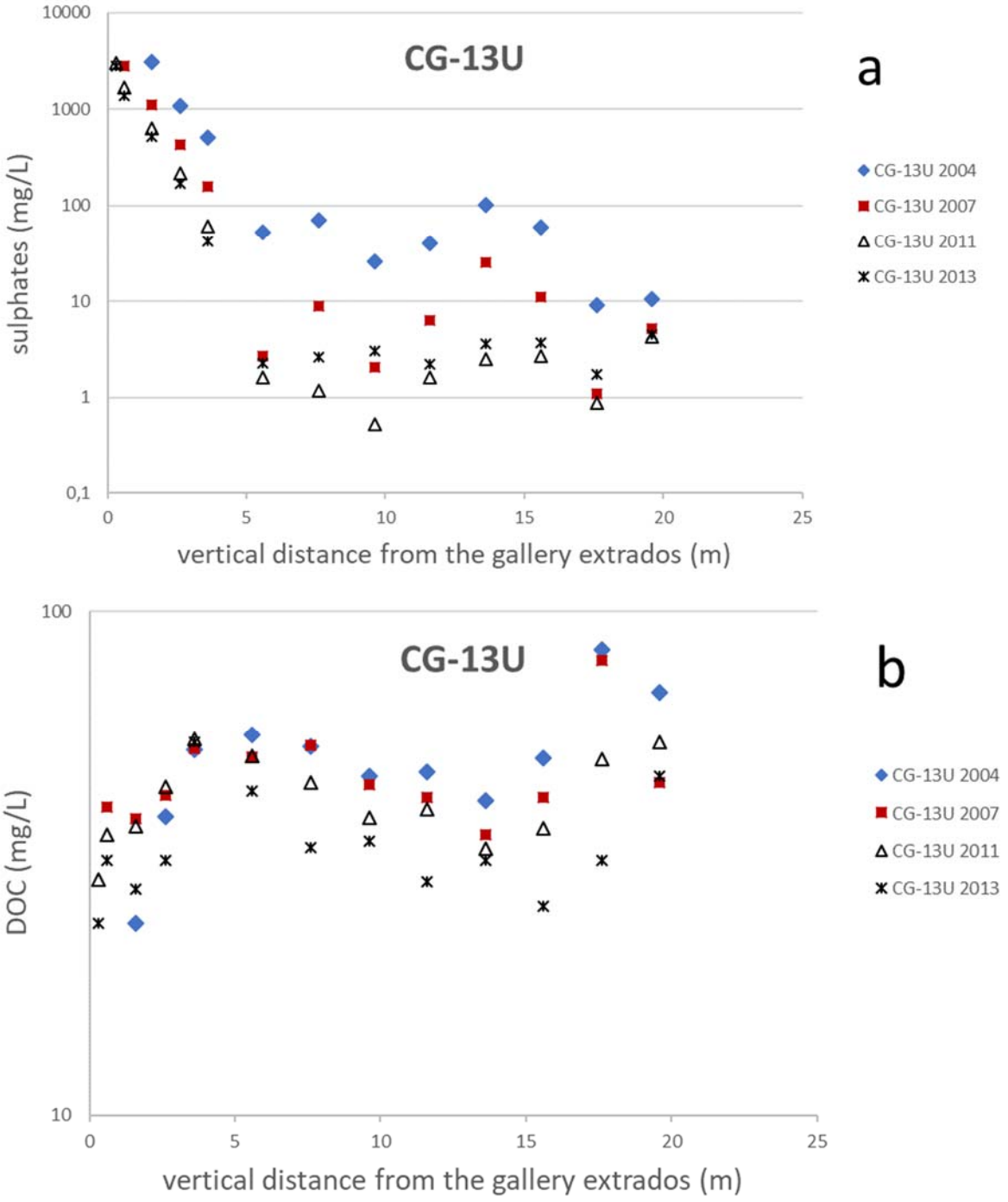

Figure 19. The concentrations of (a) sulphates and (b) the dissolved organic carbon (DOC) as a function of the vertical distance to the gallery in the piezometer CG-13U. The data demonstrate the impact of the Boom Clay layered character on the shape of the DOC and sulphate concentration profile.

While Figure 19b shows that the layered character of the Boom Clay is reflected by the shape of the concentration profiles of the DOC, the profile seems to be inversely correlated to that for sulphates for the same piezometer (Figure 19a), indicating that high sulphate concentrations are rather linked to low DOC and vice versa. The actual relationship between DOC and sulphates is discussed in the following section.

7.1.5 On the relationship between DOC and sulphate concentrations

A first attempt to find out a relationship between DOC and sulphates was made in the frame of the TD-11D (MORPHEUS) sampling campaigns in the early years after its installation (2001-2002). Van Geet (Van Geet, 2004) observed a strong decrease in DOC in the different filters over a period of 3 years, with much of the change occurring during the first year, which also coincided with a general decrease in sulphate concentration in the collected water samples. Therefore, the correlation between DOC and sulphate was suspected and examined. For several filters, a positive correlation was indeed observed but this was not the case for other filters, affected by spurious variations of DOC.

In order to further examine the relation between DOC and sulphate, the available data of all piezometers were evaluated, but no clear relation could be observed between DOC and sulphate in any other piezometer.

Here, we present DOC and sulphate data for the piezometer CG-13U (Figure 20). Clearly, no trend could be assigned to the presented data set. Considering that piezometer CG-13U is vertically oriented, one may argue that possible correlation would be smeared out by natural and variable organic and pyrite contents in different Boom Clay layers. However, no correlation between DOC and sulphate was found neither in the horizontally oriented piezometers (Figure 21). The filters of these piezometers are located within a narrow depth interval (-196.3 to -199.5 m TAW). The absence of clear correlation between the two parameters suggests that while pyrite and organic matter are both susceptible to oxidation, the fate of their oxidation products can be different. In particular, mobility of these products may differ. The oxidation of natural organic matter leads to a shift of the molecular weight distribution towards lower values (Blanchart *et al.*, 2012), which affects its mobility in the near field.

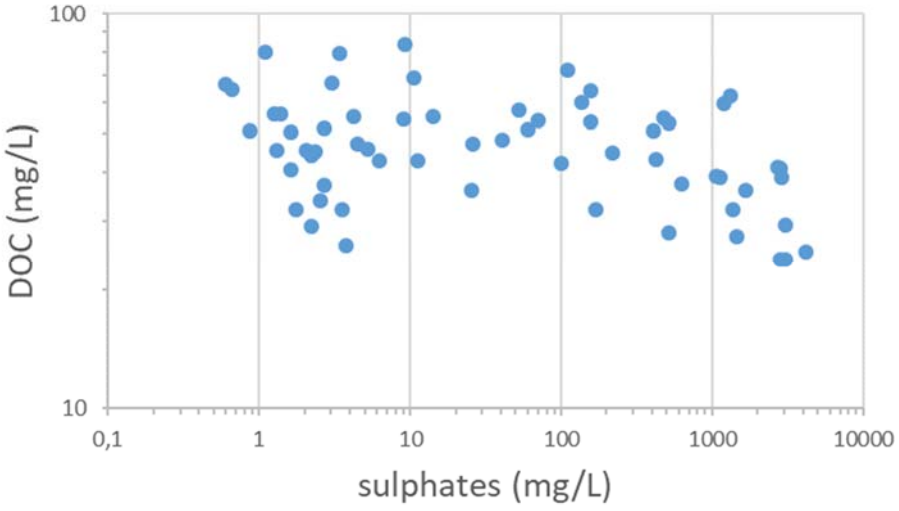

Figure 20. The relationship between DOC and sulphate concentration data in the air-installed piezometer CG-13U. No apparent trend could be established between DOC and sulphate concentrations.

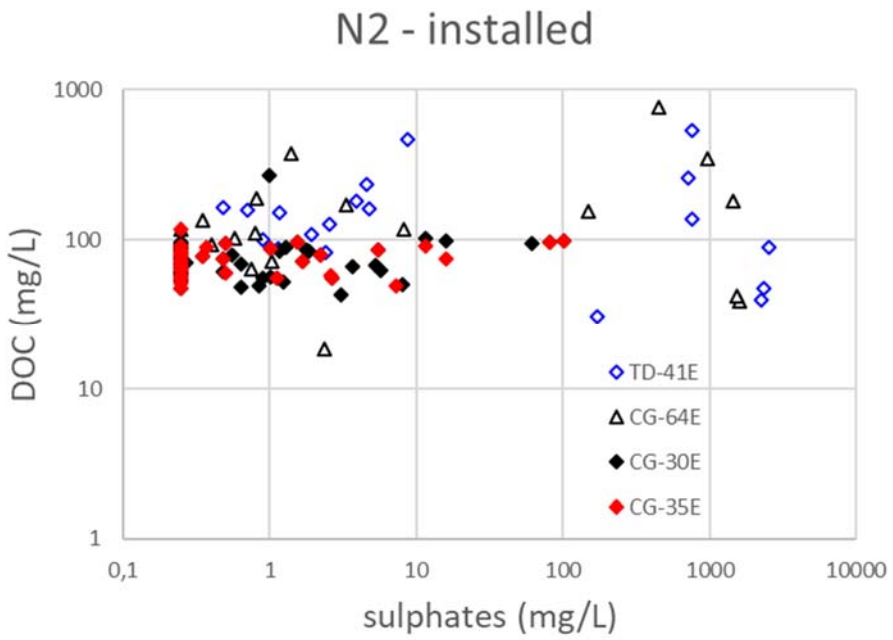

Figure 21. Sulphate concentrations against DOC in the Boom Clay pore waters showing no correlation between the two parameters. Data of the N2 – installed horizontally oriented piezometers TD-41E; CG-64E, CG-30E and CG-35E.

7.1.6 Conclusions with respect to Boom Clay pore water perturbed by oxidation

The sulphate and dissolved organic carbon contents in the pore water were studied as the most important markers of the oxidation phenomenon in the Boom Clay. What concerns sulphates, their concentrations tend to exponentially decrease with increasing distance from the gallery as previously observed by De Craen *et al.* (2008). The long-term extent of the gallery-induced oxidation around the TD and the CG appears to be limited to the first 1.2 m. Beyond this zone, sulphate concentrations values are equal to, or below 10 mg/L, considered as the upper limit for natural sulphate concentration at Mol by De Craen *et al.* (2008). Although oxidation can also lead to relatively high DOC concentrations in the pore water of some filters, it's not necessarily so in every filter close to the gallery. Sulphate concentration hence appears as a more robust indicators of oxidation than DOC. While the spatial extent of the oxidised zone around the galleries appears to be limited, the observed sulphate concentration in the pore water in this zone does not necessarily decreases with time. On one hand, accumulation of sulphate precipitates on the TD and CG galleries lining blocks show that oxidation products are transported towards the galleries. On the other hand, oxygen can diffuse from an open gallery into the clay pore water up to a distance that is limited because the pore water is flowing in the opposite direction (see also section 7.3, modelling assessment).

In the oxidised zone of an air-drilled borehole, sulphate concentration decreases with time due to repeated sampling and diffusion of sulphate into the undisturbed clay between samplings.

The Boom Clay layered character is clearly reflected in the shape of sulphate and DOC concentration profiles in the piezometers crosscutting several Boom Clay layers. The initial pyrite and organic matter contents will thus necessarily affect the overall concentrations of sulphate and DOC measured in the pore waters collected at various locations.

7.2 Mineralogy

In this part, we present the results of the mineralogical investigation of clay cores sampled in the oxidised zones of the CG, TD and PRACLAY gallery (see section 6.2). The mineralogical study involved the application of XRD, FTIR, XANES, Mössbauer spesctroscopy and cation exchange capacity (CEC) measurements.

7.2.1 XRD

The results of the XRD are presented in Figure 22 (TDR41-42E), Figure 23 (CGR68-69E) and Figure 24 (PGR70-71B).

The undisturbed Boom Clay consists of mixed-layer illite–smectite, kaolinite, detrital mica and chlorite for the clay minerals and quartz, K-feldspar, Na-plagioclase, Ca–Mg–Fe carbonate and pyrite for the non-clay minerals. The random XRD patterns allow to evaluate the changes to non-clay minerals as a result of the oxidation. The most significant feature is the presence of the 020 gypsum reflection at 7.56 Å observed in the samples from the Test Drift (Figure 22) and Connecting Gallery (Figure

23) compared to the typical pattern of the undisturbed Boom Clay lacking the gypsum diagnostic reflections. The presence of gypsum is limited to the first ~3.8 cm from the concrete/clay interface in both the TD41E and CG-68E sample sets. Further away from the clay/gallery lining interface, the XRD patterns approach those of the undisturbed rock. In contrast to the Boom Clay samples taken from the Connecting Gallery and the Test Drift, the gypsum is absent in the samples from the PRACLAY Gallery (Figure 24).

In the Connecting Gallery, jarosite ($KFe_3(SO_4)_2(OH)_6$) was identified in the clay close to the gallery lining as indicated by the reflections at 5.92, 5.72, 5.08, 3.08 and 3.11Å (Figure 23). In contrast, jarosite was absent in the samples from the Test Drift and PRACLAY Gallery respectively (Figures 22 and 24).

Interestingly, the calcite is clearly visible in the diffractograms of the Test Drift as indicated by the 104 reflection at 3.03 Å (Figure 22), while calcite could not be found in the samples of the Connecting Gallery and the PRACLAY Gallery. Worth mentioning is also pyrite, which is systematically detected in all Test Drift and the PRACLAY Gallery samples, whereas its presence is not evident in the Connecting Gallery sample set (Figure 23).

In conclusion, the mineralogical alteration is limited to maximum first ~4 cm from the gallery as indicated by the presence of gypsum and jarosite. These minerals are absent in the undisturbed Boom Clay. The alteration products can differ from place to place depending on the local pH. This is supported by the presence of jarosite in the samples close to the Connecting Gallery, whereas jarosite is missing in samples close to the Test Drift. The jarosite forms under low pH conditions, which may indicate loss of the buffering capacity in these samples. Indeed, XRD points to the absence of carbonates in the samples containing jarosite, whereas carbonates are still present in samples where gypsum is the only alteration product.

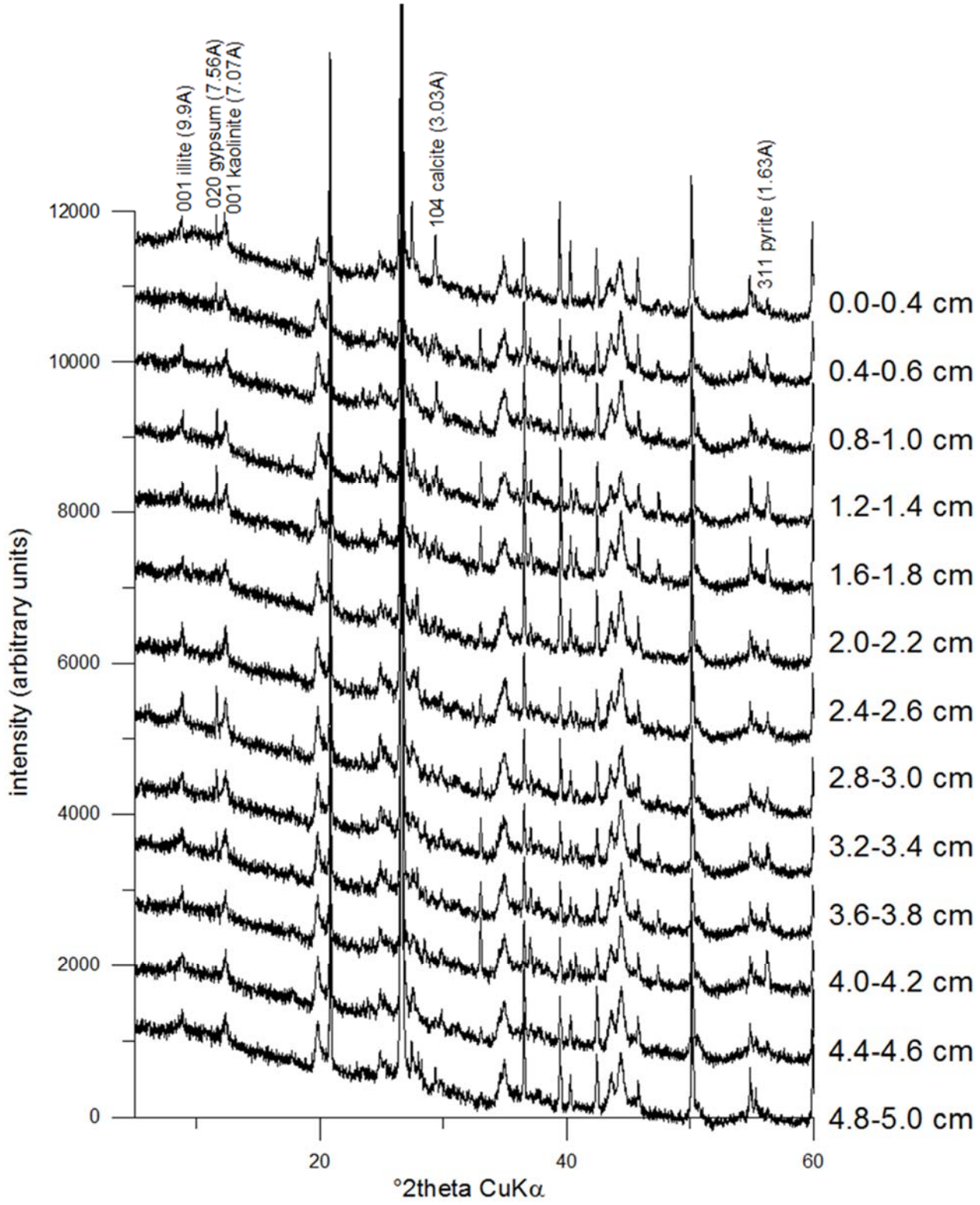

Figure 22. The whole-rock powder XRD patterns of samples from the Test Drift plotted as a function of increasing distance from the gallery lining (top to the bottom), showing gypsum as a major mineral alteration product. The lowermost pattern (4.8-5.0 cm) represents the XRD data of BC similar to undisturbed clay (modified after De Craen *et al.*, 2008a).

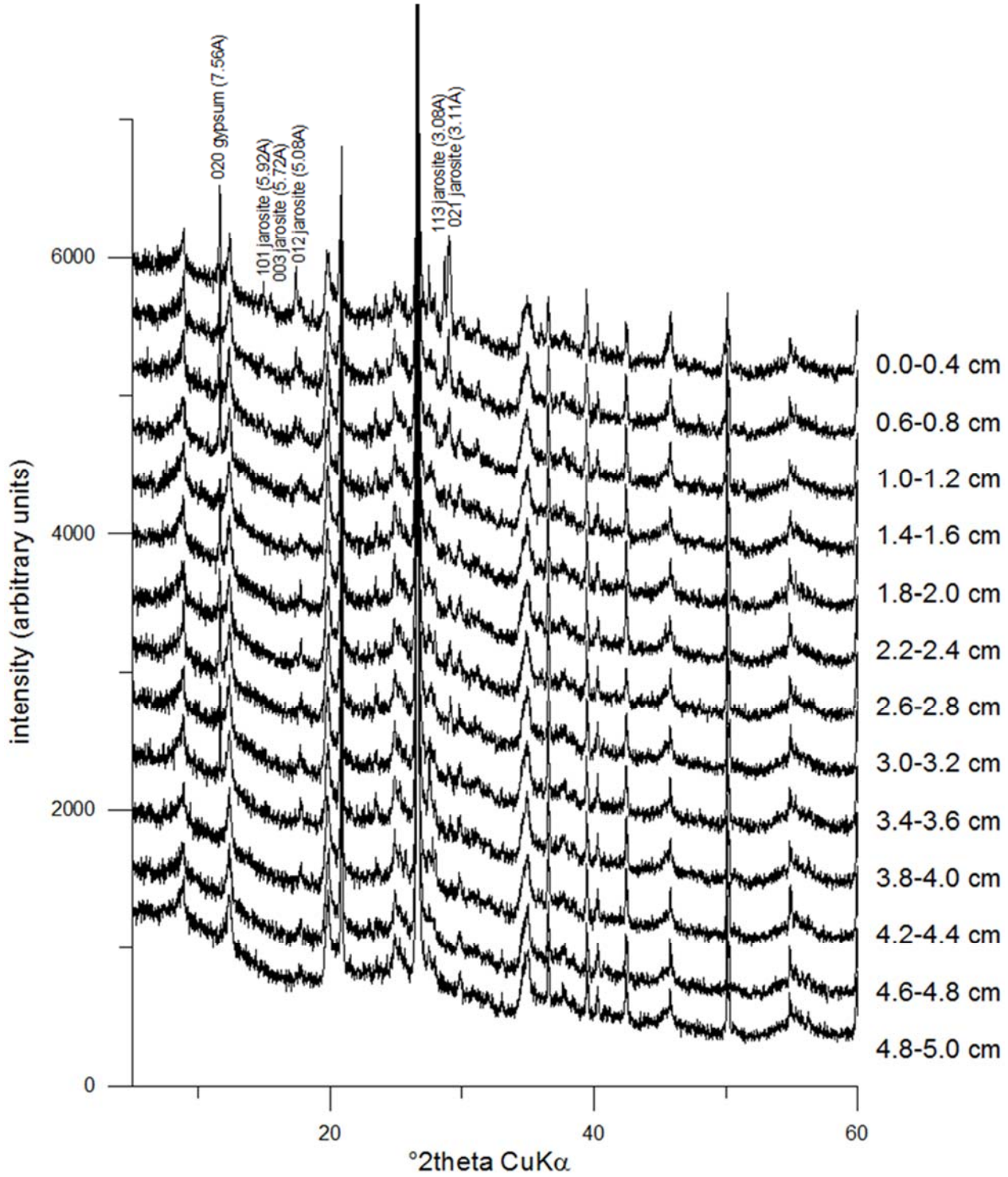

Figure 23. The whole-rock powder XRD patterns of samples from the Connecting Gallery plotted as a function of increasing distance from the gallery lining (top to the bottom), showing gypsum and jarosite as major alteration products. The lowermost pattern (4.8-5.0 cm) represents the XRD data of BC similar to undisturbed clay (modified after De Craen *et al.*, 2008a).

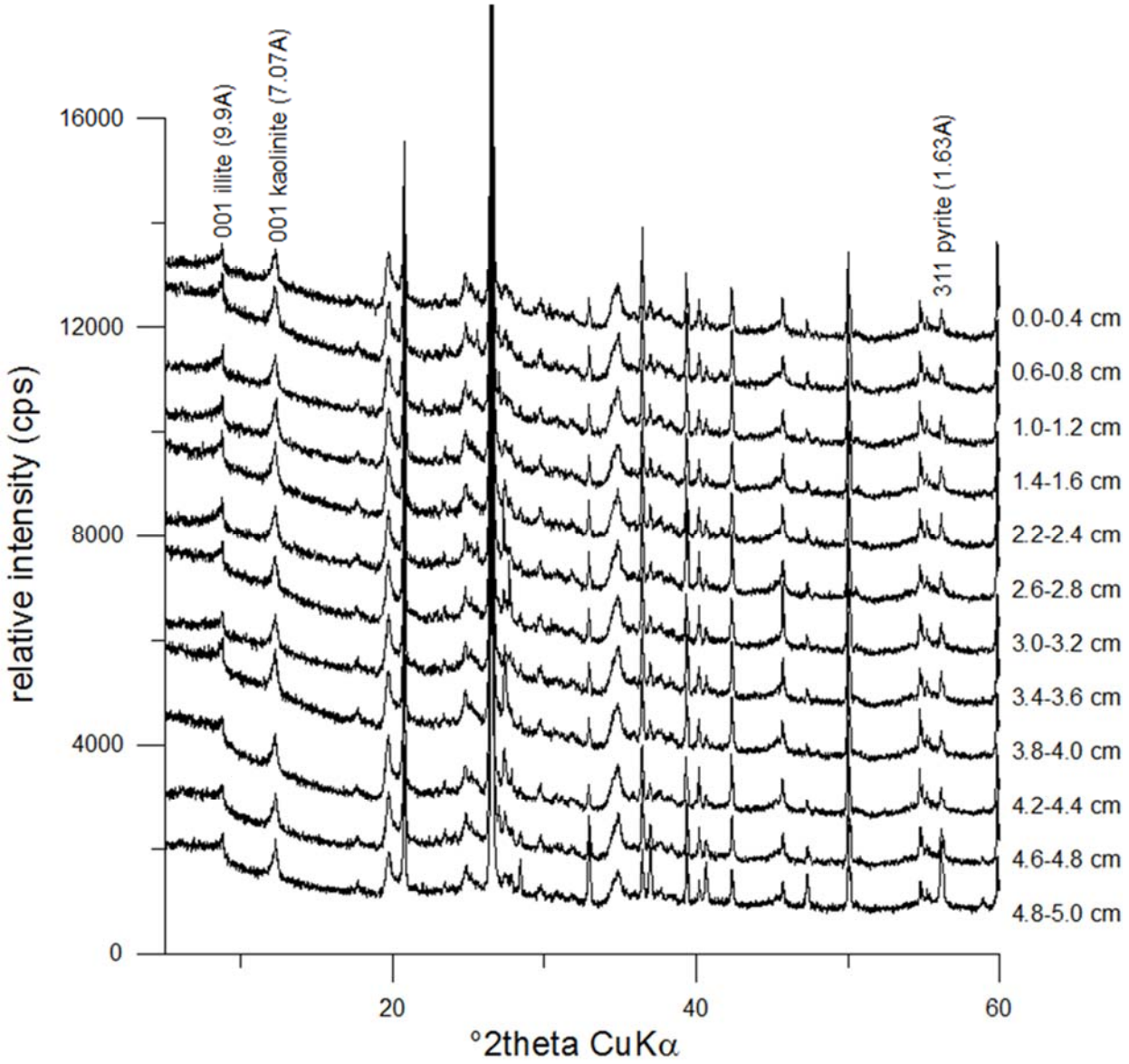

Figure 24. The whole-rock powder XRD patterns of samples from the Praclay Gallery plotted as a function of increasing distance from the gallery lining (top to the bottom), showing limited mineral alterations in these samples. The lowermost pattern (4.8-5.0 cm) represents the XRD data of BC similar to undisturbed clay.

7.2.2 FTIR

The results of the FTIR analysis are presented in Figure 25 (TD-41E), Figure 26 (CG68E) and Figure 27 (PG-70D).

The OH stretching region (4000-3000 cm^{-1}) shows three bands. The absorption band near 3698 cm^{-1}, assigned to the stretching vibrations of the surface OH groups of kaolinite (1:1 clay mineral), is diagnostic for this mineral and together with a band at 3551 cm^{-1} confirms the presence of kaolinite in the sample. The band at 3622 cm^{-1} is due to vibrations of the inner OH groups of kaolinite. A higher intensity of 3622 cm^{-1} band in comparison with that of 3698 cm^{-1} reveals the contribution of another OH vibration, i.e. the OH vibration of dioctahedral 2:1 clay mineral (e.g. illite or smectite.). A strong complex band near 1030 cm^{-1} is due to Si-O stretching vibrations of both, 2:1 clay mineral and kaolinite. The absorption at 914 cm^{-1} corresponds to AlAlOH bending vibrations. A pronounced doublet at 797 and 779 cm^{-1} together with a sharp band at 694 cm^{-1} confirms a presence of quartz admixture in the sample. The absorption bands in the 600-400 cm^{-1} region are due to Si-O bending vibrations. These bands are common in all studied samples. The main difference is related to presence or absence of carbonate and sulphate groups. Two bands at 1428 and 878 cm^{-1}, related to stretching and bending vibrations of CO_3^{2-} anion, confirm the presence of carbonates in the TD-41E sample set, while no CO_3^{2-} band near 1430 cm^{-1} in the CG-68E serie point to its absence. A broad inflection in this region is also identifiable in the PG-70D sample serie (Figure 27), but to a much lesser extent than in the TD-41E sample set. As such, this observations points to a lower carbonate content in the PG-R70D sample set compared to TD-41E serie.

Several new bands appear in the spectra of the CG-R68 sample serie (Figure 26). The most pronounced is a sharp band at 3385 cm^{-1} with a shoulder near 3410 cm^{-1}, less intensive and/or resolved bands occur at 1195, 1089, 1012, 667 and 633 cm^{-1}. All these bands indicate the presence of jarosite ($KFe_3(SO_4)_2(OH)_6$) in the sample. The 3385 and 3410 cm^{-1} bands are due to stretching vibrations of the OH groups in the $FeO(OH)_4$ octahedron, while the stretching vibrations of the SO_4 tetrahedra absorb near 1100 cm^{-1}. The bands at 667 and 633 cm^{-1} correspond to the bending SO_4 vibrations (Serna et al, 1986; Bishop and Murad, 2005).

The intensity (or area) of the band near 3385 cm^{-1} varies from sample to sample, indicating different amounts of jarosite in the CG-68E set. The highest content was found in the CG-68_0.0-0.4 sample. The amount of jarosite gradually decreases with the increasing distance of the sample from the Boom Clay/gallery lining interface. No sulphate is identifiable by the FTIR spectroscopy for the samples beyond the distance of 3.2 cm.

In summary, FTIR spectroscopy confirms the results of the XRD investigation. The jarosite was found in samples from the Connecting Gallery, but it was absent in samples from the Test Drift and the Praclay Gallery. The carbonates are still present in Boom Clay next to the Test Drift and the PRACLAY Gallery, whereas carbonates were not identified in the Connecting Gallery. No secondary minerals were identified in Boom Clay samples next to the recently excavated PRACLAY Gallery.
These findings point to the variable local geochemical conditions. It is likely that in samples with the initially lower carbonate content, the buffering capacity of the Boom Clay might be lost with significant decrease of pH as a consequence.

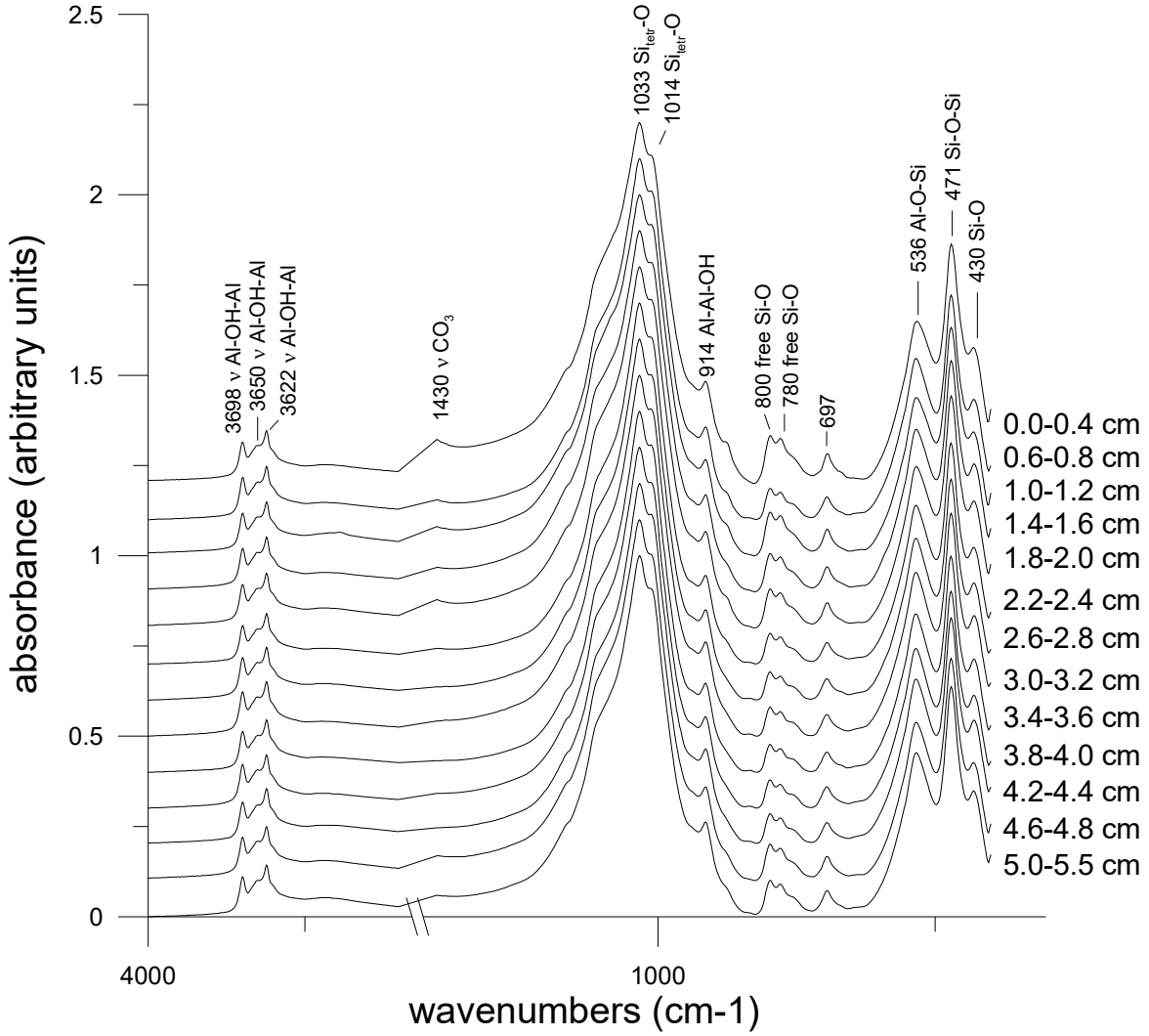

Figure 25. FTIR spectra of TD-41E sample series showing the presence of carbonates based on the CO_3 groups stretching vibrations at 1430 cm^{-1}.

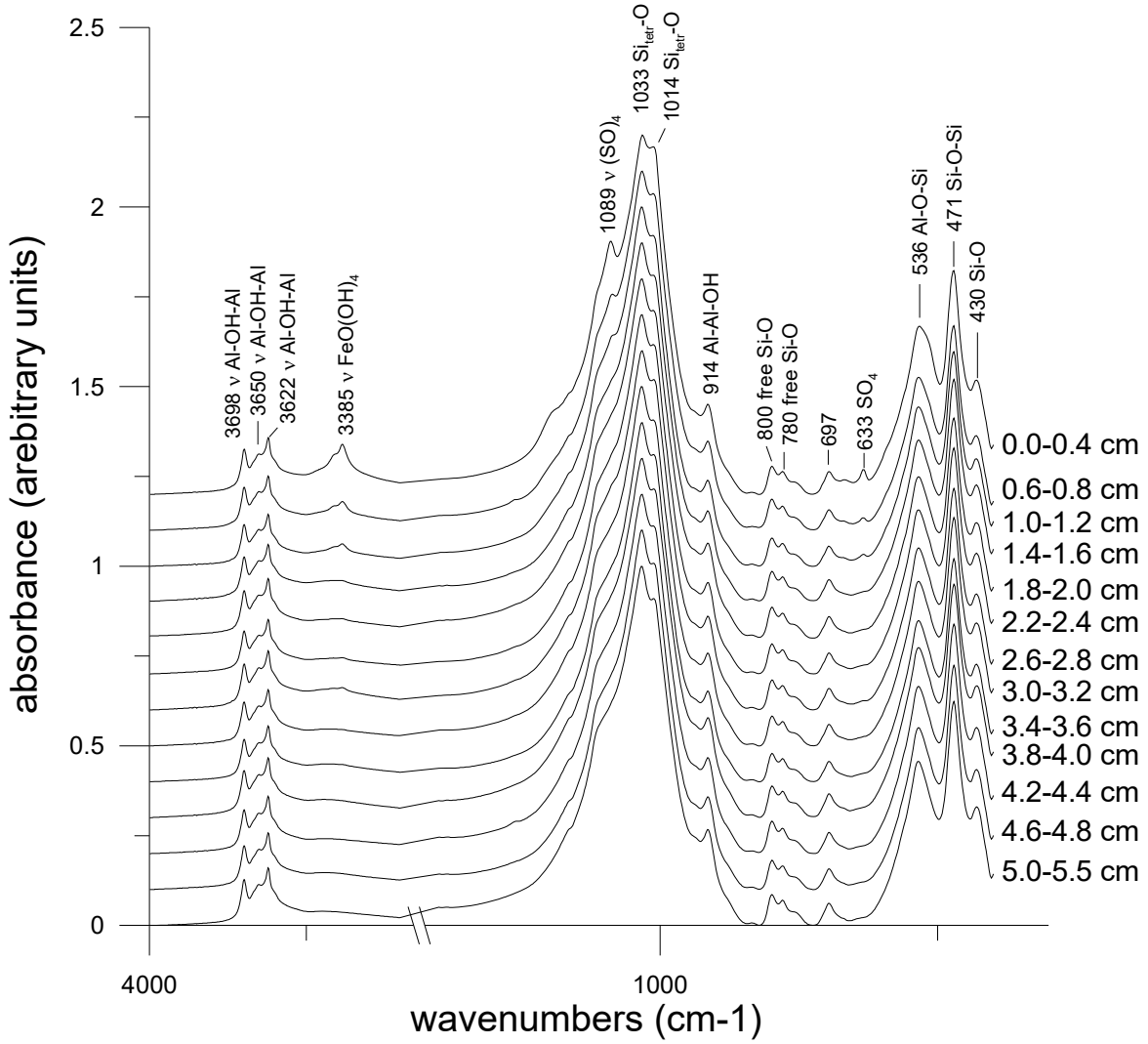

Figure 26. FTIR spectra of CG-68E sample series showing the presence of jarosite ($KFe_3(SO_4)_2(OH)_6$). The diagnostic bands occur at 3385 and 3410 cm^{-1} due to stretching vibrations of the OH groups in the $FeO(OH)_4$ octahedron and stretching vibrations of the SO_4 tetrahedra at 1089 cm^{-1}.

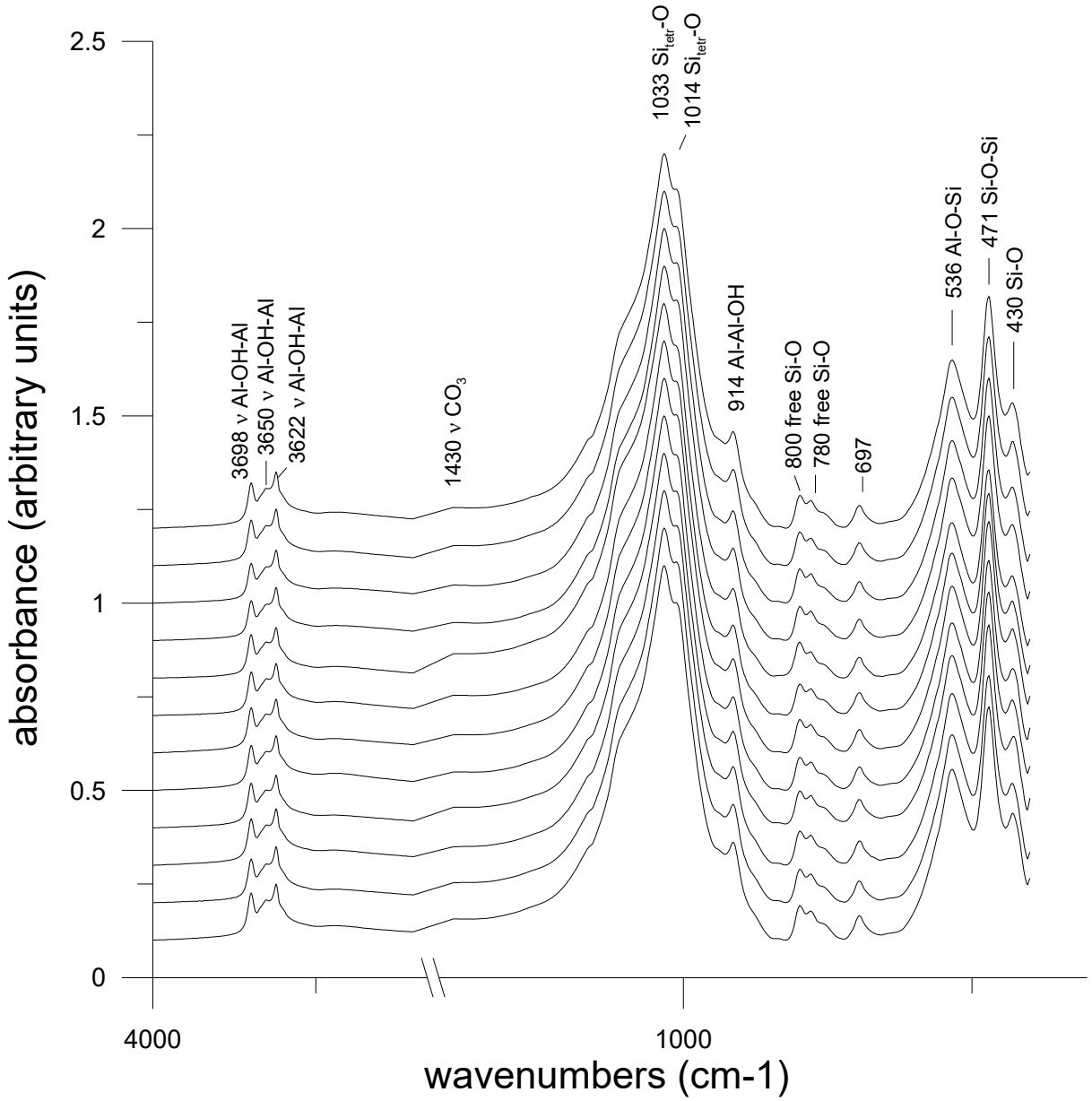

Figure 27. FTIR spectra of the PG-70D sample series showing the presence of carbonates based on the CO_3 groups stretching vibrations at 1430 cm^{-1}. No alteration products were identified in Boom Clay samples next to PRACLAY Gallery.

7.2.3 XANES

To unveil the speciation of iron in the oxidized zone of the Boom Clay, the synchrotron X-ray was employed within the study presented here. The oxidation of pyrite often leads to the formation of secondary poorly crystalline Fe minerals which are very difficult to identify with the conventional techniques. The precipitation of secondary Fe minerals might be of importance for migration of radionuclides, because of their extremely small size (nanoparticles) and related large surface area.

Normalized and first derivative XANES spectra of the measured clay and non-clay Fe-bearing mineral standards are shown in Figure 28 and Figure 29. The example of the fitting result is shown for sample CG-68E 0.0-0.4 (Figure 30) and sample TD-41E 0.0-0.4 (Figure 31). Table 2 shows the relative contribution of various Fe-bearing minerals to the total Fe pool in the core samples from the Test Drift and the Connecting Gallery. The graphical illustration of the Table 2 is given in Figures 32 and 33.

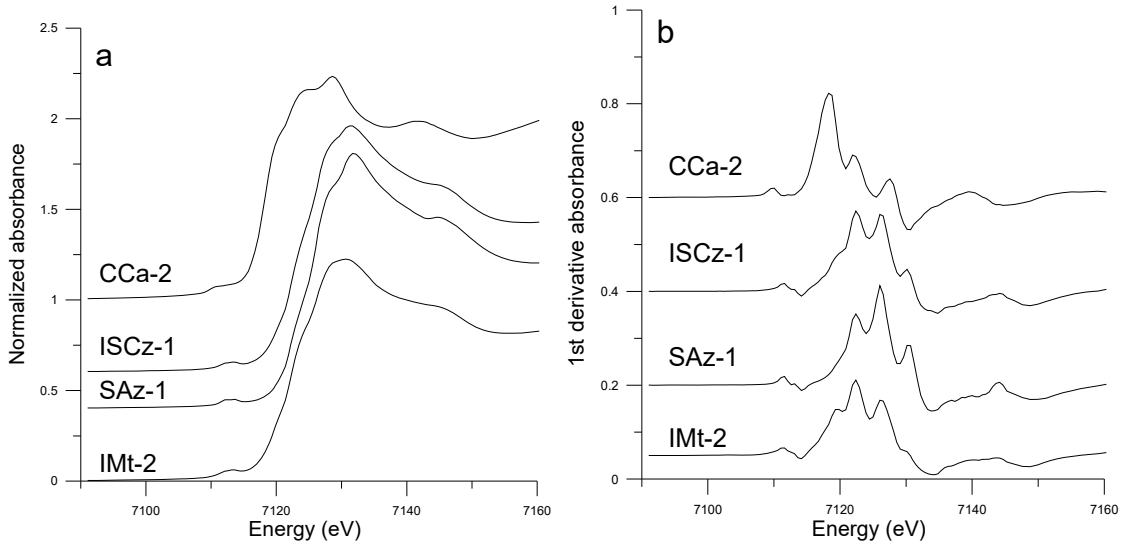

Figure 28. Normalized XANES (a) and first derivative spectra (b) for Fe-bearing clay mineral standards.

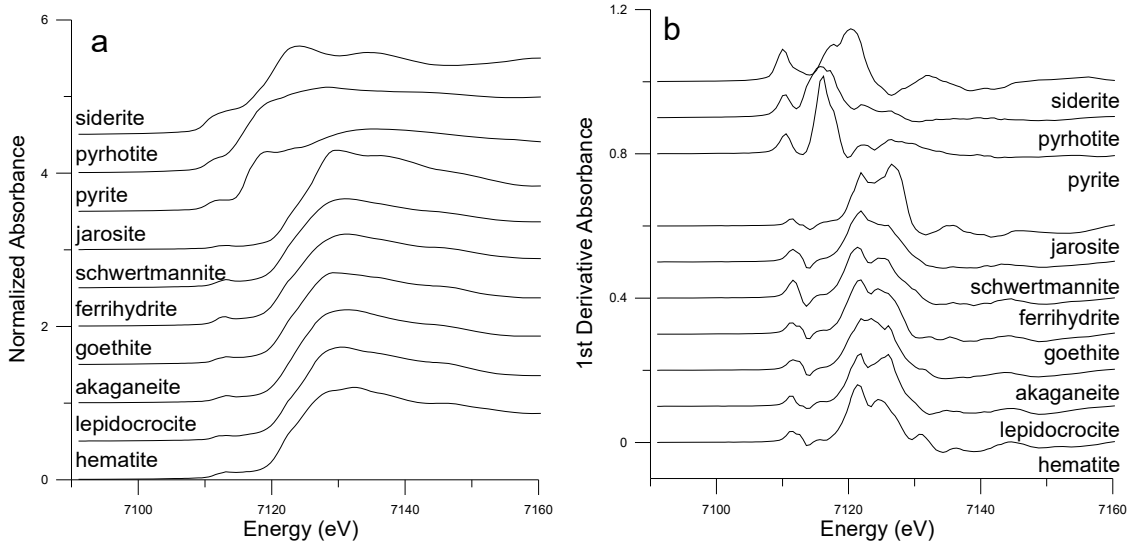

Figure 29. Normalized XANES (a) and first derivative spectra (b) for Fe-bearing non-clay mineral standards.

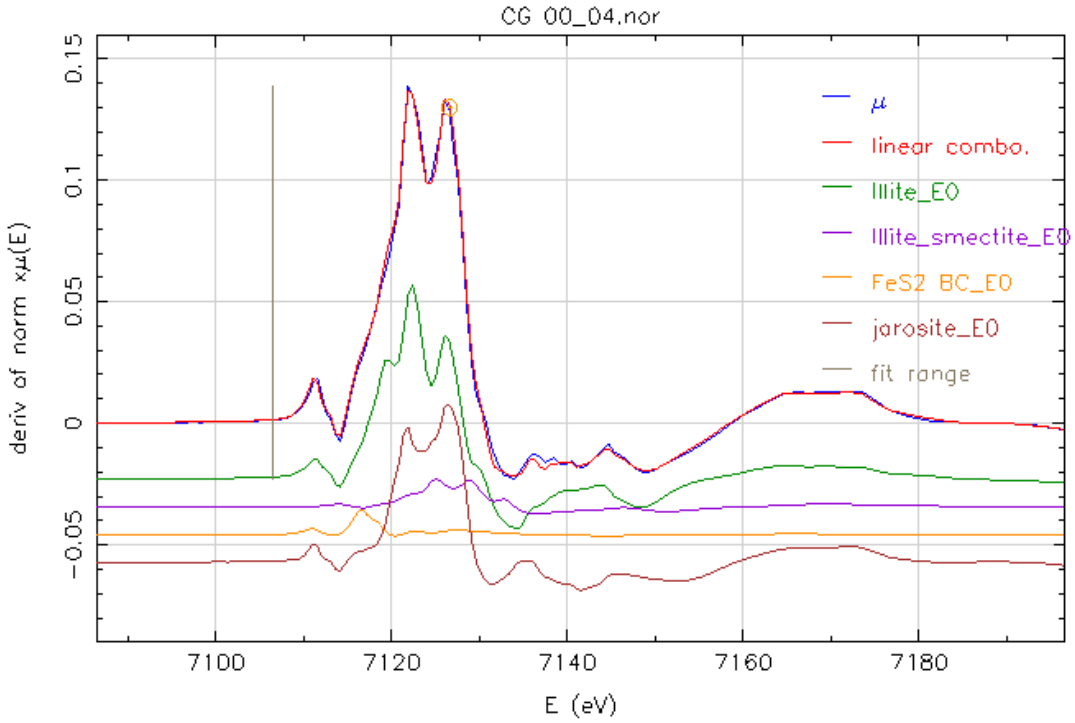

Figure 30. Example of the linear combination fitting of the sample CG-68E 0.0-0.4 cm using illite, illite-smectite, pyrite and jarosite as components. The blue pattern corresponds to the absorption coefficient (•) of the natural Boom Clay sample.

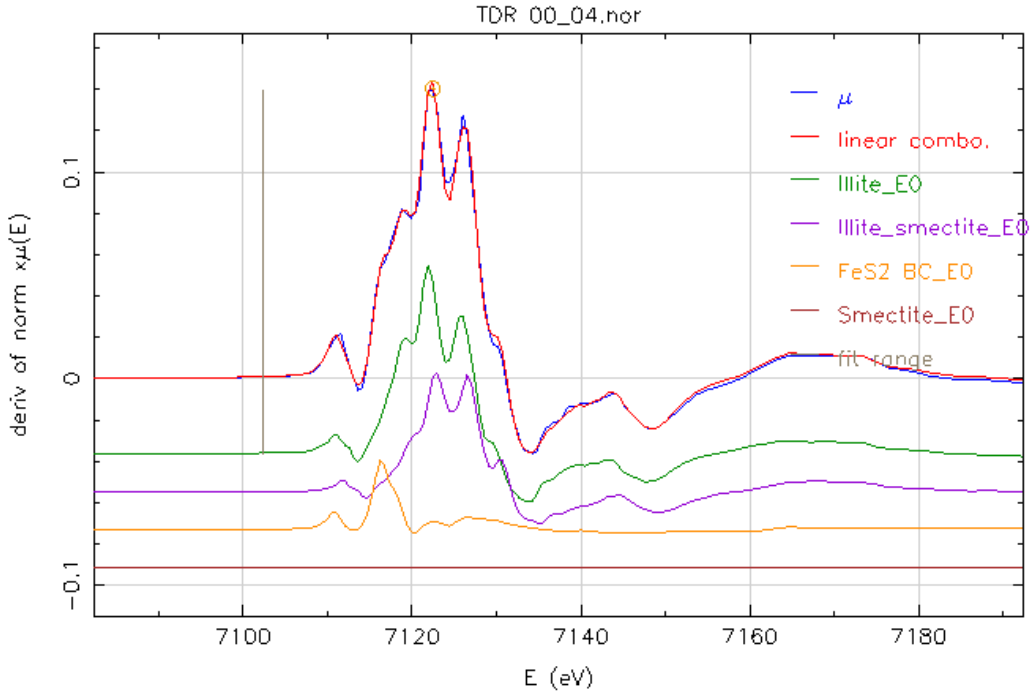

Figure 31. Example of the linear combination analysis of the sample TD-41E 0.0-0.4 cm using illite, illite-smectite and pyrite mineral assemblage. The blue pattern corresponds to the absorption coefficient (•) of the natural Boom Clay sample.

XANES investigation of the Boom Clay samples from the oxidized zone confirms the findings of the XRD and FTIR results. The jarosite is present in the sample series of the Connecting Gallery in contrast to Test Drift, where it is absent. The jarosite is the only secondary Fe containing mineral found in the oxidised Boom Clay by XANES. Since XANES probed only Fe atoms

and the mode of its bonding to neighbouring atoms, the detailed information could be gained on the structure of Fe bearing minerals. Here XANES was applied with the aim to identify secondary amorphous Fe bearing mineral phases, such as poorly crystallized Fe oxyhydroxides, which would otherwise be undetectable by conventional XRD. None of these phases were either identified by XANES. However, the added value of the XANES application lies in the quantification (relative abundance) of all Fe containing mineral phases. The majority of iron in Boom Clay is present as Fe^{3+} in the octahedral sheets of the layered phyllosilicates, of which illite and illite-smectite account for the majority of ferric atoms held in their structure (more than 75% of all Fe in the intact Boom Clay). A minor amount of Fe is present as Fe^{2+} in the pyrite (up to 27%), which can be partially, or almost fully oxidized to Fe^{3+} in the form of jarosite (Table 2, Figure 33).

Table 2. Result of the linear combination fitting of the XANES spectra of the oxidized Boom Clay samples – a relative abundance of Fe-bearing minerals contributing to the total Fe pool.

	illite	*illite-smectite*	*pyrite*	*jarosite*
			weight %	
TDR41-42E 0.0-0.4	57.3	34.5	15.5	-
TDR41-42E 0.8-1.0	52	30.2	17.8	-
TDR41-42E 1.8-2.0	36.9	35.5	27.6	-
TDR41-42E 5.0-5.5	53.8	23.8	22.4	-
CGR68-69E 0.0-0.4	50.1	6.8	4.8	38.4
CGR68-69E 0.8-1.0	49.9	30.6	4	15.5
CGR68-69E 1.8-2.0	58.3	29	7.3	5.4
CGR68-69E 5.0-5.5	66.9	18.7	6.2	8.2

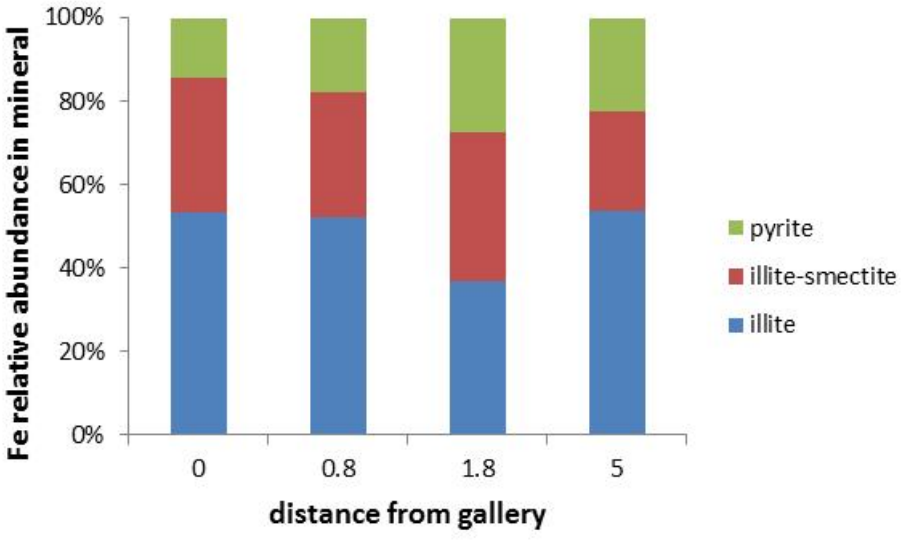

Figure 32. Distribution of Fe over prevailing Fe-bearing minerals in the sample serie TD-41E.

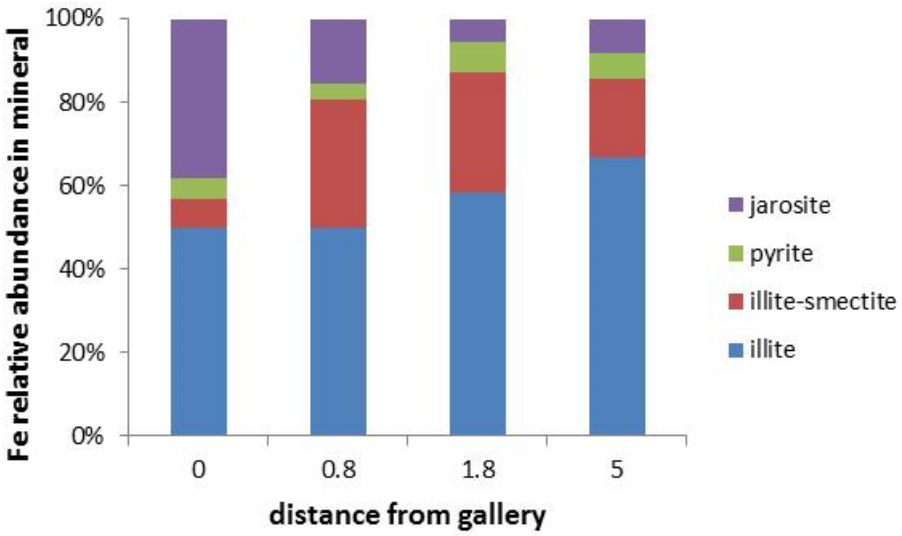

Figure 33. Distribution of Fe over prevailing Fe-bearing minerals in the sample serie CG-68E.

7.2.4 Mössbauer spectroscopy

Mössbauer spectra of the Boom Clay samples are presented in Figure 34 (CGR68-69E) and 35 (TDR41-42E). The hyperfine parameters and relative areas of the spectral components are shown in Table 3.

The general pattern in all spectra is the presence of Fe^{3+} and Fe^{2+} high spin (S=5/2 and 2 respectively) paramagnetic ions in the structure of the clay minerals. There are clearly two different distinct Fe^{3+} states and one Fe^{2+} state in all spectra. Two Fe^{3+} states most likely belong to structural iron in the octahedral sheets of the clay minerals, namely illite and illite-smectite. The Fe^{2+} state can be attributed to octahedrally coordinated iron atoms in the structure of pyrite. The relative population of the iron ions varies between the samples, but it turns out that the majority is attributed to the ferric states (Fe^{3+}) in all cases, as the sum of the absorption areas for these states is above 70% for all spectra. Very minor contributions from some magnetically split components could be seen only in some of the 77 K spectra (CG-68E/0.0-0.4, CG-68E/0.8-1.0, CG-68E/2.8-3.0 and TD-41E/0.8-1.0). These belong most probably to the presence of Fe in the jarosite.

In conclusion, Mössbauer spectroscopy confirms the results of XANES analysis: two Fe^{3+} states dominate in all samples accounting for more than 70% of the total Fe. These states are related to the iron present in the octahedral sheets of illite and illite-smectite. The rest of the iron is present as Fe^{2+} in the structure of the pyrite in most of the studied samples. Some minor contribution can be also attributed to Fe^{3+} in the jarosite. With respect to small amounts of this mineral, the XANES technique seems to have a better resolution than Mossbauer spectroscopy. Fe oxyhydroxides were not detected by any of these techniques.

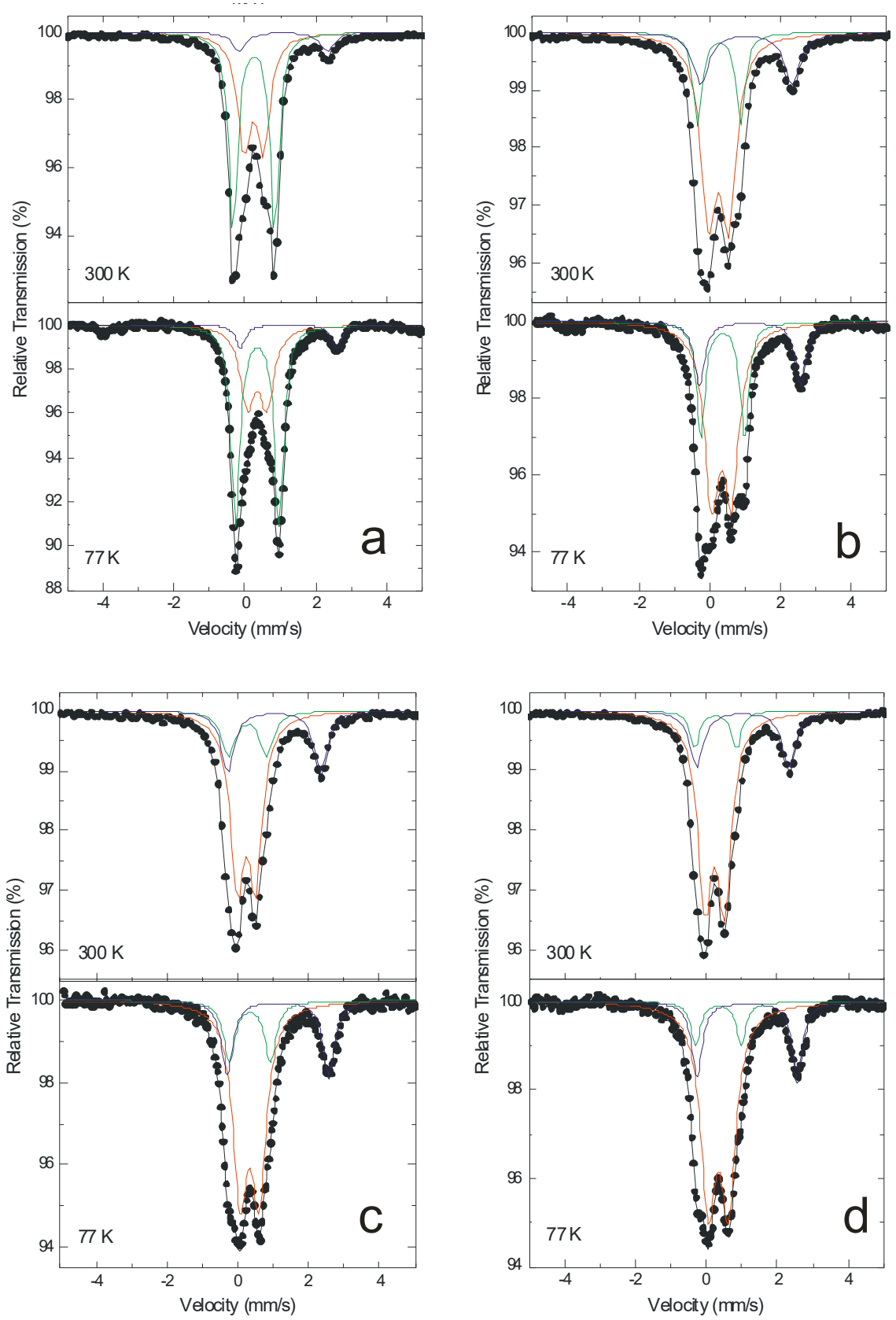

Figure 34. Mössbauer spectra of samples (a) CG-68E 0.0-0.4, (b) CG-68E 0.8-1.0, (c) CG-68E 1.8.-2.0 and (d) CG-68E 2.8-3.0 as measured at 300K (upper part) and 77K (lower part) showing that ferric states (Fe^{3+}) predominate in the Boom Clay. Red and green pattern – Fe^{3+} states in the illite and illite-smectite respectively, blue pattern – Fe^{2+} state present in the form of pyrite. Dotted line – experimental spectra.

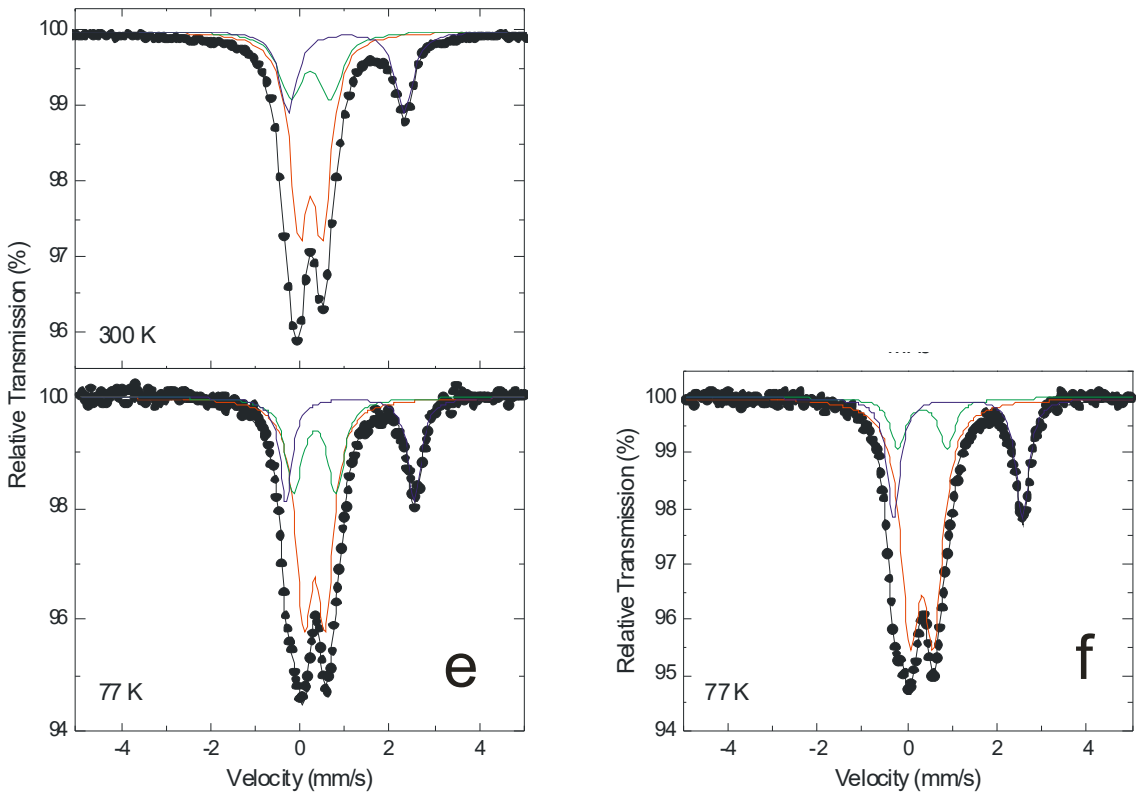

Figure 34 continued. Mössbauer spectra of samples (e) CG-68E 3.8-4.0 and (f) CG-68E 5.0-5.5 as measured at 300K (upper part) and 77K (lower part) showing that ferric states (Fe^{3+}) prevail over Fe^{2+} states in the Boom Clay. Red and green pattern – Fe^{3+} states in the illite and illite-smectite respectively, blue pattern – Fe^{2+} state present in the form of pyrite. Dotted line – experimental spectra.

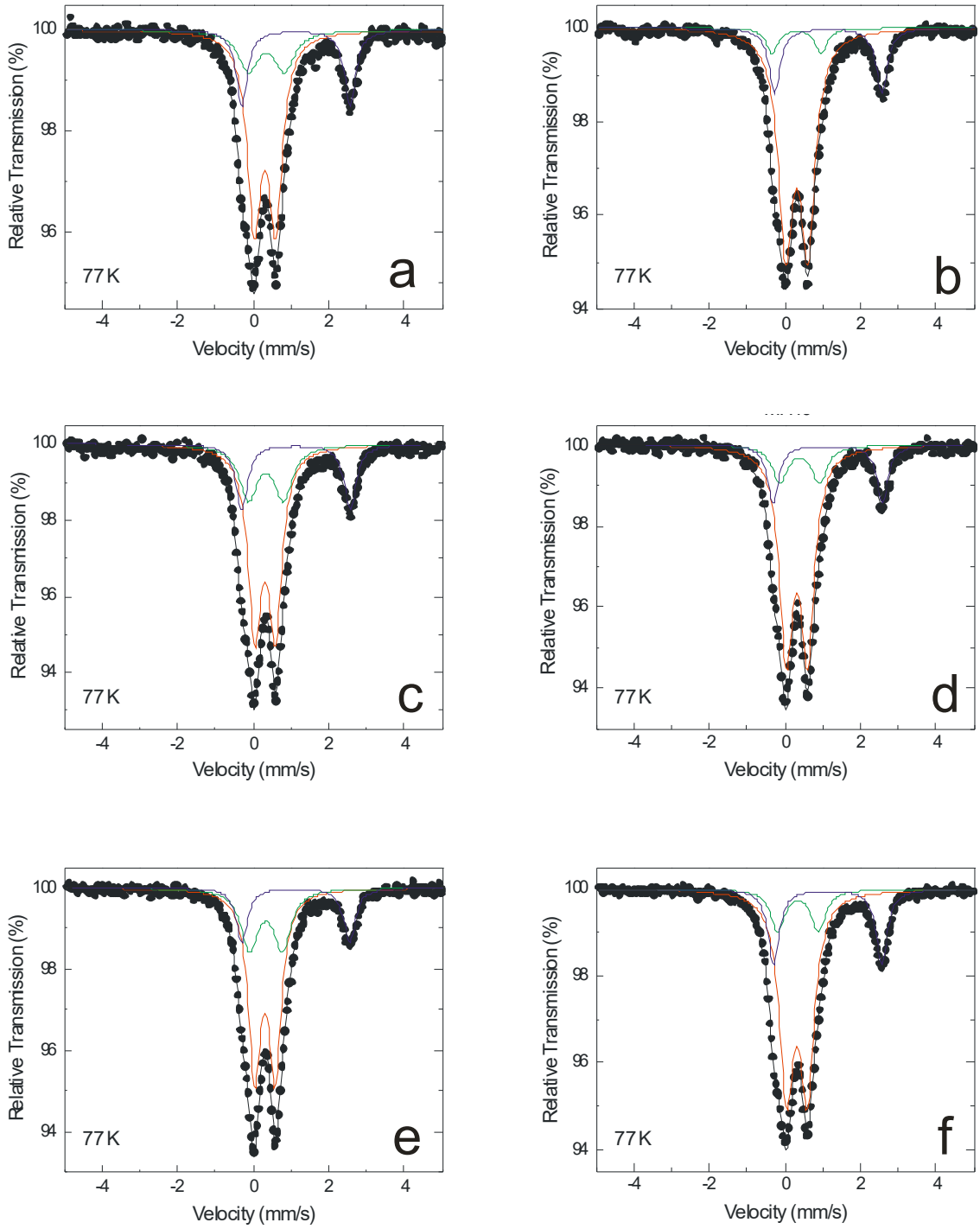

Figure 35. Mössbauer spectra of samples TD-41E (a) 0.0-0.4, (b) 0.8-1.0, (c) 1.8-2.0, (d) 2.8-3.0, (e) 3.8-4.0 and (f) 5.0-5.5 as measured at 77K, showing that ferric states (Fe^{3+}) prevail over Fe^{2+} states in the Boom Clay. Red and green pattern – Fe^{3+} states in the illite and illite-smectite respectively, blue pattern – Fe^{2+} state present in the form of pyrite. Dotted line – experimental spectra.

Table 3. Hyperfine parameters (I.S. – isomer shift, Q.S. – quadrupole splitting) and relative areas of spectral components derived from Mössbauer spectra. The data on the coloured background correspond to colours used in the spectra.

Sample	*T (K)*	*I.S. (mm/s)*	*HWHM (mm/s)*	*Q.S. (mm/s)*	*Area (%)*	*Ion*
CGR68-69E 0.0-0.4	300	0.35	0.23	0.54	41	Fe3+
		0.36	0.15	1.16	51	Fe3+
		1.19	0.23	2.49	8	Fe2+
	77	0.45	0.24	0.54	35	Fe3+
		0.46	0.15	1.22	58	Fe3+
		1.34	0.17	2.70	7	Fe2+
CGR68-69E 0.8-1.0	300	0.36	0.26	0.57	62	Fe3+
		0.38	0.15	1.20	19	Fe3+
		1.14	0.27	2.56	19	Fe2+
	77	0.44	0.26	0.56	60	Fe3+
		0.47	0.15	1.24	24	Fe3+
		1.24	0.18	2.86	16	Fe2+
CGR68-69E 1.8-2.0	300	0.35	0.24	0.52	62	Fe3+
		0.38	0.24	1.08	16	Fe3+
		1.13	0.22	2.63	22	Fe2+
	77	0.44	0.25	0.54	63	Fe3+
		0.45	0.19	1.15	16	Fe3+
		1.24	0.20	2.86	21	Fe2+
CGR68-69E 2.8-3.0	300	0.35	0.24	0.55	70	Fe3+
		0.37	0.16	1.17	9	Fe3+
		1.14	0.23	2.60	21	Fe2+
	77	0.44	0.26	0.57	70	Fe3+
		0.44	0.15	1.28	10	Fe3+
		1.25	0.18	2.83	20	Fe2+
CGR68-69E 3.8-4.0	300	0.34	0.24	0.52	53	Fe3+
		0.34	0.30	0.89	24	Fe3+
		1.14	0.23	2.59	23	Fe2+
	77	0.44	0.22	0.48	53	Fe3+
		0.45	0.22	0.94	25	Fe3+
		1.23	0.18	2.87	22	Fe2+
CGR68-69E 5.0-5.5	77	0.43	0.24	0.53	62	Fe3+
		0.45	0.21	1.09	12	Fe2+
		1.23	0.18	2.86	26	Fe2+
TDR41-42E 0.0-0.4	77	0.42	0.22	0.57	61	Fe3+
		0.46	0.32	0.97	19	Fe3+
		1.24	0.18	2.86	20	Fe2+
TDR41-42E 0.8-1.0	77	0.42	0.23	0.59	75	Fe3+
		0.42	0.19	1.30	7	Fe3+
		1.25	0.18	2.83	18	Fe2+
TDR41-42E 1.8-2.0	77	0.43	0.21	0.55	58	Fe3+
		0.45	0.29	0.93	23	Fe3+
		1.24	0.19	2.87	19	Fe2+
TDR41-42E 2.8-3.0	77	0.43	0.22	0.57	70	Fe3+
		0.50	0.24	1.04	14	Fe3+
		1.24	0.17	2.88	16	Fe2+
TDR41-42E 3.8-4.0	77	0.42	0.20	0.55	58	Fe3+
		0.45	0.28	0.87	26	Fe3+
		1.23	0.19	2.85	16	Fe2+
TDR41-42E 5.0-5.5	77	0.43	0.23	0.55	66	Fe3+
		0.45	0.22	1.08	14	Fe3+
		1.23	0.18	2.85	20	Fe2+

7.2.5 Cation exchange capacity

The results of the CEC measurements are summarized in Table 4 and Figure 36. The variations of the CEC parameter in the Putte Member of the undisturbed Boom Clay was found between 17-27 meq/100g and the average of 22.7 ± 1.58 meq/100g in the Mol-1 borehole (Honty, 2010). Similarly, (Zeelmaekers et al., 2015) reported a CEC value of 21 meq/100g for the Boom Clay sample corresponding to a depth level of the HADES URF. Due to relatively large relative errors in the CEC determinations, the observed variations can hardly be ascribed to oxidation phenomena. The sum of the exchanged cations varies from 17 to 21 meq/100g in the oxidized zone around the studied samples of the PRACLAY Gallery, between 18-24 meq/100g in samples of the Connecting Gallery and between 15-20 meq/100 in samples of the Test Drift. As such, these variations can be considered as natural feature of the clay reflecting local heterogeneities in the smectite content, rather than response to the oxidation. The CEC values fit within the range of values measured in the undisturbed Boom Clay. The natural Boom Clay variability is another aspect to consider. The local variations of the smectite content will inevitably affect the measured CEC value. Therefore, if there is any influence of the oxidation on the CEC, such effect might be hidden by mineral heterogeneity inherent to Boom Clay.

In conclusion, oxidation has no such impact on the total cation exchange capacity of the Boom Clay that would exceed either measurement error of the CEC determination or its natural variability.

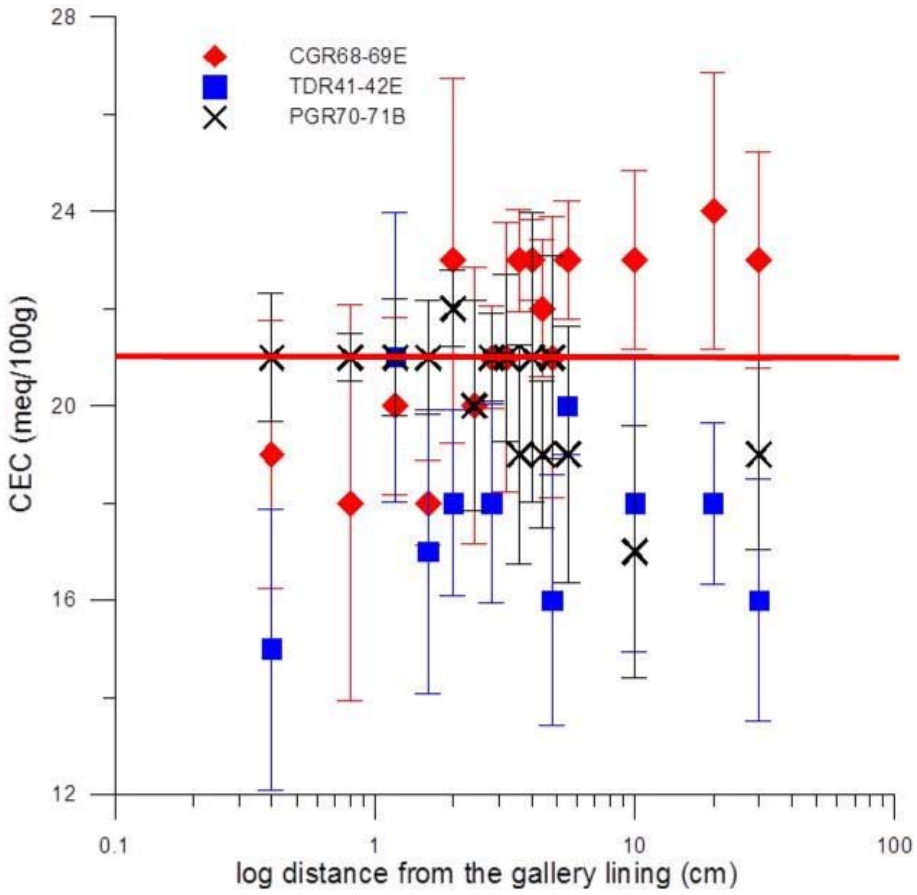

Figure 36. CEC parameter as function of increasing distance from the gallery lining. The samples are from the Test Drift (blue squares), the Connecting Gallery (red diamonds) and the PRACLAY Gallery (black crosses). Whiskers indicate error bars. Red horizontal line indicates the CEC value of the undisturbed Boom Clay from the depth level of the HADES URF (Zeelmaekers et al., 2015).

Table 4. CEC parameter as measured on samples from the Test Drift, the Connecting Gallery and the PRACLAY Gallery.

sample serie	*distance*	*CEC*	*standard deviation*
	(mm)	(meq/100g)	(± meq/100g)
PG-R70-71B	0.0-0.4	21	1,307
PG-R70-71B	0.6-0.8	21	0,493
PG-R70-71B	1.0-1.2	21	1,209
PG-R70-71B	1.4-1.6	21	1,18
PG-R70-71B	1.8-2.0	22	0,78
PG-R70-71B	2.2-2.4	20	2,16
PG-R70-71B	2.6-2.8	21	0,9
PG-R70-71B	3.0-3.2	21	1,72
PG-R70-71B	3.4-3.6	19	2,259
PG-R70-71B	3.8-4.0	21	2,97
PG-R70-71B	4.2-4.4	19	1,5
PG-R70-71B	4.6-4.8	21	2,1
PG-R70-71B	5.0-5.5	19	2,65
PG-R70-71B	10.0-10.5	17	2,59
PG-R70-71B	27.5-28.0	19	1,95
CG-R68-69E	0.6-0.8	18	4,08
CG-R68-69E	1.0-1.2	20	1,82
CG-R68-69E	1.4-1.6	18	0,87
CG-R68-69E	1.8-2.0	23	3,75
CG-R68-69E	2.2-2.4	20	2,84
CG-R68-69E	2.6-2.8	21	1,06
CG-R68-69E	3.0-3.2	21	2,76
CG-R68-69E	3.4-3.6	23	1,05
CG-R68-69E	3.8-4.0	23	0,84
CG-R68-69E	4.2-4.4	22	1,41
CG-R68-69E	4.6-4.8	21	2,9
CG-R68-69E	5.0-5.5	23	1,21
CG-R68-69E	10.0-10.5	23	1,85
CG-R68-69E	20.0-20.5	24	2,84
CG-R68-69E	30.0-30.5	23	2,23
TD-R41-42E	1.0-1.2	21	2,99
TD-R41-42E	1.4-1.6	17	2,92
TD-R41-42E	1.8-2.0	18	1,91
TD-R41-42E	2.6-2.8	18	2,05
TD-R41-42E	4.6-4.8	16	2,57
TD-R41-42E	5.0-5.5	20	1,01
TD-R41-42E	10.0-10.5	18	3,06
TD-R41-42E	20.0-20.5	18	1,66
TD-R41-42E	30.0-30.5	16	2,49

7.2.6 Conclusions with respect to Boom Clay mineralogy perturbed by oxidation

The integrated mineralogical investigation (XRD, FTIR, XANES, Mössbauer spectroscopy and CEC) point to the fact that the effect of the oxidation on the mineralogy is even more spatially restricted than the effect on the pore water chemistry. In all cases the extent of the mineralogically altered zone does not exceed 4.5 cm from the gallery. Further away, the mineralogical composition is typical of the undisturbed Boom Clay. Jarosite and gypsum are the most frequently observed secondary oxidation products.

Unsurprisingly, XANES and Mössbauer spectroscopy jointly point to the fact that ferric iron (Fe^{3+}) is present as structural iron in the octahedral sheets of the phyllosilicates. No Fe present in the form of (oxi)hydroxides could be detected by any of the two techniques, probably because of the absolute predominance of Fe bound to oxy- and hydroxyl groups in the octahedral sheets (up to 90% of the total Fe in the bulk Boom Clay) of phyllosilicates.

The CEC measurements indicate that, irrespective of the sulphate content, the exchange capacity of the bulk Boom Clay is not significantly compromised in the oxidised zone of the Boom Clay. Although the CEC of the undisturbed Boom Clay is variable around the Test Drift, the Connecting Gallery and the PRACLAY Gallery (16, 23 and 19 meq/100g respectively), the CEC of the clay in the altered zone remains in the range of values typical of the undisturbed Boom Clay.

7.3 Modelling assessments

In this Chapter we discuss the results of the scoping calculations realized in the frame of the NF-PRO project (De Craen et al., 2011) and new modelling results.

A first set of scoping calculations involves simple transport calculations to evaluate oxygen diffusion into the host rock from the ventilated gallery and sulphate redistribution by diffusion and also advection due to the flow of pore water towards the gallery. These calculations considered only transport, but not geochemical reactions. In a second set of calculations, geochemical reactions are accounted for in the model, i.e. oxygen is consumed by the oxidation of pyrite. The results of the scoping calculations are compared with the experimental data, including new data acquired after the NF-PRO project, i.e. after 2007. Lastly, equilibrium reaction modelling was carried out in order to explain the mechanism of the oxidation process and related changes in pore water composition as observed in the *in-situ* sampled pore waters. The approach used in the geochemical (equilibrium) modelling is the same as the one presented by De Craen *et al.* (2004b), but again using new pore water chemistry data as input parameters.

7.3.1 Transport modelling

Near field scoping calculations were performed to evaluate the spatial extent of oxidising conditions in the clay around a disposal gallery. Gallery dimensions correspond to the concept for VHLW described by NIROND (2004) and Wickham (2005). These calculations gave an idea of the volume of host formation that is possibly chemically altered due to oxidation due to ventilation during the construction and operational phases of the repository.

Oxygen in-diffusion into the host rock

During the construction and operational phases of the repository, the clay in contact with the gallery is exposed to air[4]. Oxygen present in the air will dissolve into the pore water of the clay. Dissolved oxygen will then diffuse into the clay massif and can potentially oxidise redox sensitive minerals, in particular pyrite (FeS_2). However, since the HADES gallery is still at atmospheric pressure, pore water is also flowing radially from the host rock towards the gallery, adding an advective component to the diffusive transport of O_2, in the opposite direction. This advective-diffusive transport process was modelled in a pseudo-1D radial geometry using the PORFLOW 3.07 numerical flow and transport code (Runchal, 1997). In a first approximation, only transport is considered and consumption of oxygen is not accounted for.

A 1D radial transport model is used. The model specifications are described in detail in the report of De Craen *et al.* (2011). At the interface between the gallery and the clay (r_i = 1.615 m), a constant concentration of dissolved oxygen of 2.73×10^{-4} mol/L is set. This value is obtained using Henry's law: $X(O_2)_{aq} = k_{H,O2} \times P_{O2}$ with P_{O2} = 0.21 bar and $k_{H,O2}$ = 0.0013 mole/(L×bar) (Henry's constant for oxygen).

The transport properties of dissolved O_2 used in the model are listed in Table 4.

Table 4. Transport properties of dissolved O_2 in Boom Clay used for the calculation

Property	Symbol	Value
porosity (-)	η	0.39
retardation factor for dissolved O_2 (-)	R	1
pore diffusion coefficient for O_2 (m^2/s)	D_p	2×10^{-10}

[4] Directly during the construction phase. After installation of the lining, through the porosity of the concrete lining segments, interfaces between these segments and other openings.

The pore water velocity field around the gallery was obtained from a quasi-steady flow calculation, considering a hydraulic conductivity of the Boom Clay of 4.5 × 10^{-12} m/s (Boisson, 2005).

Figure 37 shows the radial profile of the dissolved oxygen concentration after 3 and 20 years. Note that the concentration axis is expressed in a logarithmic scale with a minimum of less than 0.1 % of the boundary concentration. We can see that even after 20 years of open gallery conditions, the oxygen would not diffuse further than 2 meters away from the gallery in the absence of advection (plain lines on Figure 37, diffusion only). Dashed lines profiles in the figure illustrate the impact of advection, which acts in the opposite direction of the oxygen diffusion. As expected, because the pore water flows towards the gallery, the extent of the oxygen penetration into the host rock is less than in the case without advection. Figure 38 shows the instantaneous and cumulative oxygen fluxes from the gallery into the host rock. The results of this simulation indicate that after 20 years of ventilation, the total amount of oxygen that could diffuse into the clay should not exceed 0.5 mole per metre of gallery and, after 50 years, less than 1 mole per metre of gallery.

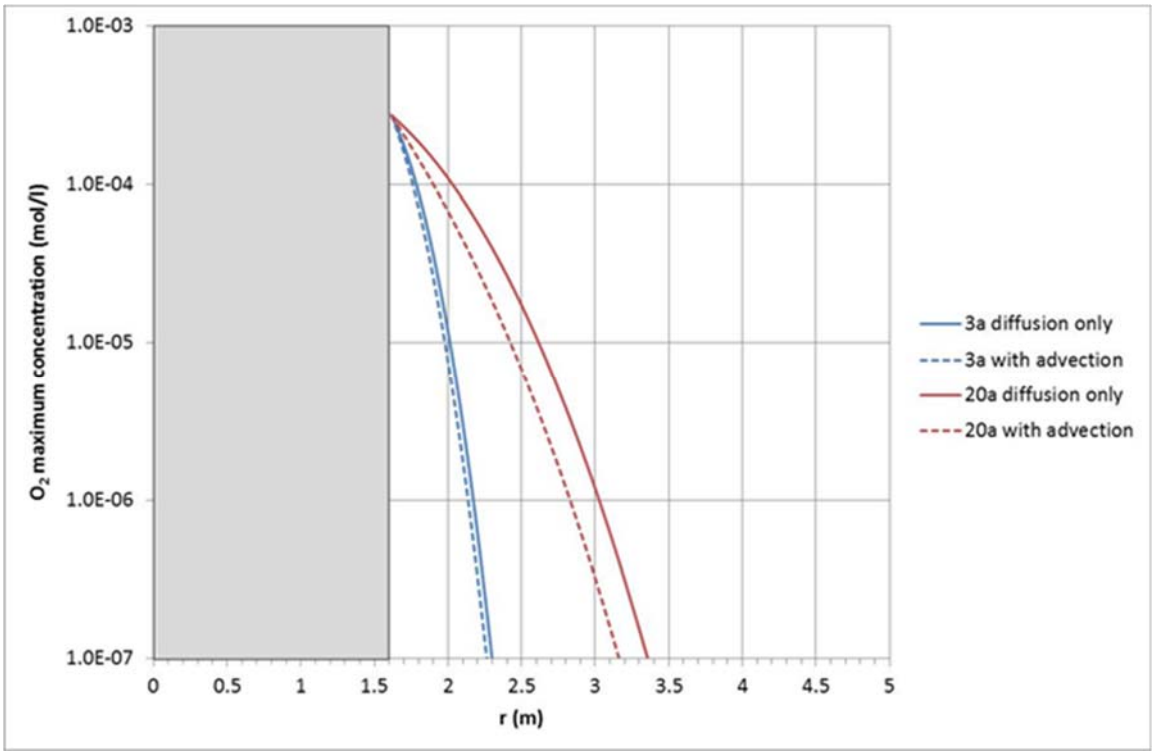

Figure 37. Simulated oxygen profiles as function of the distance from the gallery after 3 and 20 years involving purely diffusive (solid lines) and combined diffusive-advective transport (dashed lines).

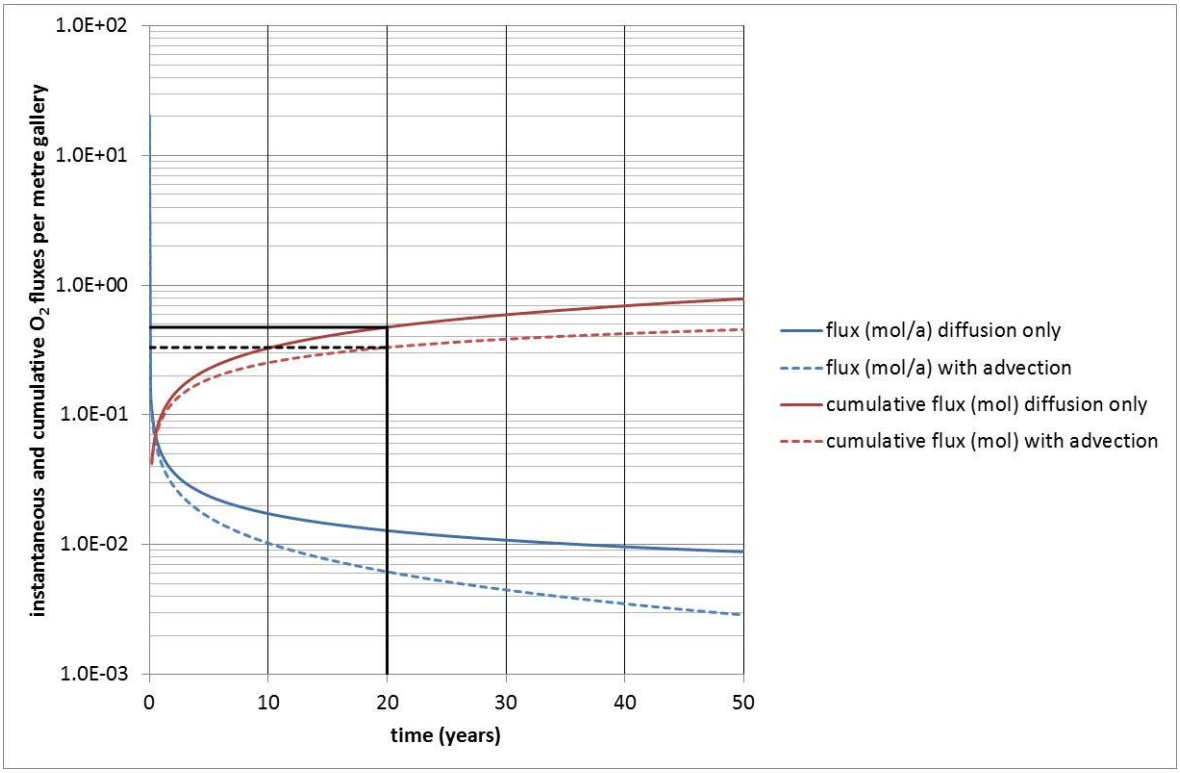

Figure 38. Instantaneous and cumulative oxygen fluxes as a function of time considering diffusion only (solid lines) and diffusion counteracted by advection towards gallery (dashed lines), over a gallery length of 1 metre.

7.3.1.1 Sulphate diffusion in the host rock

In the course of the excavation of the galleries in the HADES URF, open fractures are created in the surrounding Boom Clay to a depth of about 1 m (Bastiaens *et al.*, 2003; Bernier *et al.*, 2007). Pyrite oxidation occurs and sulphate is produced. Due to the self-sealing capacity of the Boom Clay, closure and sealing of the fractures occur fast. Hence, sulphate is trapped within this first meter around the gallery. The question arises what will happen with this (quasi-instantly formed) sulphate. Will the sulphate diffuse further into the massif or will it predominantly be transported towards the gallery by the flowing pore water? PORFLOW 3.07 was used to simulate the transport of sulphate.

The geometry of the model and the hydraulic conditions are the same as those mentioned above. The thickness of the fractured zone is assumed to be 1 m. Because the amount of sulphate initially present is unknown (we set time = 0 when the fractures are sealed), a unit (normalised) concentration is used as initial condition in that zone. The pore diffusion coefficient D_p of sulphate was set to 2×10^{-10} m^2/s (De Cannière et al., 2010). The pore water velocity field was computed assuming an hydraulic conductivity of 4.5 $\times10^{-12}$ m/s the Boom Clay and a rather high value of 1 $\times10^{-11}$ m/s was selected for the EDZ, based on experimental evidence (Bernier *et al.*, 2005). Since SO_4^{2-} is a bivalent anion, transport in Boom Clay can be substantially influenced by anion exclusion. Hence, only a fraction of the porosity is accessible for diffusion. Therefore, the accessible porosity was lowered to 0.1. Sulphate was assumed not to be sorbed in Boom Clay.

The results of these scoping calculations are shown in Figure 39. The sulphate concentration within the EDZ diminishes fast. This figure furthermore illustrates that the majority of the sulphates are transported by advection towards the gallery, while the diffusion of the sulphates further into the Boom Clay is extremely limited, even after 50 years.

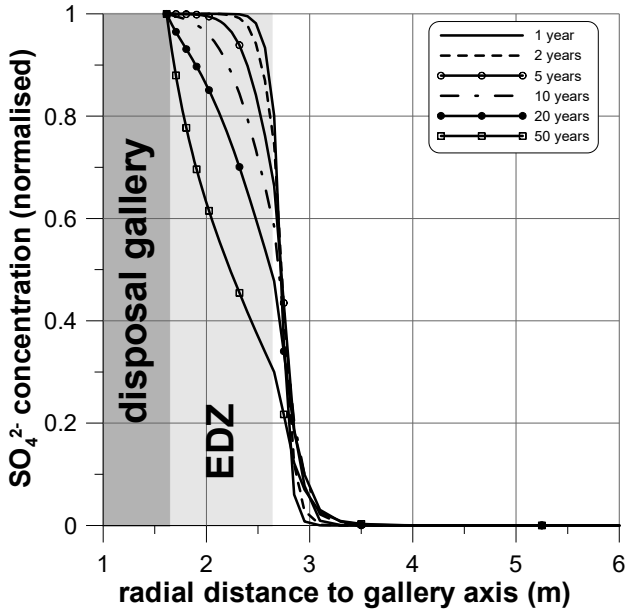

Figure 39. SO_4^{2-} concentration profiles as a function of the distance to the gallery axis (De Craen *et al.*, 2008).

7.3.2 Reactive transport modelling

In Section 7.3.1, diffusive transport of oxygen from the gallery into the clay without any geochemical reactions was simulated with PORFLOW. In this section, the geochemical transport code PHREEQC-2 (version 2.14.02; Parkhurst and Appelo, 1999) is used in order to include geochemical reactions. The oxygen flux is calculated for different scenarios. The model calculations are then compared in terms of oxygen consumption with the experimental data.

The model specification is similar to that described in Section 7.3.1.1. In the first calculation run, the pure effect of diffusive transport is simulated. In the next run, a kinetic oxidation reaction for pyrite (Williamson and Rimstidt, 1994) is included in the model:

$$FeS_2 + 7/2\ O_2 + H_2O = Fe^{2+} + 2\ SO_4^{2-} + 2\ H^+ \quad (1)$$

with the reaction rate:

$$r = 10^{-8.19} m_{O_2}^{0.5} m_{H+}^{-0.11} \quad (mol/m^2/s)$$

where m_{O2} and m_{H+} are the concentrations of dissolved O_2 and proton in the pore water respectively.

An initial amount of 0.833 moles of pyrite per kg clay is assumed. This corresponds to 2.5 dry wt%. This value is in the experimental determined range of 1-5 dry wt% of Boom Clay (De Craen *et al.*, 2004b). A reactive surface area of 100 m^2/kg of pyrite is taken. The model further assumes the equilibrium of calcite, siderite, kaolinite and chalcedony, pH = 8.5, p_{CO_2} = $10^{-2.62}$ and pe = -4.8 (E_h = -0.274 V) (De Craen *et al.*, 2004b).

For the last simulation, geochemical reactions are also included, but not the kinetic oxidation reaction for pyrite, i.e. equilibrium is assumed for the oxidation of pyrite.

Firstly, *purely diffusive transport* is simulated with PHREEQC and PORFLOW to compare oxygen profiles acquired by the two codes. The two codes produce the same profiles. After 20 years, only about *0.5 moles O_2* have entered the model domain. Secondly, the simulation result for the simulation including a *kinetic* oxidation *reaction* for pyrite is also given in Figure 40. The oxygen diffusing into the clay is rapidly consumed by pyrite oxidation according to reaction (1), creating a higher oxygen flux than for the case no reactions are included. As such, PHREEQC simulated that 0.7 moles of pyrite in Boom Clay have dissolved after 20 years. This means, based on reaction (1), that about *2.4 moles O_2* have diffused into the clay, which is five times higher than the flux calculated from the simulation not including reactions. However, the O_2 disturbed zone is much smaller and becomes negligible compared to the case where no pyrite is included.

Thirdly, in the last simulation, assuming *thermodynamic equilibrium* for the pyrite oxidation reaction, the flux is higher (as expected). More specifically, PHREEQC results show that 1 mole of pyrite dissolves in 20 years, which means about *3.5 moles* O_2 have diffused into the clay. These quantities of O_2 are much too low to account for the observed sulphate concentrations in the pore waters of the EDZ in the Boom Clay, which also reflect the rapid oxidation around open fractures during the excavation, as shown in the next section.

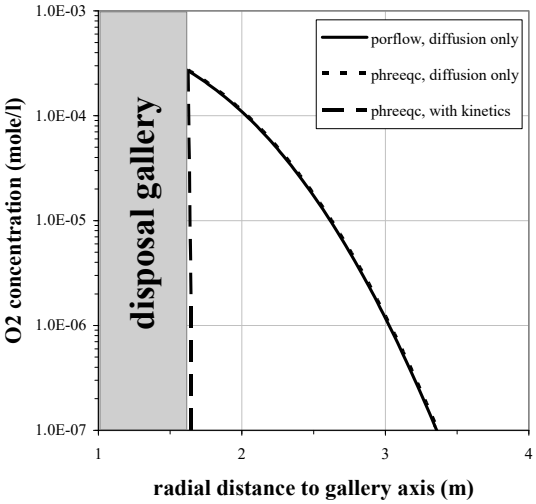

Figure 40. Oxygen profiles as function of the distance from the gallery after 20 years, for a simulation including diffusion only (with PORFLOW and PHREEQC) and another simulation also including kinetic dissolution of pyrite (with PHREEQC). (De Craen *et al.*, 2011)

7.3.3 Mass balance check: transport calculations versus experimental data

Figure 41 shows the combined batch and *in-situ* sulphate concentrations around the Test Drift, the Connecting Gallery and PRACLAY Gallery as a function of the distance from the concrete/clay interface. If a trendline is fitted through these experimental data, the total amount of sulphate that is present in the clay up to a distance of 2.5 meter of the gallery can be estimated by integration of that trendline along the radial direction. Knowing the total amount of sulphates, we can estimate the amount of oxygen and pyrite needed to produce a given amount of sulphates according to reaction

(1) $FeS_2 + 7/2\ O_2(aq.) + H_2O \leftrightarrow Fe^{2+} + 2\ SO_4^{2-} + 2\ H^+$

Integrating the exponential trendline through the data points of the Connecting Gallery, a total of 162 moles SO_4^{2-} is found per meter gallery length. According to the above reaction 81 moles of pyrite and 284 moles of O_2 need to be consumed to produce these 162 moles of sulphates. These 81 moles represent less than 2% of the pyrite present up to a distance of 2.5 m from the Connecting Gallery if one assumes an initial amount of 2.5 dry wt% of the pyrite present in the first metre. Drawing an exponential trendline through the sulphate concentration data of the Test Drift, the following values are found: the total amount of sulphates – 228 moles, pyrite – 114 moles and oxygen needed – 399 moles. No fitting was assayed through the data points in the PRACLAY gallery as these were too scattered. However, lower values of the sulphate concentrations and accordingly lower values of the pyrite and oxygen consumed would be attained than in the case of the Connecting Gallery and the Test Drift.

In the previous chapters, different scenarios were proposed in order to offer a plausible explanation to the experimental data. The addressed scenarios involved (a) diffusion of oxygen without advection, (b) diffusion of oxygen counteracted by advection towards gallery and (c) diffusion of oxygen taking into account a kinetic reaction with pyrite. It is clear that none of these scenarios is adequate to explain the measured sulphate concentrations in the EDZ of the HADES galleries. The comparison of the modelling and experimental results indicates that the contribution of oxygen in-diffusion into the clay to the oxidation is very small in the studied case. In contrast, the oxidation along the open fractures (quasi-instantaneous) by gaseous O_2 is probably the most important process affecting the total sulphate concentrations around the galleries.

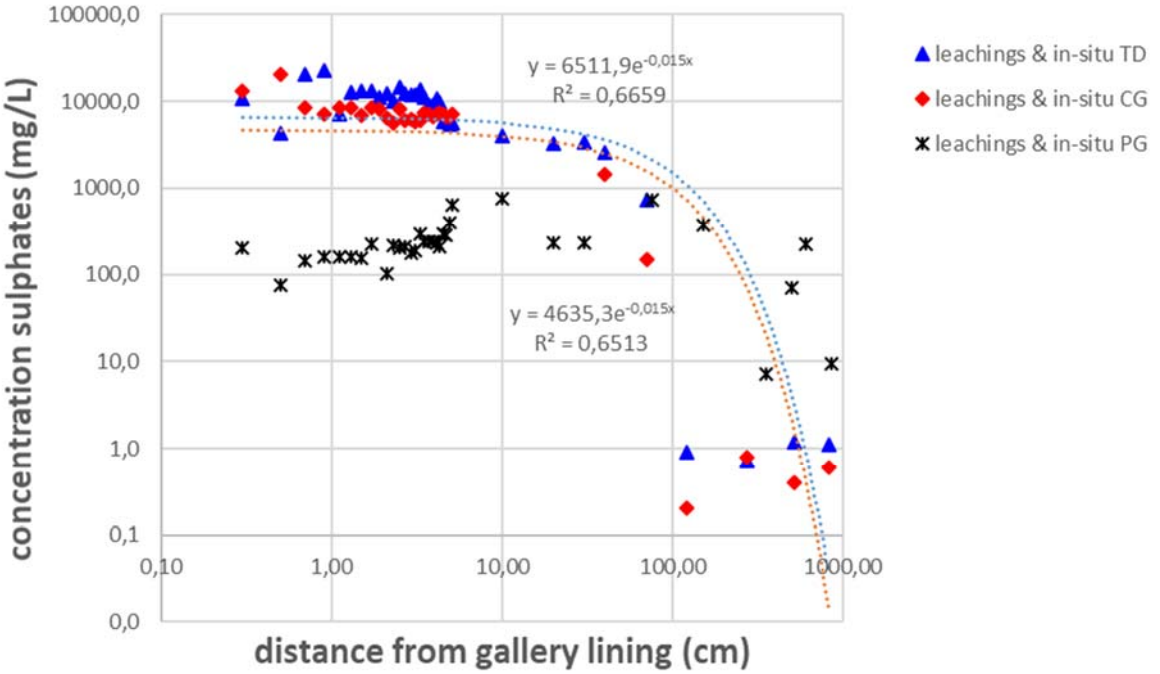

Figure 41. Combined batch (r < 40 cm) and *in- situ* (r ≥ 40 cm) pore water data to construct sulphate concentration profiles around the Test drift, the Connecting Gallery and the PRACLAY Gallery as a function of distance from the gallery.

7.3.4 Geochemical modelling

To demonstrate if pyrite oxidation is the probable process controlling the observed pore water data, an equilibrium reaction modelling was performed to explain the correlation found among the major ion concentrations. The computer code used is 'react', one of the programs from the software package The Geochemist's Workbench® (Bethke and Yeakel, 2009). The thermodynamic database is the compilation from Blanc *et al.*, (2012).

The model system consists of one kilogram of water in equilibrium with several reactive minerals known in Boom Clay. The pore water composition of the system is constrained by the solubility of the composite minerals and cation exchange reactions. Details about the model development can be found in the report of De Craen *et al.* (2004b).

Concerning the minerals in Boom Clay, two model compositions were tested (Table 5). Model I considers that the Boom Clay pore water composition is controlled by the solubility of seven minerals calcite, dolomite, chlorite, kaolinite, quartz, pyrite, and siderite. Constrained by the phase law, each mineral regulates the concentration of one major element, i.e., calcite for the concentration of dissolved inorganic carbon, dolomite for calcium, chlorite for magnesium, kaolinite for aluminium, quartz for silicon, pyrite for oxygen (redox potential), and siderite for iron. The concentration of sodium, potassium, and sulphate is the one measured in non-disturbed pore water samples as initial condition. The variation of sodium and potassium is controlled by cation exchange. The equilibrium of the initial concentration of sulphate with pyrite will decide the initial, non-oxidised redox potential. The system pH is assigned as charge balance variable. A distinct feature of this model is that the mineral assemblage defines the system partial pressure of CO_2 (g) via the following reaction:

$$5 \text{ calcite} + \text{chlorite} + 5\ CO_2\ (g) \rightarrow \text{kaolinite} + \text{quartz} + 5 \text{ dolomite} + 2\ H_2O$$

At chemical equilibrium, all minerals involved in the above reaction have a unit activity so that the fugacity (approximately equal to the partial pressure) of CO_2 (g) can be calculated if the stability constants of all minerals are known. The model was proposed by Coudrain-Ribstein *et al.* (1993; 1998). These authors found that pCO_2 in a clay rich aquitard depends only on the temperature if a certain mineral assemblages exist. Model II is similar to model I but without dolomite and chlorite. Model II emphasizes the fact that although both dolomite and chlorite are present in Boom Clay, their equilibrium with respect to the currently known solubility data has not been demonstrated. This may be due to the complexity of dolomite and chlorite for which simple stoichiometric solubility mechanism is too simple and a solid-solution model might be necessary to describe their equilibrium in water. Without dolomite and chlorite, two elements are needed to constrain the system and these are magnesium and inorganic carbon. This second model assumes that magnesium is controlled by cation

exchange together with Na, K, and Ca while the inorganic carbon is constrained by the measured value of pCO_2 (g) in non-disturbed water samples. Table 5 and 6 summarize the model assumptions, solubility, and cation exchange data used.

Table 5. Model constrains to calculate Boom Clay pore water composition

Constrain on concentration in PW	Model I (clay assemblage model)	Model II (ion exchange on Mg)
SO_4^{2-}	measured in PW (initial)	measured in PW (initial)
carbonate or pCO_2 (g)	calcite	measured in PW (initial)
Redox (O_2)	pyrite	pyrite
pH	charge balance	charge balance
Na	cation exchange	cation exchange
K	cation exchange	cation exchange
Ca	dolomite	calcite
Mg	chlorite	cation exchange
Si	quartz	quartz
Al	kaolinite	kaolinite
Fe	siderite	siderite

Table 6. Reaction constants (Blanc *et al.*, 2012) and ion exchange data used in the modelling

Minerals*	formula	Reaction constants (16/25 °C)
calcite	$CaCO_3$	1.9806/1.8470
dolomite	$CaMg(CO_3)_2$	3.8801/3.5328
quartz	SiO_2	-3.856/-3.7398
chlorite	$Mg_5Al(AlSi_3)O_{10}(OH)_8$	64.9993/61.6899
kaolinite	$Al_2Si_2O_5(OH)_4$	7.4038/6.4722
	reaction	selectivity coefficient#
cation exchange	$>X{:}Na + K^+ \Leftrightarrow >X{:}K + Na^+$	$\log K_C = 1.3279$ (K_C 21.28)
	$2\ >X{:}Na + Mg^{2+} \Leftrightarrow >X_2{:}Mg + 2\ Na^+$	$\log K_C = 0.6778$ (K_C 4.76)
	$2\ >X{:}Na + Ca^{2+} \Leftrightarrow >X_2{:}Ca + 2\ Na^+$	$\log K_C = 0.8413$ (K_C 6.94)

* reaction constants are formation constants written with Ca^{2+} , HCO_3^- ,Mg^{2+} , SiO_2 (aq), Al^{3+}, H^+ , and H_2O as basis species
# temperature independent

Modelling results and a comparison with observed data are presented in Figure 42. The computed (lines) and observed (markers) concentrations of cations Na, K, Ca, Mg, and Fe are shown as a function of increasing content of sulphate in the pore water.

The computed concentrations were obtained using the equilibrium model defined in Table 6 by adding increased amounts of O_2 into the original non-oxidized Boom Clay system defined in Table 5. Modelling results showed that about 60 mmol of O_2 is needed to produce the observed concentration of sulphate, i.e., a few thousands of mg/L of sulphate.

Figure 42 shows that as a result of pyrite oxidation by O_2, the concentration of modelled cations is expected to increase and modelling results are in general agreement with measured data except for the case of iron. For monovalent cations Na and K, both models used cation exchange as the controlling mechanism and it seems the model explains the measured data well. The increased concentration of monovalent cations is the result of an increased concentration of divalent cations in the pore water so that Na and K are exchanged from clay into liquid. For divalent cations Ca and Mg, model I predicted an increasing concentration in liquid due to the dissolution of calcite and dolomite. The dissolution is induced by acidification caused by pyrite oxidation. Model II also predicted a similar trend but seems to agree better with the observed data as compared to model I. Apparently model I, based on the solubility of dolomite, under-predicted the concentration of Mg while model II explained Mg data better by cation exchange. Model II illustrated that pyrite oxidation results in acidification which in turn triggers the dissolution of calcite. As a result, the increased concentration of calcium in solution triggered cation exchange, so the increased amount of Mg (also Na and K) is released from clay into solution. As for another divalent cation Fe, both models seem to predict the initial total Fe concentration correctly but failed to explain the variation when sulphate concentration is increased. Model assumption here is that oxidation will enhance the dissolution of siderite and the dissolved concentration of Fe should increase. This is however only true if Fe in the liquid remains as Fe(II) without being oxidised. If Fe(II) is being oxidized to Fe(III) which precipitates as iron oxides or $Fe(OH)_3$ phases, as Fe(III) has lower solubility than Fe(II) so that the total Fe in the pore water might drop as shown by the *in-situ* measured data. The mineralogical investigation was undertaken, among others, to prove or disprove the formation of the secondary Fe^{3+} bearing phases.

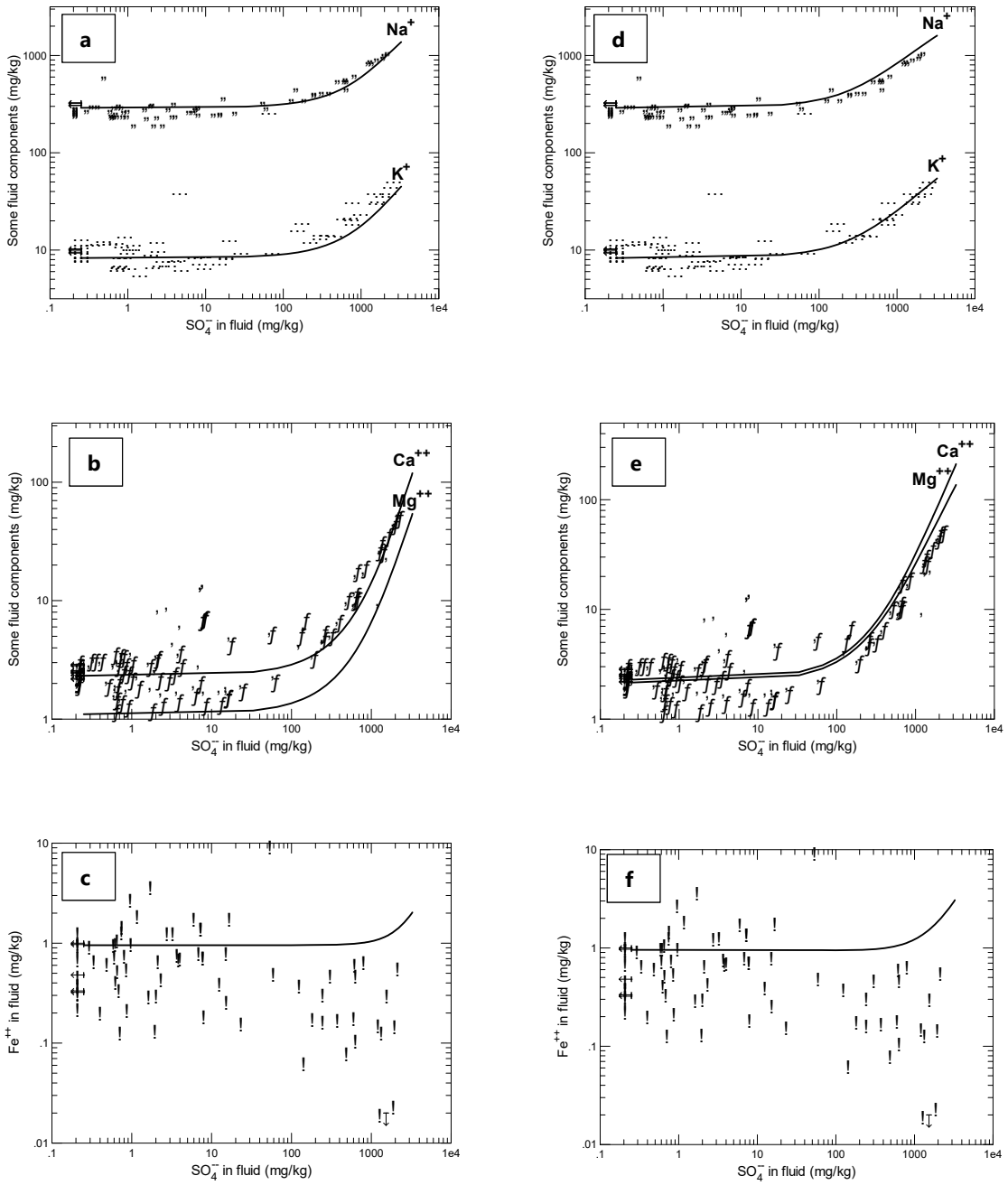

Figure 42. Evolution of the Na (point down triangles), K (diamonds), Ca (triangles), Mg (circles) and Fe (squares) as a function of increasing sulphate concentrations in the in situ pore waters (all piezometers) using the model I (a, b and c) and model II (d, e and f). Solid line – model prediction, symbols – experimental data.

8 Conclusions

Pore water composition data and mineralogical data obtained from samples taken from the Test Drift, the Connecting Gallery and the PRACLAY Gallery were used in order to study the oxidation phenomena in the Boom Clay around the galleries of the HADES URF. The experimental data are complemented by modelling assessment to test various oxidations paths and their relevance in the studied case.

In general, the new data confirm the previously established conceptual model of De Craen *et al.* (2008, 2011) in that oxidation locally occurs immediately in the course of the gallery excavation due to the creation of the fractures. The extent of these fractures dictates the extent of the oxidation in the host rock, which is limited to a maximum of 1.2 m ahead of the galleries of the HADES URF. In other words, the extent of the fractured zone is equal to the extent of the oxidized zone of the Boom Clay.

Due to the plastic character of the Boom Clay, sealing of the open fractures occurs relatively fast (Bernier *et al.*, 2005, 2007). The oxidation products are then trapped within the first meter around the gallery. From this moment, further oxidation occurs only through oxygen in-diffusion into the clay from the open space of the gallery. However, scoping calculations suggest that the contribution of in-diffusion to oxygen ingress into the clay is negligible compared to the introduction of oxygen during the excavation phase. A combined diffusion-advection regime is present around the galleries and the oxidation products will be re-distributed. The redistribution of the oxidation products has been proven by plotting the radial sulphate concentration profiles at different times after excavation. The decrease of the sulphate concentrations has been observed in the deep filters of the piezometers, whereas increase was recorded in the filters nearest to the galleries (at a distance of 0.4 m) in the time span between 2005 and 2011, indicating that oxidation products are transported towards the gallery wall by drainage of pore water. Concentrations as high as 2560 mg/L sulphate were observed in the water sampled from the piezometer filters closest to the gallery wall.

The sulphate concentrations tend to increase towards the gallery in every studied case (Test Drift, Connecting Gallery and PRACLAY Gallery). The trend of increasing sulphate concentrations towards the gallery, as observed in the piezometer waters, is further continued in the pore waters obtained from the leaching of the clay cores. Very close to the gallery lining, the effect of oxidation is the most pronounced and sulphate concentrations up to 20 000 mg/l are obtained when the concentrations in the leachates are converted to in situ S/L ratios. This value should be regarded as a conservative, upper bound of the possible sulphate concentration as no mineral dissolution or precipitation is considered in the interpretation of the leaching data. It is most likely that such a concentration would exceed the saturation index of sulphate-containing minerals in the system. The high concentrations of sulphate are associated with high concentrations of most cations. Such phenomenon can be qualitatively explained by combination of mineral dissolution/precipitation and ion-exchange reactions. Quantitatively, the geochemical model can fairly well predict the pore water compositions as measured in the piezometers.

The results suggest that the concentrations of sulphates remain relatively high in the near field even 25 years after the excavation. This points to the fact that the sulphates are not easily degradable (reducible) in the course of the open drift phase. Low concentrations of thiosulphates are generally observed. Measured concentrations of S_2O_3 are < 1 mg/L in most cases and tend to decrease in time. Even in water sampled from piezometers installed in air-drilled boreholes, concentrations are < 10 mg/L ([5]).

In contrast, the fraction of the organic matter which is dissolved in the pore water upon oxidation is relatively mobile and thus can be easily transported away from the near field. Consequently, the oxidation of the organic matter will not necessarily affect the pore water chemistry in the near field on the long-term. Although pyrite and organic matter occur together under undisturbed conditions, a lack of correlation between sulphates and DOC suggests that the oxidation of pyrite and organic matter follow different pathways. DOC also appears as a lesser indicator of oxidation than sulphates.

The Boom Clay layered character is clearly reflected in the shape of sulphate and DOC concentration profiles in the piezometers crosscutting several Boom Clay layers. The initial pyrite and organic matter contents will thus necessarily affect the overall concentrations of sulphate and DOC measured in the pore waters collected at various locations.

The integrated mineralogical investigation (XRD, FTIR, XANES, Mössbauer spectroscopy and CEC) point to the fact that the effect of the oxidation on the mineralogy is limited compared to the effect on pore water chemistry. In all cases the extent of the mineralogically altered zone does not exceed 4.5 cm from the gallery. Further away, the mineralogical composition is

[5] In one instance, a concentration of 349 mg/L was observed. Such a high concentration can only be observed if sampling occurs soon after the installation of the piezometer. This is due to the metastable character of thiosulphate in Boom Clay porewater, which has already been reported by De Craen et al. (2008)

typical of the undisturbed Boom Clay. Locally, i.e. along fractures that have been opened during excavation, stronger mineral alterations are to be expected but these were not specifically targeted when sampling the clay close to the gallery with the cutting edge tubes used for the present study.

The most frequently observed oxidation product is gypsum and sporadically jarosite. Interestingly, the jarosite is associated with the absence of carbonates, which may indicate the loss of the pH buffering capacity of the clay. Indeed, the jarosite is indicative of the low pH environment (<4). Jarosite has been observed very close to the gallery lining of the Connecting Gallery, but not in the Test Drift. Probably, the presence/absence of jarosite very close to the gallery lining may relate to the absence/presence of an alkaline plume. In the Connecting Gallery, there was probably no effect yet of an alkaline plume (3 years after the excavation and associated emplacement of the concrete lining). In contrast, in the Test Drift where the concrete lining was already present for 20 years, an alkaline plume most likely increased the pH in the clay close to the gallery lining so that the precipitation of jarosite was no longer possible. Note that combined oxidation-alkaline plume effects are out of scope of this research programme (RP.W&D.0065.E(1.0) - LTBC02-PER-05).

XANES and Mössbauer spectroscopy were employed in order to search for amorphous and poorly crystallized Fe oxyhydroxides, which are not easily detectable by XRD or FTIR. Formation of ferric precipitates was suggested by equilibrium reaction modelling of oxidized pore waters. None of these mineral phases were found in the studied sample sets. This is probably related to the absolute dominance of the Fe^{3+} present as structural iron in the octahedral sheets of the phyllosilicates, mainly illite (up to 90% of the total Fe in the bulk Boom Clay).

The CEC measurements indicate that irrespective of the sulphate content, the exchange capacity of the bulk Boom Clay is not significantly compromised in the near-field. Although the CEC of the undisturbed Boom Clay is variable in the Test Drift, the Connecting Gallery and the PRACLAY Gallery (16, 23 and 19 meq/100g respectively), the CEC of the clay in the altered zone remains in the range of values typical of the undisturbed Boom Clay.

9 Open questions and recommendations

A natural background concentration of sulphates in the Boom Clay pore water is not well constrained. Sulphate concentrations are definitely very low in undisturbed Boom Clay at the Mol site, and are often below the detection limit of our analytical technique. Until now, a limit value of 10 mg/L was arbitrary indicated to distinguish between non-disturbed and oxidized pore waters. The sulphate values well below 10 mg/L are frequently measured in some of the piezometers (e.g. CG-30E and CG-35E). It is questionable if such low sulphate values are representative of the undisturbed conditions or effect of dilution (flush-out) and/or bacterial activity.

An indirect method to deduce the upper limit of the sulphate concentrations in undisturbed Boom Clay pore water is through the use of Cl^-/SO_4^{2-} ratios in marine waters. However, in the course of the geological history both sulphates and chlorides diffused-out from the Boom Clay at different speed. The multicomponent diffusive model might be applied to simulate long-term behaviour of these natural tracers and to explain present day concentrations of sulphates in undisturbed Boom Clay pore water. In this manner, Cl^-/SO_4^{2-} ratios can be calibrated taking into account variable diffusion coefficients of the two components.

Until present, little attention has been paid to coupled oxidation/alkaline plume processes. These two processes overlap in time and space, therefore their effects should be considered in parallel. The alkaline plume will interact with the oxidation products in the near-field. In the opposite direction, the oxidation products may affect the cement-based EBS materials (e.g. sulphate attack of concrete). A simple mass balance approach might show whether the amount of oxidation products available would be sufficient to affect the EBS in a significant way. The concrete-clay interface processes has been recently tackled in the frame of the CEBAMA EC project (Phung et al., 2019).

After gallery backfilling and closure, in-diffusion of oxygen will gradually stop so reducing conditions will be re-established everywhere, but little is known about reversibility/irreversibility of the redox reactions in the realm of the Boom Clay. It is not known at this point whether part of the oxidation products (e.g. Fe^{3+} as a part of clay mineral structure, carboxylic groups of organic matter, sulphates etc.) could be reduced again. The simulations of the cycled oxidation/reduction kinetics with the redox sensitive Boom Clay constituents (various redox couples) might be an interesting topic for further phenomenological study.

Bacteria may play a role in this. Oxidation of Boom Clay results in locally high concentrations of sulphate in the pore water. Their presence, if coupled with suitable sources of energy and carbon, may trigger sulphate-reducing bacteria activity, provided that other environmental conditions (e.g. pH, sufficient space,…) are also favourable.

Acknowledgements:

The authors of this study are thankful to Xavier Sillen (NIRAS-ONDRAF) for a thorough review of this report. This work was performed in close cooperation with, and with the financial support of ONDRAF/NIRAS, the Belgian Agency for Radioactive Waste and Fissile Materials, as part of the programme on geological disposal that is carried out by ONDRAF/NIRAS. Prof. Thomas Bakas from University of Ioannina is acknowledged for the Mossbauer Spectroscopy measurements. We are also thankful to Jana Madejova from the Institute of Inorganic Chemistry of the Slovak Academy of Sciences for FTIR measurements.

References

Ammann, L., Bergaya, F., Lagaly, G. (2005) Determination of the cation exchange capacity of clays with copper complexes revisited. Clay Minerals 40, 441-453.

Baeyens, B., Maes, A., Cremers, A., and Henrion, P. N. (1985) Aging effects in Boom Clay, Radioactive Waste Management and the Nuclear Fuel Cycle, 6: 409-423.

Bastiaens, W., Bernier, F., Buyens, M., Li, X.L., Linotte, J.M. and Verstricht, J., 2003. The Connecting Gallery – EURIDICE internal report 03-293, 114pp.

Bernier F., Tsang C., Davies C.- Geohydromechanical Processes in the Excavation Damaged Zone in Crystalline Rock, Rock Salt, and Indurated and Plastic Clays.- In: International Journal of Rock Mechanics and Mining Science - Editor in Chief is John A. Hudson - Elsevier Science B.V Amsterdam, 42:01 (2005), p. 109-125.- ISSN 1365-1609.

Bernier, F., Li, X.L., Bastiaens, W., Ortiz, L., Van Geet, M., Wouters, L., Frieg, B., Blümling, P., Desrues, J., Viaggiani, G., Coll, C., Chanchole, S., De Greef, V., Hamza, R., Malinsky, L., Vervoort, A., Vanbrabant, Y., Debecker, B., Verstraelen, J., Govaerts, A., Wevers, M., Labiouse, V., Escoffier, S., Mathier, J.F., Gastaldo, L., Bühler, Ch. (2007). Fractures and self-healing within the excavation disturbed zone in clays (SELFRAC). Final report to EC (contract N°: FIKW-CT2001-00182), EUR 22585.

Bethke, C. M. and Yeakel, S., 2009. Reference Manual, The Geochemist's Workbench, Release 8.0, -Hydrogeology Program University of Illinois.

Bishop J.L., Murad E. (2005) The visible and infrared spectral properties of jarosite and alunite. American Mineralogist, 90, 1100-1107.

Blanc, Ph., Lassin, A., Piantone, P., Azaroual, M., Jacquemet, N., Fabbri, A., and Gaucher, E. C. (2012) Thermoddem: A geochemical database focused on low temperature water/rock interactions and waste materials, Applied Geochemistry, 27: 2107-2116.

Blanchart, P., 2011. Influences de l'oxydation et de la biodégradation anaerobie sur la matière organique de l'argile oligocène de Boom (Mol, Belgique): Conséquences sur la formation d'espèces organiques hydrosolubles, Institut National Polytechnique de Lorraine, Université de Nancy.

Blanchart, P., Faure, P., De Craen, M., Bruggeman, C. and Michels, R. (2012) Experimental investigation on the role of kerogen and clay minerals in the formation of bitumen during the oxidation of Boom Clay. Fuel 97, 344-351.

Boisson, J.-Y. (2005) Clay Club Catalogue of Characteristics of Argillaceous Rocks, OECD/NEA report No. 4436.

Bradbury, M. H. and Baeyens, B. (1998) A physicochemical characterisation and geochemical modelling approach for determining pore water chemistries in argillaceous rocks, Geochimica et Cosmochimica Acta, 62/5, 783-795.

Bruggeman C. and De Craen M. (2012) Boom Clay natural organic matter – status report 2011. External Report of the Belgian Nuclear Research Centre, Mol, Belgium: SCK•CEN-ER-206.

Chen, G. (2018). *In-situ* hydraulic conductivity measurement for the Boom Clay around CG and PG. EURIDICE report EUR_18_14.

Coudrain-Ribstein, A. and Gouze, P. (1993) Quantitative study of geochemical processes in the Dogger aquifer, Paris Basin, France, Applied Geochemistry, 8, 495-506.

Coudrain-Ribstein, A., Gouze, P., and de Marsily, G. (1998) Temperature-carbon dioxide partial pressure trends in confined aquifers, Chemical Geology, 145, 73-89.

De Cannière, P., Maes, A., Williams, S., Bruggeman, C., Beauwens, T., Maes, N., Cowper, M. (2010) Behaviour of Selenium in Boom Clay. State-of-the-art report. Belgium Nuclear Research Centre, Mol, Belgium: SCK-CEN-ER-120, SCK-CEN

De Craen M. (2005) Geochemical characterisation of specific Boom Clay intervals. SCK•CEN technical report of DS 2.92 for the year 2004 to NIRAS/ONDRAF, Contract nr. CO 90 01 1467.01 – CCHO 2004-2470/00/00. SCK•CEN-R-4080, Mol, Belgium, 65 p.

De Craen M., Honty M., Van Geet M., Weetjens E., Sillen X., Wang L., Jacques, D., Martens, E. (2011) Overview of the oxidation around galleries in Boom Clay (Mol, Belgium) - Final activity report for SCK•CEN. Deliverable 4.3.24.- *Brussel, Belgium: EC, 2008.- 89 p.- (EC;* Deliverable 4.3.24; FI6W-CT-2003-02389).

De Craen M., Van Geet M., Honty M., Weetjens E., Sillen X. (2008) Extent of oxidation in Boom Clay as a result of excavation and ventilation of the HADES URF: Experiment and modelling assessments: Clays in Natural and Engineered Barriers for Radioactive Waste Confinement, Lille, France, 17-20 September 2007.- In: Physics and Chemistry of the Earth, 33(2008), p. S350-S362.- ISSN 1474-7065.

De Craen M., Wang L., Van Geet, M. & Moors H. (2004b) The geochemistry of Boom Clay pore water at the Mol site, status 2004. SCK•CEN Scientific Report. BLG 990, 180 p.

De Craen, M., Van Geet, M., Wang, L., Put, M. (2004a). High sulphate concentrations in squeezed Boom Clay pore water: evidence of oxidation of clay cores. Physics and Chemistry of the Earth 29, 91–103.

De Craen, M., Moors, H. and Verstricht, J. (2018). Description of the HADES piezometers used for the study of in situ Boom Clay pore water chemistry. External report of the SCK•CEN, ER-0329, 68 pp.

Evangelou, V.P., 1995. Pyrite Oxidation and its Control. CRC Press, Boca Raton, FL.

GARNER, A., 1985, Thiosulfate corrosion in paper-machine white water, Corrosion 41(10), pp. 587-591.

George, G.N. and Pickering, I.J. (2000) EXAFSPAK: A suite of computer programs for analysis of X-ray absorption spectra. Stanford Synchrotron Radiation Laboratory.

Griffault, L, Merceron, T., Mossmann, J. R., Neerdael, B., De Cannière, P., Beaucaire, C., Daumas, S., Bianchi, A., and Christen, R. (1996) Acquisition et régulation de la chimie des eaux en milieu argileux pour le project de stockage de déchets radioactifs en formation géologique, Project <Archimède argile>, Rapport final, EUR 17454 FR.

Hem, J. D. (1985) Study and interpretation of the chemical characteristics of natural water, Third Edition, U.S Geological Survey Water-supply Paper 2254.Jerz, J. K. and J. D. Rimstidt (2004). "Pyrite oxidation in moist air." Geochimica et Cosmochimica Acta 68(4): 701-714.

Henrion, P.N., Monsecour, M., Fonteyne, A., Put M. and De Regge, P. (1985) Migration of radionuclides in Boom Clay. Radioactive Waste Management and the Nuclear Fuel Cycle, 6 (3-4) 313-359.

Honty, M. (2010) CEC of the Boom Clay - a review. Mol, Belgium: SCK•CEN, 2010.- 26 p.- (External Report of the Belgian Nuclear Research Centre; ER-134; CCHO 2009-0940000, RP Geosynthesis).- ISSN 1782-2335.

Jerz, J. K. and J. D. Rimstidt (2004). "Pyrite oxidation in moist air." Geochimica et Cosmochimica Acta 68(4): 701-714.LAYCOCK, N.J., 1999, Effects of temperature and thiosulfate on chloride pitting of austenitic stainless steels, Corrosion 55(6), pp. 590-595.

Lothenbach, B., B. t. Bary, *et al.* (2010) "Sulfate ingress in Portland cement." Cement and Concrete Research 40(8): 1211-1225.

Majzlan J., Navrotsky, A. and Schwertmann, U. (2004) Thermodynamics of iron oxides: Part III. Enthalpies of formation and stability of ferrihydrite (~$Fe(OH)_{(3)}$), schwertmannite (~$FeO(OH)_{(3/4)}(SO_4)_{(1/8)}$), and ε-$Fe_2O_3$. Geochimica et Cosmochimica Acta, 68, 1049-1059.

Majzlan, J. Grevel, K.D. and Navrotsky, A. (2003b) Thermodynamics of iron oxides. II. Enthalpies of formation and relative stability of goethite (α-FeOOH), lepidocrocite (γ-FeOOH), and maghemite (γ-Fe_2O_3), *Am. Miner.* **88**, pp. 855–859.

Majzlan, J. Lang, R. Stevens, A. Navrotsky, B.F. Woodfield and J. Boerio-Goates (2003a) Thermodynamics of iron oxides. I. Standard entropy and heat capacity of goethite (α-FeOOH), lepidocrocite (γ-FeOOH), and maghemite (γ-Fe_2O_3), *Am. Miner.* **88**, pp. 846–854.

Meier, L. and Kahr, G. (1999) Determination of cation exchange capacity (CEC) of clay minerals using the complexes of copper (II) ion with triethylenetetramine and tetraethylenepentamine. Clays and Clay Minerals 27, 417-422.

NEWMAN, R.C., 1985, Pitting of stainless alloys in sulfate solutions containing thiosulfate ions, Corrosion 41(8), pp. 450-453.

O' Day P.A., Rivera, Jr., N. Root R. and Caroll S.A. (2004) X-ray absorption spectroscopic study of Fe reference compounds for the analysis of natural sediments. Am. Mineral. 89, 572-585.

O' Day, P.A., Rehr, J.J., Zabinsky, S.I., and Brown, G.E., Jr. (1994) Extended X-ray absorption fine structure (EXAFS) analysis of disorder and multiple scattering in complex crystalline solids. Journal of the American Chemical Society, 116, 2938-2949.

ONDRAF/NIRAS (2004). Multi-criteria Analysis on the Selection of a Reference EBS Design for Vitrified High Level Waste. ONDRAF/NIRAS, Brussels 2004-03.

Parkhurst D.L., and Appelo C.A.J., 1999. User's guide to PHREEQC (version 2) - A Computer Program for Speciation, Batch-Reaction, One-Dimensional Transport and inverse Geochemical Calculations. Denver, Colorado, USA, Water-Resources Investigations Report 99-4259.

Phung Q.T, Gaboreau S., Maes N., Claret F (2019) Preliminary experimental results on the changes in microstructure, mineralogy, and transport properties of Boom Clay-concrete interface. In Proceedings of the 2nd workshop of the HORIZON 2020 CEBAMA project (Altmaier M., Montoya V., Duro L., Valls A., Eds.). KIT-SR 7752

Planel, D., J. Sercombe, *et al.* (2006). "Long-term performance of cement paste during combined calcium leaching - sulfate attack: kinetics and size effect." Cement and Concrete Research 36(1): 137-143.

Ravel, B. and Newville M. (2005) ATHENA, ARTEMIS, HEPHAESTUS: data analysis for X-ray absorption spectroscopy using IFEFFIT. J. Synchrotron Radiat. 12, 537-541.

Rounds, S.A., Wilde, F.D. (2001) Alkalinity and Acid Neutrailizing Capacity, second ed. US Geological survey, TWRI Book 9.

Runchal, A.K. PORFLOW, a software tool for multiphase fluid flow, heat and mass transport in fractured porous media. User's manual, Version 3.07 (ACRi, Bel Air, California, USA, 1997).

Serna C.J., Cortina C.P., Garcia Ramos J.V. (1986) Infrared and Raman study of alunite-jarosite compounds. Spectrochimica Acta, 42A, 729.734.

Van Geet, M., 2003. Oxidation phenomena in Boom Clay: case study from the Northern Starting Chamber in the second Shaft. In: Bastiaens *et al.* The Connecting Gallery. EURIDICE internal report 03-293, 114p.

Van Geet, M., 2004. Characterisation of Boom Clay organic matter: mobile and immobile fraction. Interim report for the period 2001-2003. SCK•CEN, Mol, Belgium.

Vandenberghe, N., De Craen, M. & Wouters, L. (2014) The Boom Clay geology From sedimentation to present-day occurrence: A review. Memoirs of the Geological Survey of Belgium, 60, 76.

Wickham,S.M. 2005. The ONDRAF-NIRAS Supercontainer Concept. Galson Sciences, UK (2005).

Williamson, M.A., and Rimstidt, J.D., 1994. The kinetics and electrochemical rate-determining step of aqueous pyrite oxidation. Geochimica et Cosmochimica Acta 58 (24), 5443-5454.

Zeelmaekers, E., Honty, M., Derkowski, A., Środoń, J., De Craen, M., Vandenberghe, N., Adriaens, R., Ufer, K. and Wouters, L. (2015) Qualitative and quantitative mineralogical composition of the Rupelian Boom Clay in Belgium. Clay Minerals 50, 249-272.

Annex 1. Position of the piezometer filters in the Lambert coordinates. SS – stainless steel, H – horizontal, V- vertical, ID – inclined downwards. * - coordinates not measured, but calculated.

piezometer	*Filter GSIS ID*	*Filter distance from the gallery (m)*	*orientation*	*Lambert coordinates*					
				x	y	z	x'	y'	z'
TD-41E (N2TD)	TD-41E-1	8.2	H	200137,0864	211805,1889	-196,5262	200137,2849	211805,2131	-196,5262
	TD-41E-2	5.2	H	200134,1085	211804,8254	-196,5262	200134,307	211804,8497	-196,5262
	TD-41E-3	2.7	H	200131,6269	211804,5226	-196,5262	200131,8254	211804,5469	-196,5262
	TD-41E-4	1.2	H	200130,1379	211804,3409	-196,5262	200130,3365	211804,3651	-196,5262
	TD-41E-5	0.7	H	200129,64	211804.3	-196.5262	200129.8	211804.3	-196.5262
	TD-41E-6	0.4	H	200129.34	211804.2	-196.5262	200129.5	211804.3	-196.5262
CG-64E (N2CG)	CG-64E-1	8.2	H	200145,5337	211741,5374	-196,51	200145,6331	211741,5486	-196,51
	CG-64E-2	5.2	H	200142,5528	211741,2	-196,51	200142,6521	211741,2113	-196,51
	CG-64E-3	2.7	H	200140,0686	211740,9189	-196,51	200140,168	211740,9302	-195,51
	CG-64E-4	1.2	H	200138,5782	211740,7502	-196,51	200138,6775	211740,7615	-195,51
	CG-64E-5	0.7	H	200138.08	211740.7	-196.51	200138.2	211740.7	-196.51
	CG-64E-6	0.4	H	200137.78	211740.7	-196.51	200137.9	211740.7	-196.51
CG13U (R13U)	CG13U-01	19.6	V	200139,2579	211689,2173	-174,5613	200139,255	211689,2166	-174,5114
	CG13U-02	17.6	V	200139,3845	211689,2252	-176,5562	200139,3808	211689,2241	-176,5064
	CG13U-03	15.6	V	200139,5216	211689,2378	-178,5511	200139,5176	211689,2369	-178,5013
	CG13U-04	13.6	V	200139,6549	211689,2362	-180,5464	200139,6518	211689,236	-180,4965
	CG13U-05	11.6	V	200139,7667	211689,2441	-182,543	200139,7629	211689,2442	-182,4932
	CG13U-06	9.6	V	200139,9098	211689,2485	-184,5377	200139,9055	211689,2488	-184,4879
	CG13U-07	7.6	V	200140,0775	211689,2903	-186,5296	200140,0745	211689,2898	-186,4797
	CG13U-08	5.6	V	200140,2342	211689,2783	-188,5231	200140,2303	211689,2779	-188,4732
	CG13U-09	3.6	V	200140,3768	211689,2773	-190,5176	200140,3729	211689,2761	-190,4678
	CG13U-10	2.6	V	200140,4546	211689,2947	-191,5144	200140,4506	211689,2944	-191,4646
	CG13U-11	1.6	V	200140,5236	211689,3148	-192,5116	200140,5209	211689,313	-192,4617
	CG13U-12	0.6	V	200140, 59	211689,34	-193.51	200140.58	211689,34	-193,46
	CG13U-13	0.3	V	200140.61	211689.34	-193.81	200140.61	211689.34	-193.76
CG13D (R13D)	R13D-01	39.6	V	200140,1722	211689,6959	-238,8595	200140,1714	211689,6964	-238,90953
	R13D-02	35.6	V	200140,2397	211689,6507	-234,8604	200140,2391	211689,6512	-234,91046
	R13D-03	30.6	V	200140,2981	211689,6073	-229,861	200140,2975	211689,6076	-229,911
	R13D-04	25.6	V	200140,3517	211689,5694	-224,8614	200140,351	211689,5699	-224,91146
	R13D-05	18.6	V	200140,4468	211689,5172	-217,8623	200140,446	211689,5173	-217,91235
	R13D-06	14.6	V	200140,5083	211689,4855	-213,8630	200140,5075	211689,4863	-213,91300

	R13D-07	11.6	V	200140,5494	211689,4598	-210,86345	200140,5489	211689,4605	-210,91344
	R13D-08	8.6	V	200140,5658	211689,4001	-207,86411	200140,5655	211689,4009	-207,91411
	R13D-09	5.6	V	200140,6105	211689,3808	-204,86460	200140,6097	211689,3811	-204,91460
	R13D-10	3.6	V	200140,6309	211689,3662	-202,86476	200140,6305	211689,3665	-202,91476
	R13D-11	2.6	V	200140,6386	211689,3595	-201,86482	200140,6382	211689,3597	-201,91481
	R13D-12	1.6	V	200140,646	211689,3581	-200,86486	200140,6461	211689,3573	-200,91485
	R13D-13	0.6	V	200140,6361	211689,3899	-199,86547	200140,6358	211689,3897	-199,91544
CG-30E (P30E)	P30E-1	1.89	ID	200163.581	211713.4541	-199.4675	200164.0564	211713.5958	-199.5299
	P30E-4	0.88	ID	200157.0721	211711.5034	-198.6023	200157.547	211711.6453	-198.668
	P30E-6	0.55	ID	200152.6598	211710.1707	-197.9878	200153.1338	211710.3145	-198.056
CG-35E (P35E)	P35E-2	1.14	H	200181.5445	211716.9759	-196.2268	200182.0402	211717.0408	-196.2208
	P35E-6	1.00	H	200166.9689	211715.0711	-196.3659	200167.4646	211715.1365	-196.3641
	P35E-11	0.88	H	200152.3916	211713.1778	-196.3285	200152.8874	211713.2427	-196.3327
PG-70S	PG70S-1	9.94	H	200178.12	211703.2	-196.5133	200178.1	211703.1	-196.515
	PG70S-2	6.96	H	200177.8	211706.2	-196.5217	200177.8	211706.1	-196.5214
	PG70S-3	4.92	H	200177.59	211708.2	-196.5259	200177.6	211708.1	-196.5257
	PG70S-4	2.93	H	200177.38	211710.1	-196.5302	200177.4	211710.1	-196.53
	PG70S-5	1.94	H	200177.27	211711.1	-196.5323	200177.3	211711	-196.5321
	PG70S-6	0.95	H	200177.17	211712.1	-196.5345	200177.2	211712	-196.5342
	PG-70S-7	0.45	H	200177.11	211712.6	-196.5355	200177.1	211712.5	-196.5353
PG-70D	PG70D-1	10	V	200176.91	211714.2	-208.8338	200176.9	211714.2	-208.3339
	PG70D-2	8.49	V	200176.91	211714.2	-208.3339	200176.9	211714.1	-205.3342
	PG70D-3	3.50	V	200176.93	211714.1	-205.3342	200177	211714	-198.335
	PG70D-4	5.00	V	200176.96	211714	-198.335	200176.9	211714.2	-208.336
	PG70D-5	6.00	V	200176.91	211714.2	-208.336	200177	211714.1	-200.3348
	PG70D-6	1.50	V	200176.95	211714.1	-200.3348	200177	211714	-199.3349
	PG70D-7	0.75	V	200176.96	211714	-199.3349	200177	211714	-198.8349

Annex 2. *In-situ* pore water chemistry of the Boom Clay from the piezometer TD-41E (previously named N2TD). All concentration values in mg/L.

Name	filter distance from the gallery extrados (m)	time since borehole drilling (months)	Br^- [mg/l]	Cl^- [mg/l]	F- [mg/l]	I- [mg/l]	$S_2O_3^-$ [mg/l]	SO_4^{2-} [mg/l]	Al^{3+} [mg/l]	B [mg/l]	Ca^{2+} [mg/l]	Fe^{2+} [mg/l]	K^+ [mg/l]	Mg^{2+} [mg/l]	Na^+ [mg/l]	Si [mg/l]	Sr^{2+} [mg/l]	Alkal [meq/l]	DIC [mg C/l]	DOC [mg C/l]
TD-41E-1/20050127/1	8,2	1	0,44	52	3,3	0,67	<1	4,8	0,085	6,8	7,1	0,73	7,5	2,98	286	6,4	0,175	11,29	135,7	161,2
TD-41E-2/20050216/1	5,2	2	0,46	26,2	3,5	0,73	<1	2,54	0,0107	7,5	9,6	0,69	8,3	2,28	233	4	0,074	12,64	153,3	128,4
TD-41E-2/20051107/1	5,2	11	0,56	24,2		0,74	<1	1,16	0,02	8	4,2	1,03	13,6	3,1	330	6,6	0,137	13,9	150	153
TD-41E-3/20050318/1	2,7	4	0,51	28,5	3,9	0,71	<1	3,9	0,081	8,1	5,1	1,32	9,2	2,51	340	5,1	0,087	13,45	153,2	180,7
TD-41E-3/20051212/1	2,7	12	0,65	23,7		0,75	<1	0,7	0,017	8,2	3,3	1,01	14,1	3,7	330	7,2	0,082	13,66	149,2	158
TD-41E-4/20050407/1	1,2	5	0,64	156	2,9	0,65	<1	8,7	0,03	6	14,9	1,45	10,3	7,2	340	10,6	0,63	10,77	182,5	470,8
TD-41E-4/20051107/1	1,2	11	0,76	28,3		0,93	<1	0,9	0,0123	8,5	4,1	1,53	16,5	3,5	370	7,2	0,111	15,37	174,2	100,7
TD-41E-5/20050523/1	0,7	6	0,72	31,2	2,9	0,61	<1	760	0,063	7,7	11	0,11	22	10,8	670	13,8	0,36	13,7	209,9	532,5
TD-41E-5/20051220/1	0,7	12	1,05	26,8		0,68	<1	720	0,035	7,6	10,7	0,187	26	10,7	670	10,2		14,29	181,4	258,3
TD-41E-6/20050609/1	0,4	7	0,51	24,6	2,4	0,77	<1	760	0,0254	6,9	19	0,49	37	18,5	550	20,1	0,61	10,17	103,4	137,6
TD-41E-1/20060124/1	8,2	13	0,5	27,3	2,26	0,64	<1	1,14	0,078	8,3	2,8	2,85	12,2	2,29	290	6,7	0,068	31,76	139,7	86,8
TD-41E-2/20061002/1	5,2	22	0,52	33	3,1	0,75	<1	0,96	0,034	8,2	3,6	0,77	11,1	3	360	5,8	0,099	15,73	174,5	88,16
TD-41E-6/20060119/1	0,4	13	0,76	22,5		0,36	4,2	2560	0,0246	7,2	62	0,58	61	53	1280	9,4	1,8	9,93	134,7	88,77
TD-41E-1/20071207/1	8,2	36	0,51	38,7	2,75	0,56	<1	<0.25	0,048	8,3	2,26	0,23	11,6	2,04	296	5,6	0,059	12,59	147,6	60,16
TD-41E-2/20071207/1	5,2	36	0,54	64	2,65	0,56	<1	0,48	9.900E-3	8,6	3,55	0,21	14,8	3,29	362	6,6	0,104	14,39	136,5	164,9
TD-41E-3/20071210/1	2,7	36	0,71	33,5	3,07	0,65	<1	<0.25	0,0116	9,5	3,03	0,4	13,7	2,98	339	6,3	0,081	15,05	169,6	94,25
TD-41E-4/20070622/1	1,2	30	0,73	375	3,22		<1	64		8,7	6,2	9,7	309	5,6	395	6,4	0,195	11,87	88,2	262,9
TD-41E-4/20071210/1	1,2	36	0,66	65	3,41	0,76	<1	4,58	0,0194	10,1	4,1	0,71	46	3,86	393	7	0,097	14,66	140,1	236,5
TD-41E-5/20071127/1	0,7	35	0,47	90	3,44	0,42	5,1	171	0,011	10,6	6,8	0,065	22,5	7,2	550	9,1	0,203	19,58	224,4	30,91
TD-41E-6/20071127/1	0,7	35	0,61	18,3	2,12	0,36	<1	2340	7.600E-3	7,9	52	0,152	53	52	1230	7,2	1,68	12,43	144,2	47,43
TD-41E-1/20111010/1	8,2	82	0,51	26,9	2,95	0,71	<1	1,94	<0.02	7,3	3,47	0,306	10,7	2,94	342	5,2	0,122	14,31	151,4	108,2
TD-41E-2/20111017/1	5,2	82	0,58	29,1	2,82	0,69	<1	<0.25	<0.02	7	2,83	0,322	10	2,48	325	5,6	0,104	13,51	155,1	89,38
TD-41E-3/20111103/1	2,7	82	0,58	23	3,13	0,67	<1	<0.25	<0.02	7,7	2,34	1	9,5	2,17	308	5,6	0,091	13,5	143,7	71,3
TD-41E-4/20111108/1	1,2	82	0,65	27,7	3,12	0,79	<1	2,41	<0.02	8,2	4	0,314	11,7	3,44	379	6	0,138	16,37	172,7	82,87
TD-41E-6/20111103/1	0,4	82	0,52	17,6	1,41	0,356	<1	2250	<0.02	6,6	51	0,024	46	47	1160	3,29	1,69	9,58	119,4	39,52

Annex 3. *In-situ* pore water chemistry of the Boom Clay from the piezometer CG-64E (previously named N2CG). All concentration values in mg/L.

Name	filter distance from the gallery extrados (m)	time since borehole drilling	Br^- [mg/l]	Cl^- [mg/l]	F- [mg/l]	I- [mg/l]	$S_2O_3^-$ [mg/l]	SO_4^{2-} [mg/l]	Al^{3+} [mg/l]	B [mg/l]	Ca^{2+} [mg/l]	Fe^{2+} [mg/l]	K^+ [mg/l]	Mg^{2+} [mg/l]	Na^+ [mg/l]	Si [mg/l]	Sr^{2+} [mg/l]	Alkal [meq/l]	DIC [mg C/l]	DOC [mg C/l]
CG-64E-1/20050127/1	8,2	1	0,44	21,9	3,2	0,67	<0	0,79	0,35	6,9	3,5	0,54	8,3	2,15	290	6,1	0,075	12,32	143	110
CG-64E-2/20050216/1	5,2	2	0,45	22,2	3,5	0,81	<1	3,3	0,056	7,1	10,1	1,3	8,3	2,22	235	3,6	0,061	12,56	147	170
CG-64E-2/20051128/1	5,2	11	0,62	23,9		0,76	<1	0,35	0,034	7,6	3,3	0,95	13,5	3,3	330	6	0,084	13,53	153	134
CG-64E-3/20050218/1	2,7	3	0,51	24,6	3,8	0,7	<1	8,2	0,161	7,2	3,3	0,82	8,7	2,13	320	4,1	0,061	12,42	147	118
CG-64E-3/20051212/1	2,7	12	0,69	22,6		0,71	<1	0,82	0,0131	7,8	3	0,35	12,9	3,6	310	6,6	0,07	13,31	155	190
CG-64E-4/20050322/1	1,2	4	0,52	20,1	3	0,58	<1	1,4	0,034	5,3	2,66	1,94	6,6	1,95	233	10,3	0,044	9,98	181	375
CG-64E-4/20051107/1	1,2	11	0,63	25,7		0,88	<1	<0.25	0,0115	8,1	3,3	0,39	15,5	3,2	350	6	0,089	14,84	166	118
CG-64E-4/20050407/1	1,2	4	0,64	156	2,9	0,65	<1	8,7	0,03	6	14,9	1,45	10,3	7,2	340	10,6	0,63	n.a.	n.a.	n.a.
CG-64E-4/20050407/2	1,2	4	1,14	160	2,9	0,65	<1	9,3	9.300E-3	6,6	15,7	0,75	10,2	7,5	360	11,3	0,63	n.a.	n.a.	n.a.
CG-64E-5/20050428/1	0,7	4	0,93	39	3,1	0,83	2,5	450	0,044	8,1	7,6	0,178	16,7	7	500	5,5	0,236	10,72	185	771
CG-64E-5/20051212/1	0,7	12	0,84	28		0,85	<1	149	0,024	7,9	4,8	0,39	18,9	5,4	420	7,4	0,39	14,64	118	156
CG-64E-6/20050523/1	0,4	6	0,62	27,9	2,24	0,63	47	960	0,013	7,7	20	0,67	28	20	760	4,1	0,66	12,04	217	346
CG-64E-6/20051220/1	0,4	12	0,89	31,4		0,76	62	1450	0,0183	8,2	10,8	0,157	46	27,9	1008	5,5	0,78	16,6	219	181
CG-64E-1/20060124/1	8,2	13	0,43	20,5	2,3	0,65	<1	0,58	0,077	7,3	2,4	0,64	13,8	2,01	720	5,5	0,053	12,57	309	103
CG-64E-2/20061002/1	5,2	22	0,53	27,2	3	0,78	<1	<0.25	0,077	8	3,4	1,05	11,2	2,9	350	6,2	0,095	14,97	161,3	115,6
CG-64E-1/20071207/1	8,2	36	0,51	24,4	3,12	0,58	<1	<0.25	0,038	8,2	2,29	1,31	11,3	2,16	293	6	0,061	12,98	144,6	71,75
CG-64E-2/20071207/1	5,2	36	0,49	41,5	3	0,58	<1	1,04	0,049	8,3	3,04	0,223	12,2	2,55	317	5,1	0,077	13,63	156,6	72,05
CG-64E-3/20071210/1	2,7	36	0,52	24,7	3,11	0,63	<1	<0.25	0,0144	8,9	2,67	0,71	12,6	2,48	316	5,3	0,071	14,11	161,2	77,41
CG-64E-4/20070509/1	1,2	29	0,473	28,1	3,77	0,66	<1	19,9	0,159	8,9	5,7	1,84	15,1	4,5	440	5,5	0,137	17,45	171,4	80,15
CG-64E-4/20071210/1	1,2	36	0,52	25,9	3,4	0,7	<1	0,4	0,0235	9,3	3,74	0,68	14	3,27	365	5,7	0,097	18,29	195,9	93,82
CG-64E-5/20071128/1	0,7	35	0,35	35,7	4,21	0,34	<1	2,34	0,0167	8,8	2,93	0,138	14,5	3,3	369	6,3	0,086	16,48	194,1	18,37
CG-64E-6/20071127/1	0,4	35	0,63	28,3	1,53	0,67	<1	1600	6.600E-3	7,6	25,7	0,133	37,9	27,2	1020	5,2	0,94	15,68	182,9	38,88
CG-64E-1/2011-10-14/1	8,2	82	0,46	21,6	2,7	0,63	<1	0,75	<0.02	6,8	2,23	0,43	8,2	1,88	290	5	0,082	13,04	136,5	64,36
CG-64E-2/2011-10-14/1	5,2	82	0,45	24,6	2,89	0,66	<1	<0.25	<0.02	7,1	2,57	0,333	9,3	2,2	305	5	0,097	13,19	147,5	76,7
CG-64E-3/2011-10-17/1	2,7	82	0,49	23,1	3,01	0,7	<1	<0.25	<0.02	7,5	2,9	0,48	10	2,53	323	5,2	0,106	14,09	145,1	97,48
CG-64E-4/2011-11-08/1	1,2	82	0,57	24,7	3,13	0,74	<1	<0.25	<0.02	7,7	2,82	0,97	10,3	2,44	324	5,5	0,106	14,68	154,5	70,11
CG-64E-6/2011-11-03/1	0,4	82	0,65	26,2	1,39	0,64	106	1530	<0.02	6,7	30,7	<0.02	36,1	32,2	1050	3,78	1,2	14,98	168	42,32

Annex 4. *In-situ* pore water chemistry of the Boom Clay from the piezometer CG-30E (previously named P30E). All concentration values in mg/L. n.a. – not analyzed.

Name	filter distance from the PRACLAYgallery extrados (m)	time since borehole drilling (months)	Br^- [mg/l]	Cl^- [mg/l]	F- [mg/l]	I- [mg/l]	$S_2O_3^-$ [mg/l]	SO_4^{2-} [mg/l]	Al^{3+} [mg/l]	B [mg/l]	Ca^{2+} [mg/l]	Fe^{2+} [mg/l]	K^+ [mg/l]	Mg^{2+} [mg/l]	Na^+ [mg/l]	Si [mg/l]	Sr^{2+} [mg/l]	Alkal [meq/l]	DIC [mg C/l]	DOC [mg C/l]
CG30E-1/20070313	1,89	9,0	0,486	23,4	3,35	0,69	< 1	5,26	0,16	6,4	2,87	0,84	9,3	2,24	299	3,11	0,076	0,85	134,75	67,67
CG30E-1/20071005	1,89	15,0	0,63	20,7	2,86	0,64	< 1	1,02	0,0296	6,8	1,84	1,7	8,7	1,75	280	4	0,056	12,97	143	56,63
CG30E-1/20071016	1,89	15,5	0,442	22,4	3,14	0,57	< 1	0,85	0,207	6,8	2,52	0,57	10,4	2	299	6,5	0,048	13,36	143	49,3
CG30E-1/20090617	1,89	29,0	1,42	443	3,22	0,89	< 0.25	1	< 0,02	8,3	8,9	3,95	268	5,4	490	4,4	0,191	20,76	234	269
CG30E-1/20081128	1,89	36,0	0,44	22,3	3,37	0,73	< 1	1,85	0,076	7,6	3,16	3,14	8,7	2,8	307	5,7	0,063		126	50
CG30E-1/2011-4-5	1,89	57,0	0,75	51,6	3,1	0,84	< 1	0,27	< 0,02	7,9	4,5	1,06	13,5	3,78	400	6	0,157	16,45	192	70,34
CG30E-1/2011-8-9	1,89	61,0	0,97	47,8	3,08	0,84	< 1	0,25	0,022	7,6	3,9	1,16	12,1	3,73	400	5,5	0,158	16,93	187,1	89,85
CG30E-1/2011-10-17	1,89	63,0	0,57	49,1	3,06	0,84	< 1	0,25	< 0,02	8	4,7	0,82	12,1	3,62	400	5,4	0,153	16,53	190,7	97,17
CG30E-1/2012-02-21	1,89	67,0	0,57	46,5	2,94	0,86	< 1	0,25	0,055	8,2	3,57	1,1	12,6	3,34	390	5	0,109	17,5	163,2	76,01
CG30E-1/2012-07-04	1,89	71,0	0,54	41,3	2,96	0,9	<1	0,55	0,022	8,6	3,21	0,27	11,9	2,92	340	5,2	0,088	16,08	180,5	79,09
CG30E-1/2012-10-03	1,89	74,0	0,57	42,3	2,92	0,77	<1	0,25	0,024	7,7	3,56	0,81	12,5	3,09	384	5	0,108	16,73	175,3	92,92
CG30E-1/2013-02-26	1,89	78,0	0,47	72	2,9	0,79	1,9	11,5	< 0,02	7,2	7,5	0,3	33,4	4,1	364	4,3	0,12	23,30	155,5	103,3
CG30E-1/2013-05-31	1,89	80,0	0,48	38,4	2,97	0,81	<10	1,28	<0.05	8,1	5,6	0,25	12,1	3,4	365	4,6	0,089	24,47	164,5	89,97
CG30E-1/2013-08-21	1,89	83,0	0,47	38,4	2,9	0,83	<10	0,25	<0.05	7,3	3,02	0,247	11,4	2,96	359	4,4	0,095	15,27	162,1	88,1
CG30E-1/2013-11-21	1,89	86,0	0,53	34,9	2,92	0,81	<10	0,25	<0.02	6,8	3,9	0,207	10,3	2,76	336	4,1	0,087	14,76	171,5	60,7
CG30E-4/20070313	0,88	9,0	0,478	24,4	3,55	0,67	< 1	3,66	0,151	5,9	3	1,74	10	2,37	310	2,71	0,077	10,66	138,69	66,84
CG30E-4/20071005	0,88	15,0	0,59	21,4	3,01	0,7	< 1	1,24	0,034	6,3	2,03	1,29	9,1	1,81	288	3,32	0,058	13,06	144,7	52,8
CG30E-4/20071016	0,88	15,5	0,57	23	3,14	0,68	< 1	0,9	0,075	6,2	2,69	0,84	11,7	2,22	303	3,59	0,063	13,53	146,1	56,03
CG30E-4/20071023	0,88	16,5	0,69	24,1	3,08	0,74	< 1	0,87	0,081	6,7	2,42	1,06	10,8	2,58	312	3,81	0,067	13,46	150,7	60,9
CG30E-4/20071128	0,88	17,0	0,61	79	3,23	0,76	< 1	0,25	0,0181	7	2,97	0,88	36,5	2,95	356	4	0,087	14,39	168,02	69,6
CG30E-4/20081128	0,88	29,0	0,54	67	3,52	0,88	< 1	0,34	0,024	7,6	3,47	0,54	11,5	3,7	376	4,3	0,094		146	59
CG30E-4/20090617	0,88	36,0	0,71	135	3,15	0,79	< 0.25	0,64	0,021	8,2	3,9	1,6	46	2,86	365	3,85	0,103	17,9	202	48,5
CG30E-4/20100216	0,88	43,5	0,82	89	3,33	0,75	< 0.25	0,25	0,04	6,9	2,81	1,06	10,4	2,59	358	3,8	0,081	15,14	148	66
CG30E-4/2011-4-5	0,88	57,0	0,67	70	2,96	0,78	< 1	0,64	0,031	6,7	3,02	0,41	11,4	2,79	360	4,4	0,134	14,87	167	68,82
CG30E-4/2011-8-9	0,88	61,0	0,54	64	2,88	0,78	< 1	0,25	< 0,02	7,2	2,88	0,55	11	2,82	358	4,4	0,119	15,52	168,5	64,52
CG30E-4/2011-10-17	0,88	63,0	0,54	62	3,03	0,78	< 1	0,25	0,021	7,3	3,2	0,39	11,5	2,85	360	4,2	0,122	14,70	169	67,71
CG30E-4/2012-02-21	0,88	67,0	0,57	59,4	2,92	0,78	< 1	0,25	0,032	7,8	2,89	0,52	11,7	2,79	359	4,1	0,09	14,63	146,1	75,85
CG30E-4/2012-07-04	0,88	71,0	0,52	57,3	2,88	0,81	<1	0,25	0,027	7,9	2,78	0,286	11,6	2,64	314	3,9	0,071	15,33	167,5	71,74
CG30E-4/2012-10-03	0,88	74,0	0,55	54,8	2,86	0,81	<1	0,25	0,024	7,9	3,41	0,89	12,4	2,79	366	4,3	0,095	15,11		79,81
CG30E-4/2013-02-26	0,88	78,0	0,5	51,1	2,81	0,8	<1	16	<0.02	7	6,2	0,254	12,3	3,59	346	3,45	0,091	20,13	154	98,36
CG30E-4/2013-05-31	0,88	80,0	0,53	53,3	2,8	0,79	<10	1,85	<0.05	7,9	7,4	0,23	12,3	3,87	357	3,9	0,092	13,33	154,5	84,62
CG30E-4/2013-08-21	0,88	83,0	0,48	49,9	2,79	0,81	<10	0,25	<0.05	7,3	3,06	0,252	11,6	2,98	361	3,67	0,095	14,58	149,3	85,8
CG30E-4/2013-11-21	0,88	86,0	0,52	47,5	2,84	0,82	<10	0,25	<0.02	6,7	4,3	0,236	10,4	2,84	338	3,36	0,087	14,36	172	67
CG30E-6/20070313	0,55	9,0	0,56	31,7	0,85	0,85	< 1	61,2	0,039	12,5	1,92	1,2	30,1	2,88	388	15,9	0,047	14,01	163,28	95,37
CG30E-6/20071005	0,55	15,0	0,63	22,7	2,94	0,74	< 1	8,1	0,041	6,5	2,34	0,77	9,6	2,1	303	3,9	0,067	12,96	150,6	50,51
CG30E-6/20071015	0,55	15,5	0,55	24,2	2,97	0,72	< 1	5,67	0,34	6,5	3,71	1,55	12	2,49	320	5,6	0,074	14,12	151,2	62,3
CG30E-6/20071023	0,55	15,8	0,67	24,7	3,12	0,75	< 1	5,39	0,4	6,6	2,54	0,83	12,2	2,75	317	4,6	0,072	15,29	152	67,31
CG30E-6/20071128	0,55	17,0	0,82	303	3,23	0,75	< 1	2,14	0,0198	7,4	3,52	0,207	302	3,23	353	4,7	0,104	15,27	168,39	82,18
CG30E-6/20081128	0,55	29,0	0,72	49,7	3,53	0,84	< 1	1,87	0,041	7,4	3,17	0,87	29,6	3,44	358	4,4	0,078		138	55
CG30E-6/20090617	0,55	40,0	0,62	77	3,44	0,83	< 0.25	3,07	0,031	7,8	3,4	1,09	31,2	2,96	377	3,57	0,098	20,54	220	43,3
CG30E-6/20100216	0,55	43,5	0,78	72	3,47	0,84	< 0.25	0,25	< 0,04	6,8	3,6	0,32	11,6	3,18	387	3,5	0,106	16,34	166	74
CG30E-6/2011-4-5	0,55	57,0	0,74	41,3	2,95	0,72	< 1	0,48	0,021	7,2	2,58	0,205	10,5	2,25	325	4,8	0,092	13,80	156,8	61,7
CG30E-6/2011-8-9	0,55	61,0	0,47	35,5	2,9	0,72	< 1	0,25	< 0,02	7,3	2,33	0,54	9,9	2,18	316	4,3	0,095	13,18	154	58,24
CG30E-6/2011-10-17	0,55	63,0	0,49	35,3	2,93	0,71	< 1	0,25	< 0,02	7,7	2,41	0,238	10	2,2	320	4,3	0,096	12,40	153,7	59,89
CG30E-6/2012-02-21	0,55	67,0	0,49	34,1	2,81	0,72	< 1	0,25	0,021	7,5	2,22	0,218	10,2	2,13	313	3,61	0,068	13,37	140,3	60,56
CG30E-6/2012-07-04	0,55	71,0	0,5	40	2,92	0,84	<1	0,25	0,037	10,1	3,03	0,46	11,2	2,19	301	5,7	0,063	16,63	166,7	71,44
CG30E-6/2012-10-03	0,55	74,0	0,48	31,2	2,85	0,74	<1	0,25	<0.02	7,7	2,32	0,218	11	2,13	322	3,9	0,072	12,80	148,6	72,8
CG30E-6/2013-02-26	0,55	78,0	0,46	34,9	2,84	0,74	<1	1,78	<0.02	7,6	4,6	0,174	11,3	2,57	319	3,26	0,073	21,76	147,2	86,06
CG30E-6/2013-05-31	0,55	80,0	0,44	31,7	2,9	0,73	<10	1,17	<0.05	8	5,8	0,15	10,9	3,19	332	3,5	0,077	13,07	145,6	83,95
CG30E-6/2013-08-21	0,55	83,0	0,43	30,4	2,9	0,74	<10	0,25	<0.05	7,5	2,92	0,147	10,5	2,69	329	3,17	0,083	14,16	143,5	82,2
CG30E-6/2013-11-21	0,55	86,0	0,44	29,1	2,93	0,75	<10	0,25	0,029	7,1	4,5	0,127	9,9	2,71	314	2,99	0,078	13,68	161,3	53,6

Annex 5. *In-situ* pore water chemistry of the Boom Clay from the piezometer CG-35E (previously named P35E). All concentration values in mg/L.

Name	filter distance from the PRACLAYgallery extrados (m)	time since borehole drilling (months)	Br^- [mg/l]	Cl^- [mg/l]	F- [mg/l]	I- [mg/l]	$S_2O_3^-$ [mg/l]	SO_4^{2-} [mg/l]	Al^{3+} [mg/l]	B [mg/l]	Ca^{2+} [mg/l]	Fe^{2+} [mg/l]	K^+ [mg/l]	Mg^{2+} [mg/l]	Na^+ [mg/l]	Si [mg/l]	Sr^{2+} [mg/l]	Alkal [meq/l]	DIC [mg C/l]	DOC [mg C/l]
CG35E-2/20070313	1,14	9,00	0,414	25,1	3,48	0,66	< 1	2,67	1	7,6	2,5	1,66	8,7	2,4	299	4,7	0,034	1,09	135,29	55,98
CG35E-2/20071005	1,14	15,00	0,56	19,9	2,72	0,66	< 1	1,12	0,048	6,8	1,81	1,66	8,1	1,64	272	4,9	0,053	12,04	135,9	55,8
CG35E-2/20071015	1,14	15,50	0,515	21,8	2,79	0,69	< 1	0,58	0,063	7	2,94	0,82	10,1	2,08	291	5,1	0,057	13,06	140,7	62
CG35E-2/20071129	1,14	17,00	0,48	29,5	3,04	0,69	< 1	0,36	0,032	7,7	2,84	2,93	12,4	2,4	309	5,9	0,069	13,91	155,01	69,45
CG35E-2/20081128	1,14	29,00	0,8	92	2,97	0,81	< 1	0,25	0,0172	7,9	4,7	1,63	13,3	4,6	389	6,2	0,107	n.a.	150	64
CG35E-2/20090617	1,14	36,00	0,67	103	2,9	0,75	< 0,25	0,25	< 0,02	8,8	3,9	0,83	24,6	3,07	372	5,6	0,101	17,22	166	47,5
CG35E-2/20100216	1,14	47,50	0,96	79	3,06	0,74	< 0,25	0,25	< 0,04	7,2	3,37	0,75	11,1	2,9	377	5,3	0,092	15,52	150	91
CG35E-2/2011-4-5	1,14	57,00	0,65	64	2,79	0,76	< 1	0,48	< 0,02	7,3	3,68	0,59	11,4	3,16	372	6,4	0,126	13,89	169,2	75,29
CG35E-2/2011-8-9	1,14	61,00	0,53	61,5	2,86	0,74	< 1	0,25	< 0,02	7,4	3,14	1,2	11,3	3,19	370	6,7	0,119	14,56	171,1	79,83
CG35E-2/2011-10-17	1,14	63,00	0,53	57,5	2,85	0,77	1,07	0,25	< 0,02	7,4	3,39	0,271	11,5	3,17	370	5,4	0,131	14,21	175,2	73,03
CG35E-2/2012-02-21	1,14	67,00	0,57	56,1	2,8	0,78	< 1	0,25	< 0.02	7,8	3,15	0,35	11,6	3,06	366	5,1	0,097	21,23	158,2	73,35
CG35E-2/2012-07-04	1,14	71,00	0,51	53,2	2,87	0,82	<1	0,25	0,072	8,5	3,38	0,51	12,1	2,93	324	4,4	0,086	15,86	n.a.	82,63
CG35E-2/2012-10-03	1,14	74,00	0,57	50,6	2,85	0,78	<1	0,25	0,038	7,8	3,32	0,337	11,9	3	368	5,4	0,1	14,39	n.a.	82,47
CG35E-2/2013-02-26	1,14	78,00	0,47	51,4	2,84	0,75	<1	101	<0.02	6,9	10,4	0,47	14,7	8,4	385	4,1	0,135	21,32	156,3	97,94
CG35E-2/2013-05-31	1,14	80,00	0,44	46,6	2,88	0,76	<10	1,54	<0.05	7,7	6,8	0,18	12,2	3,94	364	4,6	0,097	14,12	156,5	96,97
CG35E-2/2013-08-21	1,14	83,00	0,44	54,1	3,03	0,76	<10	0,5	<0.05	7,3	3,9	0,227	14	3,46	373	4,3	0,105	14,04	154,2	94,9
CG35E-2/2013-11-21	1,14	86,00	0,44	42	2,88	0,75	<10	0,25	<0.02	6,6	5,7	0,163	10,3	3,32	332	3,77	0,09	15,79	169,9	57,4
CG35E-6/20070313	1,0	9,00	0,312	24,7	3,55	0,53	< 1	5,51	2,41	7,4	2,36	3,17	12,7	2,36	343	6,7	0,039	n.a.	148,13	86,37
CG35E-6/20071005	1,0	15,00	0,59	20,6	2,76	0,68	< 1	1,68	0,2	6,9	2,14	1,13	8,7	1,95	284	4,9	0,058	12,52	134,8	71,8
CG35E-6/20071015	1,0	15,50	0,5	22	2,97	0,71	< 1	0,78	0,119	6,7	3,29	0,82	13,9	2,61	320	4,1	0,065	12,72	147,01	82,25
CG35E-6/20071129	1,0	17,00	0,55	32,8	3,03	0,72	< 1	0,5	0,044	7,6	2,92	2,64	17,5	2,79	318	5,6	0,078	13,99	161,35	79,79
CG35E-6/20081128	1,0	29,00	0,68	54,3	3,48	0,86	< 1	0,25	0,0205	8,1	4,1	0,88	11,4	3,72	352	5,8	0,089	n.a.	133	63
CG35E-6/20090617	1,0	36,00	0,72	63	3,3	0,81	< 0,25	0,25	< 0,02	8,7	3,25	0,99	16,9	2,72	341	5,2	0,091	18,84	198	56,9
CG35E-6/20100216	1,0	47,50	1,19	54,6	3,47	0,78	< 0,25	0,25	0,06	7,7	3,2	2,27	10	2,79	364	5,5	0,089	31,69	153	78
CG35E-6/2011-4-5	1,0	57,00	1,01	47,4	3,06	0,8	< 1	0,35	< 0,02	8,3	3,42	0,289	11,6	3	357	6,1	0,123	13,63	174,7	77,15
CG35E-6/2011-8-9	1,0	61,00	0,53	44,4	3,04	0,8	< 1	0,25	< 0,02	7,5	3,12	0,58	11	3,01	357	5,6	0,124	14,67	169,7	78,21
CG35E-6/2011-10-17	1,0	63,00	0,52	43,9	3,05	0,81	< 1	0,25	< 0,02	7,8	3,5	0,38	11,1	3,05	360	5,5	0,128	15,45	165,7	83,15
CG35E-6/2012-02-21	1,0	67,00	0,55	43	2,95	0,81	< 1	0,25	< 0.02	7,9	3,05	0,298	11,1	2,92	355	5,1	0,094	15,58	159,5	73,62
CG35E-6/2012-07-04	1,0	71,00	0,5	36,2	3,22	0,84	<1	2,22	<0.02	7,8	3,04	0,224	11,4	2,83	321	4,8	0,084	15,27	n.a.	79,96
CG35E-6/2012-10-03	1,0	74,00	0,54	39,4	2,88	0,8	<1	0,25	<0.02	7,9	3,06	0,6	11,6	2,77	356	5,3	0,093	15,06	n.a.	81,66
CG35E-6/2013-02-26	1,0	78,00	0,49	47,2	2,8	0,76	<1	82,1	<0.02	7,3	10,1	0,263	16,1	6,8	365	4,6	0,106	20,46	152,8	96,66
CG35E-6/2013-05-31	1,0	80,00	0,51	37	2,85	0,78	<10	1,01	0,05	7,7	6,3	0,24	10,8	3,57	344	5	0,087	13,48	151	87,31
CG35E-6/2013-08-21	1,0	83,00	0,43	34,8	2,77	0,8	<10	0,25	<0.05	7,2	2,86	0,26	10,2	2,74	333	4,7	0,085	14,50	148,8	85,43
CG35E-6/2013-11-21	1,0	86,00	0,46	32,8	2,8	0,78	<10	0,25	<0.02	6,8	3,9	0,235	10	2,59	319	4,4	0,078	13,56	165	65,9
CG35E-11/20070313	0,88	9,00	0,6	28,1	3,58	0,83	< 1	16	0,52	7	3,82	1,28	11,8	3,47	367	5,7	0,113	12,34	165,7	75,31
CG35E-11/20071005	0,88	15,00	0,56	21,4	2,95	0,71	< 1	7,35	0,034	6,6	2,29	0,47	9,8	2,27	303	3,9	0,065	14,24	151	49,1
CG35E-11/20071015	0,88	15,50	0,514	24,4	2,96	0,7	< 1	5,27	0,045	6,7	3,29	0,82	13,9	2,61	320	4,1	0,065	13,93	150	56,55
CG35E-11/20071023	0,88	15,80	0,78	198	3,01	0,69	< 1	4,82	0,252	6,8	2,89	0,37	208	2,73	315	4,7	0,074	13,53	148,4	59,73
CG35E-11/20071128	0,88	17,00	0,56	74	3,28	0,76	< 1	0,35	0,0224	7,3	3,16	0,38	47	2,99	354	4,9	0,09	15,38	174,63	65,31
CG35E-11/20081128	0,88	29,00	0,49	58,9	3,44	0,89	< 1	0,25	0,042	8,5	6	2,86	13,7	6	420	6,9	0,15	n.a.	162	118
CG35E-11/20090617	0,88	36,00	0,65	125	3,26	0,81	< 0,25	0,25	0,036	8,5	5,2	1,42	35,9	4,1	400	5	0,139	19,91	221	67,8
CG35E-11/20100216	0,88	47,50	0,95	51,3	3,65	0,84	< 0,25	0,25	0,05	7,5	3,8	0,49	11,2	3,4	382	4,5	0,109	32,93	169	83
CG35E-11/2011-4-5	0,88	57,00	0,77	42,1	3,17	0,84	< 1	0,37	0,04	8,1	3,81	0,55	12,7	3,55	393	6,9	0,141	16,53	187,9	90,08
CG35E-11/2011-10-17	0,88	63,00	0,68	41,3	3,08	0,83	< 1	0,25	0,057	8,4	3,9	0,38	13,2	3,59	391	5,2	0,146	17,32	188,7	51,35
CG35E-11/2012-02-21	0,88	67,00	0,59	40,9	3,12	0,82	< 1	0,25	0,058	8,7	3,59	0,38	12,1	3,35	378	5,1	0,105	17,29	166,4	80,07
CG35E-11/2012-07-04	0,88	71,00	0,52	36,2	3,12	0,83	<1	0,25	0,023	7,9	2,91	0,295	11,1	2,7	311	4,8	0,081	16,57	n.a.	70,51
CG35E-11/2012-10-03	0,88	74,00	0,55	30,4	3,18	0,77	<1	0,25	0,093	8,6	3,14	0,7	11,6	2,57	336	4,4	0,081	16,93	n.a.	55,71
CG35E-11/2013-02-26	0,88	78,00	0,46	40,8	3,18	0,72	<1	11,6	<0.02	7,7	6,9	0,12	18,5	3,21	309	3,35	0,092	19,67	150,3	90,84
CG35E-11/2013-05-31	0,88	80,00	0,43	35,2	3,23	0,75	<10	2,61	<0.05	8,2	9	0,13	11	4,2	336	4	0,087	12,94	153,9	58,24
CG35E-11/2013-08-21	0,88	83,00	0,43	30,6	3,07	0,76	<10	0,25	<0.05	7,7	3,12	0,174	10,3	2,85	336	3,47	0,086	14,16	151,7	56,99
CG35E-11/2013-11-21	0,88	86,00	0,46	27,1	2,84	0,69	<10	0,5	<0.02	6,6	7,1	0,1	9,1	3,12	287	3,06	0,072	13,79	154,4	60

Annex 6. *In-situ* pore water chemistry of the Boom Clay from the piezometer CG-13U (previously named R13U). n.a. – not analyzed.

Name	filter distance from the gallery extrados (m)	time since borehole drilling (months)	Br^- [mg/l]	Cl^- [mg/l]	F- [mg/l]	I- [mg/l]	$S_2O_3^-$ [mg/l]	SO_4^{2-} [mg/l]	Al^{3+} [mg/l]	B [mg/l]	Ca^{2+} [mg/l]	Fe^{2+} [mg/l]	K^+ [mg/l]	Mg^{2+} [mg/l]	Na^+ [mg/l]	Si [mg/l]	Sr^{2+} [mg/l]	Alkal [meq/l]	DIC [mg C/l]	DOC [mg C/l]
CG13U-01/20041014/1	19,6	10	0,59	14,8	2,02	0,52	<1	10,6	1,04	3,9	2,8	0,53	7,7	2,06	253	4,1	0,051	10,37	120	69
CG13U-02/20041019/1	17,6	10	0,58	15,7	2,79	0,57	<1	9,2	2,6	4,2	3,7	0,96	8,2	2,86	256	3,9	0,07	10,75	123	84
CG13U-03/20041015/1	15,6	10	0,49	14	2,45	0,49	<1	60,2	0,151	3,7	2,6	0,12	7,4	1,79	251	3,9	0,05	9,37	109	51
CG13U-04/20041018/1	13,6	10	0,51	14	2,52	0,5	<1	101	0,049	3,9	2,7	0,06	8	2,11	274	3,8	0,057	9,61	114	42
CG13U-05/20041018/1	11,6	10	0,56	15,7	2,53	0,56	<1	40,7	0,115	4,1	2,7	0,08	7,9	1,99	272	3,4	0,055	10,44	126	48
CG13U-06/20041024/1	9,6	10	0,6	17,2	2,92	0,61	<1	26,2	0,049	4,2	2,6	0,5	8,1	2,18	279	3,8	0,059	11,21	135	47
CG13U-07/20041021/1	7,6	10	0,62	17,5	2,64	0,66	<1	70	0,09	4,7	2,9	0,08	8,7	2,49	310	3,4	0,07	11,21	139	54
CG13U-08/20041021/1	5,6	10	0,62	18,9	2,91	0,7	<1	52,2	0,076	4,7	2,9	0,11	8,6	2,52	320	3,6	0,073	12,11	145	57
CG13U-09/20041021/1	3,6	10	0,98	17,8	2,32	0,67	<1	511	0,0268	4,9	5,6	<0.05	14,4	5,9	460	3,4	0,155	9,41	119	53
CG13U-10/20041020/1	2,6	10	0,66	16	1,28	0,52	<1	1070	0,065	5,9	14,2	<0.05	33	20,2	810	2,9	0,51	14,06	172	39
CG13U-11/20041021/1	1,6	10	0,74	11,3	0,6	0,48	2,97	3060	0,03	8,1	78	<0.05	73	92	1530	3,8	2,09	13,86	182	24
CG13U-01/20051021/1	19,6	22	0,43	17,2	n.a.	n.a.	<1	30,3	n.a.	n.a.	2,5	n.a.	9,3	n.a.	300	3,9	n.a.	10,95	n.a.	n.a.
CG13U-07/20051013/1	7,6	22	0,48	17,9	n.a.	n.a.	<1	111	n.a.	n.a.	6,7	n.a.	11,2	n.a.	340	4,3	n.a.	11,09	121,4	71,91
CG13U-08/20051014/1	5,6	22	0,51	19,2	n.a.	n.a.	<1	14,3	n.a.	n.a.	2,9	n.a.	10,4	n.a.	300	4,4	n.a.	11,95	135,9	54,97
CG13U-11/20051107/1	1,6	23	0,35	13,3	n.a.	n.a.	1,1	1440	n.a.	n.a.	28	n.a.	41	n.a.	990	3,5	n.a.	13,84	4,36	27,46
CG13U-12/20051006/1	0,6	22	0,45	8,9	n.a.	n.a.	<1	4190	n.a.	n.a.	90	n.a.	89	n.a.	1920	5,4	n.a.	8,67	126,8	25,1
CG13U-01/20070208/1	19,6	38	0,344	12,5	n.a.	0,43	<1	5,22	0,97	4,8	2,46	0,7	7,3	1,78	216	5,4	0,052	8,72	100,2	45,59
CG13U-02/20070208/1	17,6	38	0,368	15	n.a.	0,49	<1	1,09	0,8	5	3,54	1,26	8,8	2,51	255	5,2	0,081	8,27	89,89	79,88
CG13U-03/20070209/1	15,6	38	0,386	14	n.a.	0,48	<1	11,2	0,51	5	2,65	0,44	8,1	1,77	239	4,3	0,057	8,75	96,58	42,67
CG13U-04/20070206/1	13,6	38	0,318	13,9	n.a.	0,48	<1	25,5	0,058	5,2	2,57	0,255	8	1,61	247	3,58	0,053	9,51	105,4	35,91
CG13U-05/20070206/1	11,6	38	0,354	15,4	n.a.	0,46	<1	6,25	0,133	5,4	3,02	0,51	7,9	1,69	256	3,84	0,063	10,03	116,3	42,57
CG13U-06/20070206/1	9,6	38	0,414	16,1	n.a.	0,54	<1	2,04	0,034	5,6	2,65	0,42	7,9	1,72	259	3,58	0,057	11,19	115,6	45,33
CG13U-07/20070206/1	7,6	38	0,398	17,3	n.a.	0,61	<1	9	0,33	5,8	4,8	0,328	8	1,78	276	3,33	0,097	11,87	125,2	54,15
CG13U-08/20070206/1	5,6	38	0,433	18,2	n.a.	0,6	<1	2,72	0,02	6,2	3,05	0,137	8,7	2,04	287	4	0,067	12,25	132,5	51,38
CG13U-09/20070206/1	3,6	38	0,73	18,5	n.a.	0,65	<1	158	0,0118	6,4	4,3	0,039	11,4	3,37	367	3,39	0,112	12,79	138,3	53,27
CG13U-10/20070207/1	2,6	38	0,479	16,9	n.a.	0,59	<1	424	5.300E-3	6,7	7,6	0,027	18,1	7,1	520	2,82	0,247	15,17	166,8	43,05
CG13U-11/20070207/1	1,6	38	0,65	14,4	n.a.	<0.05	<1	1120	5.600E-3	7,2	20,9	<0.02	30,5	19,1	800	3,03	0,6	14,44	161,1	38,77
CG13U-12/20070207/1	0,6	38	0,498	11,5	n.a.	0,5	<1	2810	0,032	9,2	93	0,065	60	78	1460	3,17	2,29	11,6	168,1	40,79
CG13U-1/2011-4-14/1	19,6	87	0,27	14,2	2	0,45	<0.25	4,26	<0.04	3,7	2,46	0,14	7,5	1,45	263	4,1	0,055	9,952	115	55
CG13U-2/2011-4-14/1	17,6	87	0,27	14,1	2,6	0,45	<0.25	0,87	<0.04	3,8	2,82	0,61	7,5	1,68	254	3,9	0,064	9,871	114	50,8
CG13U-3/2011-4-15/1	15,6	87	0,31	13,6	2,5	0,43	<0.25	2,71	<0.04	3,9	2,44	0,21	7,2	1,33	241	4	0,053	9,481	113	37,1
CG13U-4/2011-4-15/1	13,6	87	0,31	14,2	2,6	0,45	0,46	2,53	<0.04	4,2	2,37	<0.04	7,4	1,3	245	4,2	0,049	9,681	112	33,7
CG13U-5/2011-4-15/1	11,6	87	0,28	15,1	2,5	0,49	<0.25	1,62	0,05	4,3	2,7	0,15	7,5	1,45	263	4,1	0,056	10,481	122	40,5
CG13U-6/2011-4-8/1	9,6	87	0,36	16,2	2,8	0,53	0,58	0,53	<0.04	4,7	2,45	0,17	7,7	1,55	266	3,9	0,06	10,555	122	38,8
CG13U-7/2011-4-8/1	7,6	87	0,4	17,1	2,6	0,57	0,51	1,19	0,07	5,1	2,65	0,12	7,9	1,65	286	3,9	0,067	11,144	127	45,7
CG13U-8/2011-4-8/1	5,6	87	0,41	18,2	2,9	0,59	<0.25	1,63	<0.04	5,4	3,16	0,13	8,5	1,89	307	4,4	0,08	11,808	136	51,5
CG13U-9/2011-4-11/1	3,6	87	0,38	19	2,9	0,61	0,54	61,3	<0.04	5,7	3,08	0,2	10	2,39	356	3,6	0,094	12,367	141	55,7
CG13U-10/2011-4-8/1	2,6	87	0,38	18	2,3	0,6	<0.25	219	<0.04	5,7	5,4	0,15	14	4,5	480	3,21	0,184	14,558	166	44,7
CG13U-11/2011-4-13/1	1,6	87	0,36	15,9	1,8	0,55	<0.25	633	<0.04	6	10,6	0,3	21,2	9,7	670	3,08	0,39	14,427	162	37,4
CG13U-12/2011-4-11/1	0,6	87	0,42	14,3	1,2	0,55	0,39	1680	<0.04	7,1	31,2	0,35	42	35,5	1150	3,7	1,11	15,047	166	36
CG13U-13/2011-4-19/1	0,3	87	0,48	14,6	1,2	0,6	0,54	3030	<0.04	7,7	59	1,99	63	87	1650	4,3	2,37	12,538	140	29,3

Annex 6 continued. *In-situ* pore water chemistry of the Boom Clay from the piezometer CG-13U (previously named R13U). n.a. – not analyzed.

Name	filter distance from the gallery extrados (m)	time since borehole drilling (months)	Br^- [mg/l]	Cl^- [mg/l]	F- [mg/l]	I- [mg/l]	$S_2O_3^-$ [mg/l]	SO_4^{2-} [mg/l]	Al^{3+} [mg/l]	B [mg/l]	Ca^{2+} [mg/l]	Fe^{2+} [mg/l]	K^+ [mg/l]	Mg^{2+} [mg/l]	Na^+ [mg/l]	Si [mg/l]	Sr^{2+} [mg/l]	Alkal [meq/l]	DIC [mg C/l]	DOC [mg C/l]
CG13U-1/2013-11-28	19,6	119	0,28	16,1	1,64	0,46	<10	4,45	0,05	4,9	3,8	0,14	8,1	1,71	220	4,2	0,044	10	121	47
CG13U-2/2013-11-28	17,6	119	0,27	15,8	2,38	0,48	<10	1,74	0,05	5,4	4,1	0,2	8,6	1,9	216	3,8	0,05	10	119	32
CG13U-3/2013-11-25	15,6	119	0,28	15,4	2,08	0,46	<10	3,74	<0.04	5,2	3,32	0,2	8,1	1,51	204	3,5	0,039	10	114	26
CG13U-4/2013-11-20	13,6	119	0,28	17,2	2,22	0,47	<10	3,57	0,05	5,8	4,3	0,28	8,2	1,8	209	4,1	0,041	10	114	32
CG13U-5/2013-12-2	11,6	119	0,31	16,8	2,1	0,51	<10	2,2	<0.04	5,9	3,9	0,45	9	1,74	230	3,6	0,052	13	127	29
CG13U-6/2013-11-26	9,6	119	0,34	20	2,29	0,55	<10	3,01	<0.04	6,5	5,1	0,42	9,2	2,14	227	4,2	0,048	14	124	35
CG13U-7/2013-12-2	7,6	119	0,29	18,6	2,19	0,59	<10	2,65	<0.05	6,3	4	0,52	8,7	1,91	258	3,6	0,046	10	133	34
CG13U-8/2013-12-2	5,6	119	0,3	18,3	2,43	0,61	<10	2,28	<0.05	6,8	4	0,17	8,9	2,01	265	3,8	0,049	14	136	44
CG13U-9/2013-11-22	3,6	119	0,43	25,8	2,61	0,68	<10	42,3	0,05	7,6	7,3	0,13	11	3,27	294	4,2	0,079	16	150	55
CG13U-10/2013-11-22	2,6	119	0,36	21,7	1,96	0,64	<10	170	<0.04	7,3	7,3	0,11	14,5	4,3	376	3,5	0,128	19	173	32
CG13U-11/2013-11-22	1,6	119	0,41	22,7	1,49	0,59	<10	520	0,05	7,4	13,5	0,08	20	8,4	510	3,6	0,263	20	170	28
CG13U-12/2013-11-28	0,6	119	0,34	17,7	0,95	0,65	<10	1380	<0.04	8,3	31,1	0,06	36	25,9	890	3,6	0,84	20	192	32
CG13U-13/2013-11-25	0,3	119	0,49	18,6	0,77	0,65	<10	2810	<0.04	9	63	<0.04	60	74	1380	4,1	2,07	16	163	24
CG13U-1/2014-9-11/1	19,6	129	0,35	13,4	1,62	0,43	<10	3,03	<0.05	5,4	2,21	0,08	8,3	1,39	227	4,5	0,042	10,19	111,9	67,12
CG13U-2/2014-9-11/1	17,6	129	0,38	13,1	2,33	0,43	<10	0,66	<0.05	5,7	2,65	0,19	9,1	1,6	223	4,1	0,05	9,827	108,7	64,41
CG13U-3/2014-9-11/1	15,6	129	0,35	13	2,2	0,42	<10	1,31	<0.05	6,1	2	0,22	9,1	1,32	212	4,2	0,04	9,549	105	45,45
CG13U-4/2014-9-23/1	13,6	129	0,37	12,9	2,13	0,44	<10	1,64	<0.05	6,6	1,7	0,13	8,5	1,2	214	4,5	0,035	9,617	98,03	50,37
CG13U-5/2014-9-23/1	11,6	129	0,42	14,5	2	0,48	<10	1,38	<0.05	6,7	2,02	0,18	10,2	1,36	234	4,2	0,041	10,383	113,4	55,8
CG13U-6/2014-9-23/1	9,6	129	0,42	15	2,22	0,5	<10	0,71	<0.05	6,9	1,8	0,45	10,2	1,35	236	4,5	0,041	10,413	116,5	50,56
CG13U-7/2014-9-23/1	7,6	129	0,44	16,3	2,15	0,54	<10	1,48	<0.05	7,3	2,11	0,62	13,6	1,51	251	4,3	0,05	11,312	120	58,24
CG13U-8/2014-9-19/1	5,6	129	0,54	17,1	2,52	0,56	<10	1,72	<0.05	7,8	2,21	<0.05	11,7	1,67	261	4,7	0,052	11,6	121,2	66,86
CG13U-9/2014-9-17/1	3,6	129	0,48	17,9	2,5	0,54	<10	35	<0.05	7,6	2,61	0,13	12,9	2,14	294	3,7	0,068	12,44	131,6	72,36
CG13U-10/2014-9-15/1	2,6	129	0,45	17,9	2,04	0,56	<10	157	<0.05	7,2	4,1	0,06	17,2	3,59	381	2,78	0,122	13,757	158,1	64,09
CG13U-11/2014-9-15/1	1,6	129	0,38	15,7	1,58	0,55	<10	479	<0.05	7,7	7,9	0,08	23,6	7,3	520	3,08	0,246	14,435	163	54,57
CG13U-12/2014-9-18/1	0,6	129	0,45	15	0,97	0,59	<10	1320	<0.05	8,9	27,9	0,18	37	25,1	890	3,7	0,8	14,77	171,4	61,91
CG13U-13/2014-9-22/1	0,3	129	0,54	14,8	0,79	0,62	<10	2860	<0.05	9,4	75	0,1	59	76	1430	4,2	2,29	12,857	164,3	38,72
CG-13U-1/2015-10-13	19,6	142	<0.5	14,7	2,14	0,44	<1	3,4	<0.05	4,8	2,03	0,14	6,1	1,11	249	4,4	0,033	10,44	119,9	79,5
CG-13U-2/2015-10-13	17,6	142	<0.5	14,1	2,06	0,43	<1	0,6	<0.05	4,8	2,68	0,07	7,1	1,33	236	4,5	0,041	10,17	115,3	66,2
CG-13U-3/2015-10-13	15,6	142	<0.5	13,2	2,03	0,42	<1	2,3	<0.05	5,0	2,26	0,12	6,4	1,04	220	4,8	0,029	9,34	107,6	45,0
CG-13U-4/2015-10-13	13,6	142	<0.5	13,5	2,13	0,42	<1	2,2	<0.05	5,2	2,30	0,25	6,5	1,08	218	5,0	0,029	9,27	108,1	43,9
CG-13U-5/2015-10-13	11,6	142	<0.5	14,7	2,06	0,47	<1	1,3	<0.05	5,6	2,32	0,09	6,0	1,27	243	4,4	0,036	10,15	117,5	55,8
CG-13U-6/2015-10-12	9,6	142	<0.5	14,9	2,18	0,48	<1	0,6	<0.05	6,0	1,91	0,06	7,2	1,28	246	4,4	0,035	9,95	118,8	50,1
CG-13U-7/2015-10-12	7,6	142	<0.5	16,4	2,13	0,52	<1	1,7	<0.05	6,2	2,10	0,08	6,8	1,47	269	4,0	0,041	11,00	129,7	64,2
CG-13U-8/2015-10-12	5,6	142	<0.5	16,5	2,41	0,52	<1	4,3	<0.05	6,6	2,27	0,08	7,7	1,64	271	4,1	0,045	11,10	127,6	64,9
CG-13U-9/2015-10-12	3,6	142	<0.5	17,6	2,49	0,58	<1	45,0	<0.05	7,0	2,93	0,18	8,5	2,07	316	4,2	0,061	13,81	138,2	68,8
CG-13U-10/2015-10-12	2,6	142	<0.5	17,5	2,12	0,57	<1	137,0	<0.05	6,9	4,30	0,29	12,7	3,29	400	3,3	0,110	11,97	162,1	59,6
CG-13U-11/2015-10-12	1,6	142	<0.5	15,9	1,77	0,54	<1	410,0	<0.05	7,0	7,60	<0.05	15,9	6,40	530	3,6	0,211	14,05	162,6	50,7
CG-13U-12/2015-10-13	0,6	142	0,50	16,4	1,18	0,59	<1	1190,0	<0.05	7,9	25,60	0,26	30,0	22,50	890	4,1	0,710	15,69	179,7	59,2
CG-13U-13/2015-10-15	0,3	142	0,57	16,6	1,09	0,61	<1	2700,0	<0.05	8,6	82,00	0,64	52,0	74,00	1440	4,5	2,310	15,21	146,3	41,1

Annex 7. *In-situ* pore water chemistry of the Boom Clay from the piezometer CG-13D (previously named R13D). n.a. – not analyzed.

Name	filter distance from the gallery extrados (m)	time since borehole drilling (months)	Br^- [mg/l]	Cl^- [mg/l]	F- [mg/l]	I- [mg/l]	$S_2O_3^-$ [mg/l]	SO_4^{2-} [mg/l]	Al^{3+} [mg/l]	B [mg/l]	Ca^{2+} [mg/l]	Fe^{2+} [mg/l]	K^+ [mg/l]	Mg^{2+} [mg/l]	Na^+ [mg/l]	Si [mg/l]	Sr^{2+} [mg/l]	Alkal [meq/l]	DIC [mg C/l]	DOC [mg C/l]
CG13D-1/2011-4-28/1	39,6	87	0,44	24,3	3,4	0,59	<0.25	0,41	<0.04	5,3	1,65	0,11	7,3	1,35	389	4,4	0,065	15,449	168	32,2
CG13D-2/2011-4-28/1	35,6	87	0,45	24,3	3,4	0,64	<0.25	<0.25	0,05	5,6	1,67	0,63	7,8	1,37	395	4,7	0,064	14,782	166	37,8
CG13D-3/2011-4-20/1	30,6	87	0,6	31,3	3,3	0,83	0,61	<0.25	0,06	5,9	2,87	0,69	8	2,1	500	4,6	0,096	18,369	202	106
CG13D-4/2011-4-15/1	25,6	87	0,48	25,9	3	0,59	<0.25	0,34	<0.04	5,8	2,4	0,09	8,1	1,69	410	3,8	0,081	15,71	173	58,8
CG13D-5/2011-4-15/1	18,6	87	0,46	25,6	2,9	0,63	<0.25	<0.25	0,26	6	2,48	0,32	8,2	1,67	383	4,9	0,078	14,484	161	60,7
CG13D-6/2011-4-15/1	14,6	87	0,52	24,1	3	0,69	0,59	0,95	<0.04	6	2,76	0,13	8,3	1,78	379	3,7	0,084	14,36	159	51,8
CG13D-7/2011-4-15/1	11,6	87	0,5	23,6	2,9	0,71	<0.25	1,59	<0.04	6,2	3,05	0,13	8,5	1,89	374	3,8	0,084	14,134	161	63,4
CG13D-8/2011-4-11/1	8,6	87	0,5	22,3	2,6	0,68	<0.25	1,29	0,05	6,2	2,27	0,19	8,4	1,79	352	3,6	0,077	13,447	149	57,2
CG13D-9/2011-4-8/1	5,6	87	0,46	22,5	2,6	0,69	<0.25	0,65	0,04	6,3	2,64	0,12	9,2	1,96	368	3,13	0,085	14,325	157	68,7
CG13D-10/2011-4-11/1	3,6	87	0,51	22,4	2,9	0,71	<0.25	28	0,09	6,1	3,02	0,26	10	2,46	397	3,43	0,104	14,651	158	73,1
CG13D-11/2011-4-11/1	2,6	87	0,53	21,9	2,7	0,67	<0.25	172	0,16	6,3	4,7	0,23	12,3	3,66	460	3,09	0,167	14,572	165	56,1
CG13D-12/2011-4-11/1	1,6	87	0,45	19,1	2,2	0,64	<0.25	410	0,04	6,5	7	0,35	16,3	6,1	580	3,5	0,278	14,716	162	56,2
CG13D-13/2011-4-18/1	0,6	87	0,51	19,6	2	0,63	<0.25	514	<0.04	6,5	8,6	0,25	19	8	650	3,15	0,34	15,509	175	54
CG13D-1/2013-11-19	39,6	119	0,41	25,7	2,73	0,61	<10	2,57	<0.05	6,5	4,6	<0.05	6,4	1,94	322	4,6	0,052	13	167	29
CG13D-2/2013-11-19	35,6	119	0,44	25,9	2,68	0,63	<10	1,83	<0.04	6,8	3,9	<0.04	8,4	1,76	294	4,7	0,054	13	164	24
CG13D-3/2013-11-22	30,6	119	0,63	32	2,86	0,91	<10	1,22	<0.04	6,8	4,1	0,68	9,9	2,38	410	4,2	0,08	18	224	128
CG13D-4/2013-11-19	25,6	119	0,52	28,4	2,47	0,76	<10	1,94	0,06	7	4	0,06	9,1	2,07	338	3,9	0,063	15	190	41
CG13D-5/2013-11-19	18,6	119	0,54	28	2,39	0,74	<10	2,48	<0.04	7,4	4,7	0,09	8,4	2,13	307	4,6	0,059	13	166	46
CG13D-6/2013-11-19	14,6	119	0,54	26,3	2,65	0,79	<10	1,56	0,05	7,3	4,9	0,1	9,9	2,39	307	3,7	0,068	14	174	46
CG13D-7/2013-11-25	11,6	119	0,45	25,2	2,46	0,75	<10	2,43	0,05	7	3,8	0,87	10,2	2,02	300	3,5	0,062	14	163	46
CG13D-8/2013-11-26	8,6	119	0,46	27,6	2,55	0,72	<10	4,66	<0.04	7,7	6,2	0,06	9,2	2,58	283	4,1	0,068	13	155	44
CG13D-9/2013-11-26	5,6	119	0,43	23,9	2,36	0,73	<10	2,03	0,04	7,5	5,2	0,21	10,4	2,52	298	3,5	0,068	14	161	51
CG13D-10/2013-11-27	3,6	119	0,51	23,9	2,72	0,76	<10	15	0,05	7,2	4,8	0,51	11,8	2,63	322	3,31	0,08	14	169	58
CG13D-11/2013-11-27	2,6	119	0,44	23,1	2,5	0,75	<10	121	0,07	7,5	6,7	0,12	11,4	3,66	375	3,3	0,104	14	170	40
CG13D-12/2013-11-29	1,6	119	0,47	22,3	2,17	0,75	<10	312	<0.04	7,7	8,5	0,12	13,1	5,4	450	3,6	0,182	15	174	36
CG13D-13/2013-11-21	0,6	119	0,45	23,2	2,03	0,72	<10	414	0,06	7,9	11	<0.04	18,9	7,2	500	3,6	0,23	17	183	47

Annex 7 continued. *In-situ* pore water chemistry of the Boom Clay from the piezometer CG-13D (previously named R13D). n.a. – not analyzed.

Name	filter distance from the gallery extrados (m)	time since borehole drilling (months)	Br^- [mg/l]	Cl^- [mg/l]	F- [mg/l]	I- [mg/l]	$S_2O_3^-$ [mg/l]	SO_4^{2-} [mg/l]	Al^{3+} [mg/l]	B [mg/l]	Ca^{2+} [mg/l]	Fe^{2+} [mg/l]	K^+ [mg/l]	Mg^{2+} [mg/l]	Na^+ [mg/l]	Si [mg/l]	Sr^{2+} [mg/l]	Alkal [meq/l]	DIC [mg C/l]	DOC [mg C/l]
CG13D-1/2014-9-23/1	39,6	129	0,46	21,6	2,58	0,56	<10	0,57	<0.05	7,1	1,33	0,29	9,3	1,19	320	4,7	0,05	13,633	159	42,99
CG13D-2/2014-9-23/1	35,6	129	0,49	22,2	2,5	0,58	<10	0,37	<0.05	7,3	1,21	0,27	9,8	1,15	320	4,9	0,045	14,254	158,8	48,2
CG13D-3/2014-9-23/1	30,6	129	0,66	30,2	2,96	0,79	<10	<0.25	<0.05	7,4	2,34	0,77	10,6	2,02	430	4,4	0,07	16,887	204,6	167,5
CG13D-4/2014-9-23/1	25,6	129	0,58	25,3	2,36	0,71	<10	0,3	<0.05	7,5	1,79	0,25	11,7	1,62	359	3,8	0,06	16,017	176,9	81,88
CG13D-5/2014-9-17/1	18,6	129	0,53	23,4	2,27	0,68	<10	<0.25	<0.05	7,5	1,49	0,3	11	1,42	311	4,2	0,052	13,485	156,6	62,98
CG13D-6/2014-9-18/1	14,6	129	0,6	22,9	2,55	0,69	<10	0,88	<0.05	8	2,09	0,52	10,2	1,87	315	3,8	0,066	13,52	145,8	77,94
CG13D-7/2014-9-22/1	11,6	129	0,53	22,8	2,32	0,69	<10	3,16	<0.05	7,4	1,98	0,63	9,8	1,6	310	3,8	0,056	12,679	156,6	74,44
CG13D-8/2014-9-17/1	8,6	129	0,51	21,3	2,38	0,65	<10	1,1	<0.05	7,7	1,84	0,05	10,2	1,52	301	3,9	0,051	13,418	144,2	76,29
CG13D-9/2014-9-17/1	5,6	129	0,52	22,1	2,36	0,68	<10	0,78	<0.05	7,7	2,11	0,4	10,7	1,81	317	3,5	0,06	13,84	147,4	96,07
CG13D-10/2014-9-17/1	3,6	129	0,54	21,6	2,56	0,69	<10	13,5	<0.05	7,8	2,53	0,12	11,6	2,14	330	3,7	0,071	14,076	149,7	93,99
CG13D-11/2014-9-15/1	2,6	129	0,5	21	2,43	0,67	<10	109	<0.05	7,7	3,3	0,65	13,5	2,88	372	3,07	0,102	13,909	160,3	73
CG13D-12/2014-9-15/1	1,6	129	0,48	19,8	2,14	0,65	<10	288	<0.05	7,9	5,4	<0.05	16,1	4,6	450	3,4	0,165	14,331	159,5	78,86
CG13D-13/2014-9-15/1	0,6	129	0,52	20,3	1,98	0,66	<10	402	<0.05	8,3	7,1	0,1	18,3	6,7	520	3,3	0,226	14,906	162,2	80,29
CG-13D-1/2015-10-13	39,6	142	0,52	21,0	2,89	0,54	<1	<0.5	<0.05	6,1	2,09	0,26	5,9	1,31	338	4,8	0,045	14,28	165,1	40,9
CG-13D-2/2015-10-13	35,6	142	0,56	21,3	2,69	0,57	<1	<0.5	<0.05	6,1	1,69	0,16	6,6	1,23	334	4,7	0,040	13,99	160,2	48,6
CG-13D-3/2015-10-13	30,6	142	0,68	27,8	3,54	0,82	<1	<0.5	<0.05	6,8	2,26	0,64	5,8	1,92	450	4,4	0,060	18,28	207,0	171,5
CG-13D-4/2015-10-13	25,6	142	0,55	21,4	2,29	0,70	<1	<0.5	<0.05	6,5	2,08	0,35	7,6	1,49	372	3,9	0,051	15,50	178,2	81,7
CG-13D-5/2015-10-13	18,6	142	0,56	24,1	2,67	0,68	<1	<0.5	<0.05	6,7	2,13	0,18	6,5	1,38	334	4,6	0,047	-	158,6	64,9
CG-13D-6/2015-10-12	14,6	142	0,52	21,2	2,28	0,65	<1	0,8	<0.05	6,5	1,69	0,60	7,0	1,31	315	3,7	0,044	13,32	154,1	66,1
CG-13D-7/2015-10-12	11,6	142	0,54	21,4	2,38	0,66	<1	1,3	<0.05	6,8	1,94	0,26	7,4	1,49	321	4,1	0,048	13,38	154,0	78,8
CG-13D-8/2015-10-12	8,6	142	0,52	19,9	2,37	0,64	<1	1,4	<0.05	6,8	1,88	0,11	6,4	1,42	306	4,1	0,046	12,84	148,4	68,0
CG-13D-9/2015-10-12	5,6	142	0,51	20,5	2,32	0,66	<1	0,5	<0.05	7,0	2,18	0,17	7,3	1,74	332	3,6	0,056	13,76	157,8	92,7
CG-13D-10/2015-10-12	3,6	142	0,51	20,3	2,60	0,67	<1	13,0	<0.05	7,1	2,72	0,14	9,0	2,01	345	3,9	0,065	13,91	159,8	80,1
CG-13D-11/2015-10-12	2,6	142	0,51	19,3	2,44	0,64	<1	95,0	<0.05	7,3	3,50	0,41	10,9	2,68	384	3,6	0,096	13,84	159,8	70,0
CG-13D-12/2015-10-13	1,6	142	<0.5	18,5	2,30	0,63	<1	247,0	<0.05	7,3	5,00	0,10	12,8	3,96	460	3,8	0,139	13,97	161,3	66,9
CG-13D-13/2015-10-15	0,6	142	0,53	19,6	2,23	0,66	<1	310,0	<0.05	7,6	5,90	<0.05	14,7	5,40	500	3,4	0,175	15,02	168,3	65,6

Annex 8. *In-situ* pore water chemistry of the Boom Clay from the piezometer P70S and P70D. All concentration values in mg/L.

Name	filter distance from the gallery extrados (m)	Br^- [mg/l]	Cl^- [mg/l]	F- [mg/l]	I- [mg/l]	$S_2O_3^-$ [mg/l]	SO_4^{2-} [mg/l]	Al^{3+} [mg/l]	B [mg/l]	Ca^{2+} [mg/l]	Fe^{2+} [mg/l]	K^+ [mg/l]	Mg^{2+} [mg/l]	Na^+ [mg/l]	Si [mg/l]	Sr^{2+} [mg/l]	Alkal [meq/l]	DIC [mg C/l]	DOC [mg C/l]
PG70S-3/2009-5-20	4.92	0,61	19,8	2,74	0,64	0,46	10,9	0,103	6,9	1,88	0,44	8,2	1,63	288	4,6	0,05	14,03	172,3	33,6
PG70S-4/2009-5-25	2.93	64	19,5	1,75	0,64	<0,25	14,2	0,093	7	3,56	1,32	9	1,77	291	4,7	0,054	18,52	174,5	42,2
PG70S-5/2009-5-20	1.94	37	22,6	3,01	0,77	<0,25	52,6	0,079	7,4	4,3	0,78	13,1	3,79	387	3,59	0,122	20,82	223,5	104,7
PG70S-6/2009-6-16	0.95	0,9	18	1,77	0,61	<0,25	850	0,029	7,9	9,6	0,72	22,2	8,7	600	3,9	0,278	13,55	157,6	74,9
PG70S-7/2009-6-16	0.45	0,78	14,2	0,7	0,61	349	3180	<0,02	10,4	59	0,94	82	93	1650	3,3	1,08	0,94	151,2	73,2
PG70S-1/2011-9-29/1	9,94	0,46	18,6	2,14	0,61	<1	2,05	0,075	5,1	2,1	3,76	7,9	1,25	276	4,1	0,062	13,371	130,7	52,16
PG70S-2/2011-9-29/1	6,96	0,52	19,1	2,21	0,61	<1	1,02	0,078	5,3	2,06	0,57	7,8	1,34	286	3,9	0,068	14,298	130,8	55,31
PG70S-3/2011-10-5/1	4.92	0,46	18,8	2,25	0,6	<1	0,85	<0.02	6	1,73	0,134	7,8	1,45	287	4,3	0,064	14,058	155,2	67,21
PG70S-4/2011-10-5/1	2.93	0,47	19,5	2,48	0,61	<1	0,74	<0.02	6,1	2,08	1,03	8	1,54	284	4,5	0,071	14,922	167,5	67,52
PG70S-5/2011-10-5/1	1.94	0,61	22,5	2,54	0,7	<1	0,78	<0.02	6,1	3,64	1,1	10,1	2,95	353	3,7	0,128	18,103	200,4	98,87
PG70S-6/2011-10-5/1	0.95	0,58	20,5	2,01	0,66	<1	293	<0.02	6,1	5,4	0,171	15,8	5,7	490	5,1	0,244	30,091	173,4	52,3
PG70S-7/2011-11-3/1	0.45	0,48	15,2	0,86	0,58	<1	1860	<0.02	6,5	26,5	0,312	43	37,9	1120	4,1	1,25	14,776	159,7	33,48
PG70D-1/2011-9-29/1	10	0,59	20,9	2,3	0,63	<1	0,72	0,066	5,6	1,85	0,76	7,5	1,23	296	3,46	0,067	14,73	140,8	45,74
PG70D-2/2011-9-29/1	8.49	0,49	21,3	2,18	0,66	<1	9,5	0,054	5,6	1,99	0,194	7,8	1,4	301	3,77	0,073	14,33	143,7	57
PG70D-3/2011-5-16/1	3.50	0,59	21,8	2,21	0,66	<1	7,18	<0.02	6,7	2,19	1,81	10	1,7	319	4,1	0,068	13,21	144,7	60,44
PG70D-4/2011-5-16/1	5.00	0,61	21,6	2,14	0,65	<1	70,9	<0.02	6,9	2,66	0,51	11,1	2,19	349	3,73	0,089	14,64	143,8	58,53
PG70D-5/2011-5-16/1	6.00	0,6	19,9	2,03	0,62	<1	219	<0.02	6,9	4	0,182	14,3	3,49	420	3,76	0,145	15,54	146,3	46,22
PG70D-6/2011-5-18/1	1.50	0,47	18,5	1,8	0,61	<1	365	<0.02	7	5,9	0,49	17,3	5,4	500	3,43	0,225	14,61	156,1	48,58
PG70D-7/2011-5-18/1	0.75	0,57	19,9	1,4	0,64	1,26	741	<0.02	7,1	13,6	0,63	24,4	11,8	690	3,82	0,49	15,05	166,5	47,81

Annex 9. Chemical composition of the leachates extracted from the core slices of the Test Drift (TD-41E). n.a. – not analyzed. (modified after De Craen *et al.*, 2008).

location	sample name/distance from the gallery extrados (cm)	S/L (g/g)	water content (wt%)	Na	K	Ca	Mg	Fe	Al	Si	SO42-	Cl	TIC	TOC
									mg/L					
TD41-42E	N2TD/0.0-0.4	1/10	23,63	144	21	45	10,8	0,12	0,2	12,8	337	0,89	24,12	25,16
TD41-42E	N2TD/0.4-0.6	1/10	27,02	179	16,3	22,6	11,8	0,64	n.a.	n.a.	157	1,82	47,52	21,44
TD41-42E	N2TD/0.6-0.8	1/10	30,22	196	32	194	42	0,02	0,0105	6,6	900	2,31	24,37	24,11
TD41-42E	N2TD/0.8-1.0	1/10	28,66	204	22,4	240	38,7	0,52	n.a.	n.a.	899	1,08	26,1	41,07
TD41-42E	N2TD/1.0-1.2	1/10	28,32	165	22	37	12,5	0,13	0,059	9	285	1,56	40,31	32,07
TD41-42E	N2TD/1.2-1.4	1/10	28,96	183	21,3	110	26,4	0,343	n.a.	n.a.	516	0,72	51,89	23,83
TD41-42E	N2TD/1.4-1.6	1/10	29,32	189	22,7	112	27,6	1,04	n.a.	n.a.	548	0,76	44,77	18,83
TD41-42E	N2TD/1.6-1.8	1/10	31,48	182	22	72	26,2	2,96	n.a.	n.a.	612	0,64	6,81	19,12
TD41-42E	N2TD/1.8-2.0	1/10	31,46	172	20,9	82	22,9	0,207	n.a.	n.a.	507	0,71	32,45	19,54
TD41-42E	N2TD/2.0-2.2	1/10	31,50	176	27	88	25	0,02	0,0075	7,9	560	1,1	28,7	20,62
TD41-42E	N2TD/2.2-2.4	1/10	32,97	171	19,6	47	18	0,83	n.a.	n.a.	486	0,63	14,32	23,08
TD41-42E	N2TD/2.4-2.6	1/10	32,32	174	23,4	113	31,4	0,43	n.a.	n.a.	695	0,69	19,06	21,16
TD41-42E	N2TD/2.6-2.8	1/10	33,61	181	24	72	25,5	1,28	n.a.	n.a.	614	0,97	9,15	20,44
TD41-42E	N2TD/2.8-3.0	1/10	34,34	197	24,2	66	24,8	0,315	n.a.	n.a.	616	0,68	9,99	20,25
TD41-42E	N2TD/3.0-3.2	1/5	33,44	320	43	134	43	0,49	1,13	9,8	1040	3	33,49	32,98
TD41-42E	N2TD/3.0-3.2	1/10	33,44	186	28	57	22	0,76	0,0283	13,6	590	1,83	2	15,81
TD41-42E	N2TD/3.0-3.2	1/50	33,44	39	9,4	10,9	4,6	1,23	3,5	10,9	123	0,37	3	6
TD41-42E	N2TD/3.0-3.2	1/100	33,44	22	6,7	39	6,7	0,12	1,08	5,1	149	0,31	6,34	3
TD41-42E	N2TD/3.2-3.4	1/10	33,38	182	26,9	86	30,2	6,8	n.a.	n.a.	690	0,62	1,93	16,21
TD41-42E	N2TD/3.4-3.6	1/10	33,64	173	22,8	59	22,1	1,73	n.a.	n.a.	562	0,63	6,63	17,63
TD41-42E	N2TD/3.6-3.8	1/10	33,33	176	19,6	35,6	15,6	2	n.a.	n.a.	448	0,68	12,4	24,77
TD41-42E	N2TD/3.8-4.0	1/10	33,36	170	20,3	37,3	16	0,97	n.a.	n.a.	451	0,65	13,26	21,33
TD41-42E	N2TD/4.0-4.2	1/10	32,43	175	26	57	21	0,02	0,0162	6,7	520	0,85	15,9	16,67
TD41-42E	N2TD/4.2-4.4	1/10	32,36	169	21,3	49	19,5	4,84	n.a.	n.a.	470	0,56	9,87	23,16
TD41-42E	N2TD/4.4-4.6	1/10	30,00	173	17	30,4	10,4	0,9	n.a.	n.a.	251	0,66	51,56	26,17
TD41-42E	N2TD/4.6-4.8	1/10	27,23	152	17	40	11,5	0,95	n.a.	n.a.	234	0,56	53,83	26,55
TD41-42E	N2TD/4.8-5.0	1/10	28,53	145	16	42	11,4	0,72	n.a.	n.a.	216	0,63	52,49	26,74
TD41-42E	N2TD/5.0-5.5	1/10	23,54	123	14,9	15,4	4,4	0,54	0,1	5,5	172	0,65	29,13	31,93

Annex 9 continued. Chemical composition of the leachates extracted from the core slices of the Test Drift (TD-41E). (modified after De Craen *et al.*, 2008).

location	sample name/distance from the gallery extrados (cm)	S/L (g/g)	water content (wt%)	Na	K	Ca	Mg	Fe	Al	Si	SO42-	Cl	TIC	TOC
									mg/L					
TD41-42E	N2TD/10.0-10.5	1/2	28,31	470	53	34	16,5	0,71	1,46	8,3	770	2,24	78,08	73,4
TD41-42E	N2TD/10.0-10.5	1/5	28,31	240	24	17,4	7,5	0,75	0,52	4,6	326	0,98	58,96	42,62
TD41-42E	N2TD/10.0-10.5	1/10	28,31	134	22	8,4	2,9	0,26	0,32	3,9	158	0,78	31,39	45,76
TD41-42E	N2TD/10.0-10.5	1/50	28,31	40	14,2	13,4	3,4	0,22	0,56	3,5	31,5	0,25	27,56	7,03
TD41-42E	N2TD/10.0-10.5	1/100	28,31	24	9,8	13	2,8	0,49	1,78	5,4	17,2	0,25	20,95	4,74
TD41-42E	N2TD/20.0-20.5	1/2	23,41	400	39	18,4	11,5	1,14	2,73	8,4	530	3	83,28	103,9
TD41-42E	N2TD/20.0-20.5	1/5	23,41	200	25	9,9	4,7	1,05	0,86	4,5	196	0,78	64,97	86,59
TD41-42E	N2TD/20.0-20.5	1/10	23,41	125	18	6,6	2,8	1,24	2,23	7,6	100	0,77	35,59	74
TD41-42E	N2TD/20.0-20.5	1/50	23,41	38	17	10,8	6,9	10	36	58	21,9	0,25	24,33	16,18
TD41-42E	N2TD/20.0-20.5	1/100	23,41	25	10	11,1	3,1	0,06	0,185	3,3	12,1	0,32	21,63	5
TD41-42E	N2TD/30.0-30.5	1/2	22,50	410	49	17,3	16,9	12,3	21	63	520	1,74	87,55	118,5
TD41-42E	N2TD/30.0-30.5	1/5	22,50	230	31	11,8	6,3	1,93	0,44	4,3	227	0,75	65,9	83,34
TD41-42E	N2TD/30.0-30.5	1/10	22,50	126	18	6,3	2,5	0,89	0,97	5,3	99	0,83	36,77	73,24
TD41-42E	N2TD/30.0-30.5	1/50	22,50	48	15,6	7,9	4,4	3,7	7,2	22	8	0,25	26,58	17,37
TD41-42E	N2TD/30.0-30.5	1/100	22,50	21	8,8	14,4	3,7	0,05	0,13	3,5	13,5	0,25	21,12	3,73

Annex 10. Chemical composition of the leachates extracted from the core slices of the Connecting Gallery (CG-68E). n.a. – not analyzed.

location	sample name/distance from the gallery extrados (cm)	S/L (g/g)	water content (wt%)	Na	K	Ca	Mg	Fe	Al	Si	SO42-	Cl	TIC	TOC
									mg/L					
CG68-69E	CG-R68-69E/0.0-0.4	1/10	37,12	246	53	280	67	15,2	0,05	13	1410	0,67	9,64	0,56
CG68-69E	CG-R68-69E/0.4-0.6	1/10	35,92	223	46	172	53	4,8	n.a.	n.a.	1080	0,96	8,84	15,17
CG68-69E	CG-R68-69E/0.6-0.8	1/10	35,63	239	47	440	74	0,239	0,051	9,6	1740	0,52	9,44	9,18
CG68-69E	CG-R68-69E/0.8-1.0	1/10	35,05	218	46	256	62	9,7	n.a.	n.a.	1240	0,95	10,08	13,65
CG68-69E	CG-R68-69E/1.0-1.2	1/10	34,92	229	41	311	68	1,19	0,029	5,2	1400	0,51	14,72	9,64
CG68-69E	CG-R68-69E/1.2-1.4	1/10	34,96	222	45	231	59	4,3	n.a.	n.a.	1180	0,9	10,25	15,09
CG68-69E	CG-R68-69E/1.4-1.6	1/10	34,21	212	41	164	52	0,96	n.a.	n.a.	1000	0,59	14,44	15,73
CG68-69E	CG-R68-69E/1.6-1.8	1/10	33,37	211	41	175	54	0,38	n.a.	n.a.	1020	0,65	11,91	16
CG68-69E	CG-R68-69E/1.8-2.0	1/10	32,04	200	34	75	32,7	0,6	n.a.	n.a.	639	0,59	17,42	15,46
CG68-69E	CG-R68-69E/2.0-2.2	1/10	31,76	216	38,30	141	47	0,132	0,095	3,37	900	0,45	17,34	10,27
CG68-69E	CG-R68-69E/2.2-2.4	1/10	32,07	207	42	110	39,9	0,91	n.a.	n.a.	783	0,67	15,26	18,5
CG68-69E	CG-R68-69E/2.4-2.6	1/10	31,26	217	50	322	65	0,98	n.a.	n.a.	1480	1,06	10,66	14,38
CG68-69E	CG-R68-69E/2.6-2.8	1/10	30,68	226	47	220	56	0,034	n.a.	n.a.	1110	n.a.	11,51	16,5
CG68-69E	CG-R68-69E/2.8-3.0	1/10	30,31	200	36,6	75	32,3	0,49	n.a.	n.a.	652	0,96	17,16	18,09
CG68-69E	CG-R68-69E/3.0-3.2	1/10	30,09	221	35,1	125	43	0,24	0,117	3,51	862	0,43	14,68	9,7
CG68-69E	CG-R68-69E/3.2-3.4	1/10	30,19	214	50	360	70	0,257	n.a.	n.a.	1540	0,65	11,15	19,99
CG68-69E	CG-R68-69E/3.4-3.6	1/10	30,22	205	44	178	51	0,41	n.a.	n.a.	980	1,05	16,19	16,62
CG68-69E	CG-R68-69E/3.6-3.8	1/10	29,99	207	42	193	53	0,095	n.a.	n.a.	1030	0,65	16,81	14,21
CG68-69E	CG-R68-69E/3.8-4.0	1/10	29,47	199	37,9	102	37,1	0,272	n.a.	n.a.	709	0,58	21,88	14,58
CG68-69E	CG-R68-69E/4.0-4.2	1/10	30,01	196	24,2	33,8	19,8	0,55	0,33	3,81	447	0,44	27,58	16,74
CG68-69E	CG-R68-69E/4.2-4.4	1/10	29,41	176	24,3	20,3	13,6	1,09	n.a.	n.a.	321	0,75	33,15	23,74
CG68-69E	CG-R68-69E/4.4-4.6	1/10	29,53	163	19,9	11,3	8,7	1,59	n.a.	n.a.	223	0,89	39,4	31,17
CG68-69E	CG-R68-69E/4.6-4.8	1/10	29,41	165	22,1	12,2	9,7	1,71	n.a.	n.a.	243	0,63	37,04	30,45
CG68-69E	CG-R68-69E/4.8-5.0	1/10	29,35	151	23,3	7,2	7	4,6	n.a.	n.a.	191	0,81	34,74	50,04
CG68-69E	CG-R68-69E/5.0-5.5	1/10	29,15	158	21	6,5	5,9	1,81	1,2	4,9	206	0,42	35,55	32,44

Annex 10 continued. Chemical composition of the leachates extracted from the core slices of the Connecting Gallery (CG-68E). n.a. – not analyzed.

location	sample name/distance from the gallery extrados (cm)	S/L (g/g)	water content (wt%)	Na	K	Ca	Mg	Fe	Al	Si	SO42-	Cl	TIC	TOC
									mg/L					
CG68-69E	CG-R68-69E/10.0-10.5	1/2	27,12	510	35,8	33	25,3	0,335	0,64	6,4	877	1,66	75,9	67,95
CG68-69E	CG-R68-69E/10.0-10.5	1/5	27,12	269	24	17,6	10,7	0,253	0,49	4	372	0,67	59,27	36,94
CG68-69E	CG-R68-69E/10.0-10.5	1/10	27,12	152	19	8,7	5,2	0,54	0,52	3,12	175	0,41	40,73	31,18
CG68-69E	CG-R68-69E/10.0-10.5	1/50	27,12	44	10	5,2	3,43	0,47	0,96	4,4	36,2	0,25	21,46	10,71
CG68-69E	CG-R68-69E/10.0-10.5	1/100	27,12	23,4	6,7	6	3,48	0,53	1,3	4,9	17,7	0,25	17,04	5,39
CG68-69E	CG-R68-69E/20.0-20.5	1/2	25,76	410	30,7	13,7	12,4	1,06	1,9	9,7	561	1,7	69,39	107,94
CG68-69E	CG-R68-69E/20.0-20.5	1/5	25,76	228	23	8,6	5,8	1,02	0,73	5	242	0,7	55,25	72,89
CG68-69E	CG-R68-69E/20.0-20.5	1/10	25,76	135	17,6	6,1	3,9	2,41	4,6	11,9	119	0,48	44,15	51,18
CG68-69E	CG-R68-69E/20.0-20.5	1/50	25,76	43	11	4,6	2,49	1,33	3,2	8,9	25,3	0,25	20,94	13,66
CG68-69E	CG-R68-69E/20.0-20.5	1/100	25,76	24,5	8,5	5,7	3,03	1,26	3,4	8,6	14	0,25	15,35	7,13
CG68-69E	CG-R68-69E/30.0-30.5	1/10	25,94	136	21,9	7	7,3	12	25	57	88,1	0,36	39,68	89,39
CG68-69E	CG-R68-69E/40.0-40.5	1/2	24,57	366	27,8	10,4	8,2	2,09	3,5	13,3	350	1,69	50,37	141,78
CG68-69E	CG-R68-69E/40.0-40.5	1/5	24,57	196	18,6	7,4	4,4	1,62	2,8	7,6	117	0,69	50,8	153,89
CG68-69E	CG-R68-69E/40.0-40.5	1/10	24,57	128	14,8	5,6	3,37	3,08	2,1	15,5	59,4	0,34	44,56	90,64
CG68-69E	CG-R68-69E/40.0-40.5	1/50	24,57	43	9,7	5	1,94	0,61	6,1	5,3	12	0,25	22,71	17,43
CG68-69E	CG-R68-69E/40.0-40.5	1/100	24,57	25,1	7,7	6,2	2,32	0,41	1,6	4,5	9,6	0,25	18,3	7,15

Annex 11. Chemical composition of the leachates extracted from the core slices of the PRACLAY Gallery (PG-70D).

location	distance from the gallery extrados (cm)	S/L (g/g)	water content (wt%)	Na	K	Ca	Mg	Fe	Al	Si	SO42-	Cl	TIC	TOC
									mg/L					
PGR70-71D	0.0-0.4	1/10	22,00	93	13,9	6,3	2,4	1,6	18	7	4,4	0,6	69	112
PGR70-71D	0.4-0.6	1/29	21,41	52	9,1	3,9	1,5	0,4	11	3	1,6	0,6	46	43
PGR70-71D	0.6-0.8	1/10	23,25	90	21,2	8,2	5,1	6,4	54	30	3,4	0,9	68	111
PGR70-71D	0.8-1.0	1/10	23,21	87	12,3	6,4	2,6	9,9	18	7	3,7	1,0	63	112
PGR70-71D	1.0-1.2	1/10	23,26	88	13,0	6,3	2,5	1,5	16	6	3,6	0,5	64	111
PGR70-71D	1.2-1.4	1/10	23,37	88	12,7	6,6	2,9	2,4	20	10	3,7	0,6	62	113
PGR70-71D	1.4-1.6	1/11	23,04	86	22,4	8,3	5,2	6,7	52	30	3,5	0,5	65	107
PGR70-71D	1.6-1.8	1/10	23,47	93	32,3	9,9	9,1	15,6	87	76	5,2	0,7	66	121
PGR70-71D	2.0-2.2	1/23	22,65	55	16	4,7	2,8	2,7	33	10	1,7	0,4	46	55
PGR70-71D	2.2-2.4	1/10	23,06	90	11,4	6,0	2,5	2,1	14	7	4,9	0,8	64	118
PGR70-71D	2.4-2.6	1/11	22,88	87	18,2	7,3	4,0	4,5	39	18	4,6	0,7	63	111
PGR70-71D	2.6-2.8	1/11	23,10	88	19,5	8,0	4,6	5,6	44	24	4,7	0,6	64	113
PGR70-71D	2.8-3.0	1/11	23,05	88	23,4	8,1	5,9	8,8	60	39	4,1	0,8	64	111
PGR70-71D	3.0-3.2	1/11	23,01	90	28,6	9,4	9,1	16,1	79	187	4,3	0,5	65	118
PGR70-71D	3.2-3.4	1/9	23,16	99	54,0	12,6	13,8	24,6	150	355	6,8	0,7	68	139
PGR70-71D	3.4-3.6	1/10	23,09	93	18,5	7,6	3,4	3,1	43	10	5,4	0,5	67	113
PGR70-71D	3.6-3.8	1/10	22,68	96	51,0	11,6	11,2	18,8	134	353	5,5	0,7	67	142
PGR70-71D	3.8-4.0	1/10	22,54	95	33,4	10,0	6,3	7,9	94	250	5,4	0,6	67	135
PGR70-71D	4.0-4.2	1/10	23,11	94	24,2	8,3	5,7	7,9	63	153	5,1	0,6	68	127
PGR70-71D	4.2-4.4	1/11	23,26	90	17,3	6,8	3,8	4,2	39	14	4,7	0,5	66	110
PGR70-71D	4.4-4.6	1/11	22,96	91	17,2	7,5	3,4	3,1	36	12	6,8	0,7	67	110
PGR70-71D	4.6-4.8	1/11	22,87	88	19,6	7,1	4,2	5,6	44	22	6,4	0,8	65	108
PGR70-71D	4.8-5.0	1/10	21,28	90	9,0	5,4	2,2	1,7	5	4	9,0	0,9	65	116
PGR70-71D	5.0-5.5	1/8	22,86	107	22,0	8,5	4,5	5,5	51	121	13,5	1,1	73	132
PGR70-71D	10.0-10.5	1/2	21,99	252	44,0	20,5	10,5	7,8	75	23	53,4	2,2	143	403
PGR70-71D	10.0-10.5	1/5	21,99	156	18,2	9,6	4,0	2,5	20	8	28,8	0,8	100	171
PGR70-71D	10.0-10.5	1/11	21,99	98	20,7	8,4	3,9	3,9	40	16	16,5	0,6	69	99
PGR70-71D	10.0-10.5	1/50	21,99	31	9,4	4,8	1,5	0,1	1	2	11,4	0,3	31	13
PGR70-71D	10.0-10.5	1/255	21,99	8	4,0	7,4	2,1	0,1	0	1	0,7	0,3	20	4
PGR70-71D	20.0-20.5	1/2	23,06	257	22,3	13,1	6,3	3,1	11	7	25,1	2,2	164	299
PGR70-71D	20.0-20.5	1/5	23,06	149	17,2	7,9	3,1	1,3	13	4	9,9	0,7	106	124
PGR70-71D	20.0-20.5	1/10	23,06	101	12,3	6,5	2,3	6,6	13	3	5,3	0,6	77	77
PGR70-71D	20.0-20.5	1/55	23,06	28	6,6	5,2	1,6	0,1	0	2	1,6	0,3	32	14
PGR70-71D	20.0-20.5	1/108	23,06	16	5,5	6,7	1,9	0,1	0	1	0,5	0,3	26	4
PGR70-71D	27.5-28.0	1/2	22,75	261	21,1	15,0	6,8	3,0	9	5	31,0	2,8	157	376
PGR70-71D	27.5-28.0	1/5	22,75	146	15,5	9,5	3,6	2,3	19	7	10,6	0,9	100	179
PGR70-71D	27.5-28.0	1/11	22,75	95	22,5	7,9	3,8	4,0	58	127	5,3	0,7	72	95
PGR70-71D	27.5-28.0	1/46	22,75	37	12,6	3,8	1,9	2,7	6	2	1,8	4,5	39	14
PGR70-71D	27.5-28.0	1/101	22,75	18	4,0	3,6	2,2	0,3	0	2	0,5	0,3	26	8

sck cen

Registered Office
Herrmann-Debrouxlaan 40
1160 Brussel – Belgium

Foundation of Public Utility
VAT BE 406.568.867

Research Centres
Boeretang 200
2400 Mol – Belgium

Chemin du Cyclotron 6
1348 Ottignies-Louvain-la-Neuve – Belgium

Reference N°	Creation Date	
SCK CEN/36148856	2020-04-20	
Alternative Reference N°	Revision	Version
N/A	1.0	12
ISC	Revision Status	
Public	Approved	

ER-0609 Overview of oxidation phenomena in Boom Clay around galleries of the HADES URF URF – Status 2019

Authors*
Miroslav Honty ; Mieke De Craen ; Lian Wang ; Eef Weetjens

Review information since previous revision*		
Name	**Outcome**	**Date**
Elke Jacops	Reviewed	2020-04-20

Approval information for current revision*		
Name	**Outcome**	**Date**
Norbert Maes	Approved	2020-04-22

Change log*				
Revision	**Version**	**Status**	**Date**	**Description of change**
1.0	12	Approved	2020-04-20	

Internal Distribution List*	
Name	**Expert Group/Unit**
Miroslav Honty	EHS | W&D | RDD
Mieke De Craen	EHS | EUR
Lian Wang	EHS | W&D | RDD
Eef Weetjens	EHS | W&D | EGA

External Distribution List*	
Name	**Affiliation**
Xavier Sillen	NIRAS/ONDRAF

**This automatically generated cover page shows references and workflow status information as were available in the Alexandria document*